The Dissertation Committee for Andrew Scott Thornburg
certifies that this is the approved version of the following dissertation:

Analysis of Millimeter Wave Ad Hoc Networks

Committee:

Robert W. Heath, Jr., Supervisor

Jeffrey Andrews

François Baccelli

John Hasenbein

Gustavo de Veciana

Analysis of Millimeter Wave Ad Hoc Networks

by

Andrew Scott Thornburg

DISSERTATION

Presented to the Faculty of the Graduate School of

The University of Texas at Austin

in Partial Fulfillment

of the Requirements

for the Degree of

DOCTOR OF PHILOSOPHY

THE UNIVERSITY OF TEXAS AT AUSTIN

December 2017

Dedicated to my grandfather,

Dr. Kenneth L. Garver M.D. Ph.D.

Acknowledgments

I extend my sincere gratitude to my supervisor, Professor Robert Heath, for his guidance, patience, and support. Professor Heath continually extended help and opportunities for growth academically, professionally, and personally. I also wish to thank my committee for their questions and feedback: Professors Jeff Andrews, François Baccelli, John Hasenbein, and Gustavo de Veciana. I am very grateful to Professor Matthew McKay for hosting a summer at Hong Kong University of Science and Technology. My thanks extend to my colleagues from the WSIL lab. The lab consistently provided help and ideas to shape my research, as well as friendly faces on a daily basis. My lab mates, past and present, helped through our shared experience at UT: Anum Ali, Travis Cuvelier, Rebal Jurdi, Talha Khan, Preeti Kumar, Sungwoo Park, Vutha Va, Yuyang Wang, Dalin Zhu, and Drs. Amin Abdel-Khalek, Ahmed Alkhateeb, Salam Akoum, Tianyang Bai, Omar El Ayach, Namyoon Lee, Jeonghun Park, Ken Pesyna, and Kiran Venugopal. I am very grateful to the WNCG and Electrical Engineering department staff for their help throughout the graduate program. I thank Brother Ernest J. Miller, FSC, D. Min for teaching the importance of talking nuance, especially outside the bubble of engineering.

The friendships I formed during my time Austin with my fellow grad students proved invaluable at remaining positive throughout the graduate ex-

perience: Andrew Kerns, Chris Brennan, Ethan Elenberg, Xin Xu, and Kyle McNicholas. A special thanks to my roommates, Jeff Smith and Kyle McNicholas, these past several years. I really do not know if I would have made it to the end without the laughing, goofiness, and venting I get to experience on a daily basis. My family has given me their endless support and inspiration over the past years. I am so grateful for my mother Maureen and siblings Alyssa and Bartley.

Lastly, I must thank Ani for her unyielding support and encouragement. I cannot wait for what comes next.

Analysis of Millimeter Wave Ad Hoc Networks

Publication No. _____

Andrew Scott Thornburg, Ph.D.
The University of Texas at Austin, 2017

Supervisor: Robert W. Heath, Jr.

Over the coming few years, the next-generation of wireless networks will be standardized and defined. Ad hoc networks, which operate without expensive infrastructure, are desirable for use cases such as military networks or disaster relief. Millimeter wave (mmWave) technology may enable high speed ad hoc networks. Directional antennas and building blockage limit the received interference power while the huge bandwidth enables high data rates. For this reason, understanding the interference and network performance of mmWave ad hoc networks is crucial for next-generation network design.

In my first contribution, I derive the SINR complementary cumulative distribution function (CCDF) for a random single-hop mmWave ad hoc network. These base results are used to further give insights in mmWave ad hoc networks. The SINR distribution is used to compute the transmission capacity of a mmWave ad hoc network using a Taylor bound. The CDF of the interference to noise ratio (INR) is also derived which shows that mmWave ad

hoc networks are line-of-sight interference limited. I extend my work in the second contribution to include general clustered Poisson point processes to derive insights in the effect of different spatial interference patterns. Using the developed framework, I derive the ergodic rate of both spatially uniform and cluster mmWave ad hoc networks. I develop scaling trends for the antenna array size to keep the ergodic rate constant. The impact of beam alignment is computed in the final part of the contribution. Finally, I account for the overhead of beam alignment in mmWave ad hoc networks. The final contribution leverages the first two contributions to derive the expected training time a mmWave ad hoc network must perform before data transmission occurs. The results show that the optimal conditions for minimizing the training time are different than the optimal conditions for maximizing rate.

Table of Contents

List of Tables

List of Figures

Chapter 1

Introduction

When wireless is perfectly applied, the whole earth will be converted into a huge brain, which in fact it is, all things being particles of a real and rhythmic whole. We shall be able to communicate with one another instantly, irrespective of distance. Not only this, but through television and telephony we shall see and hear one another as perfectly as though we were face to face, despite intervening distances of thousands of miles; and the instruments through which we shall be able to do his will be amazingly simple compared with our present telephone. A man will be able to carry one in his vest pocket.

–Nikola Tesla, 1926

1.1 Introduction

Nearly every industry has been affected by the emergence of the ubiquitous mobile data connection: bridges communicate information about cracks or failures, farmers in rural Africa check the market prices in cities to ensure a fair price, any fact or idea can be queried instantly, medical devices in the home

communicate directly with doctors. There are now more mobile connected devices than people on the planet. The growth in devices has coincided with an explosion of demand for wireless data; it is expected that the capacity of wireless networks must increase 1000 fold this decade to meet the demand. An overwhelming majority of this data is sent over ad hoc networks using protocols like IEEE 802.11 wireless LAN (WLAN); WLANs transmit roughly 4× the data per month compared to cellular networks as of late 2016 [2].

Ad hoc networks are characterized by their lack of infrastructure. Users in cellular networks only communicate with fixed base stations, but users in ad hoc networks communicate with each other directly; all users transmit or receive data. A fantastic use-case for ad hoc networks is after a natural disaster. Disasters, such as Hurricane Maria in Puerto Rico, the earthquake in Haiti, or the typhoon in the Philippines, destroy the cellular infrastructure. Collaboration of rescue crews, communication with loved ones, and coordination of aid delivery is hindered by the devastation. An ad hoc network transforms a smart phone into both a cell tower and cell phone. By doing this, data can be transmitted throughout the disaster area. However, such features are largely ignored because ad hoc networks are notoriously inefficient.

1.2 Next-generation Ad Hoc Networks

Modern wireless communication systems are interference limited meaning that unintended transmissions, e.g. other users, obfuscate the intended message. Newer fixed, planned networks such as cellular systems utilize so-

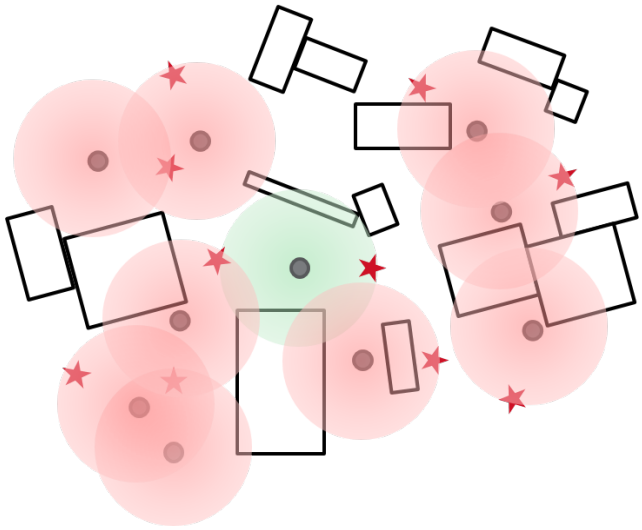

Figure 1.1: In a typical ad hoc network, the omni-directional transmissions of neighboring users limits performance. Interference mitigation strategies must be used or the interference must be tolerated for communication to occur.

phisticated techniques to minimize unwanted interference. The less organized nature of ad hoc networks limits the opportunity to use these techniques. Ad hoc networks, illustrated in Fig. 1.1, consistently underperform compared to fixed, planned networks. A main reason is due to the self-interference created in the network. There is often little coordination between users which creates residual interference that leads to poor signal-to-interference-plus-noise ratios (SINRs) [3].

A fundamental concept of wireless communication is the *spectral efficiency* in $bits/s/Hz$ of the communication which is a function of the SINR and primarily limited by interference in modern wireless systems. Broadly speaking, a user must consume time s or frequency Hz resources to receive

their data *bits*. As more users communicate with ad hoc protocols like IEEE 802.11 [4], IEEE 802.15.3 [5], Bluetooth [6], Zigbee [7], and others, an inefficiency feedback loop begins. A user must spend more time or frequency resources to receive their data which in turn creates more interference for other users because the time/frequency resources are occupied. MmWave band communication aims to remedy some of these issues. MmWave networks use directional antennas which limit the interference and boost the SINR to increase efficiency. Users may require less time or frequency resources to complete their tasks. The mmWave band is also much wider than current frequencies used for wireless communication. MmWave communication has the potential to be *more efficient* while having access to *more resources*.

1.3 The Challenges of mmWave Ad Hoc Networks

The vast and underutilized millimeter wave (mmWave) band between $30-300$ GHz appears to be an outstanding candidate for the next generations of ad hoc networks, shown in Fig. 1.2. By moving to the mmWave spectrum, many gigahertz of bandwidth are available making it possible to achieve data rates of gigabits per second even with conventional modulation strategies. While mmWave systems provide an enormous benefit in their bandwidth, there are several constraints that are not present in lower frequency systems. First, the mostly digital MIMO implementations found at lower frequencies are unlikely; high-speed, high-bandwidth analog-digital converters require too much power to include many in a mobile device [8]. As a result, mmWave sys-

tems are more likely to use analog beamforming, or hybrid approaches [9], [10]. Second, mmWave propagation is much more sensitive to blockages than lower frequency signals [11]. While non-line-of-sight (NLOS) communication is possible, system design parameters may be different between line-of-sight (LOS) / NLOS regimes as the path-loss exponent can be vastly different [12]. Third, mmWave devices will have dozens, perhaps hundred of antennas to overcome the path-loss. Historically, path loss has been viewed as a limiting factor for employing mmWave wireless systems; by fabricating many mmWave antennas in the same physical size of a single UHF antenna, the path-loss difference can be eliminated. This dissertation develops a framework to evaluate single-hop ad hoc networks while incorporating the key characteristics of mmWave communication.

The first two contributions of this dissertation argue mmWave ad hoc networks can be more efficient in their spectrum usage even with NLOS communication; these contributions show that analog beamforming and building blockage of mmWave ad hoc networks help decrease the overall interference if properly designed for. This dissertation extends the current literature by deriving signal and interference metrics for mmWave single-hop ad hoc networks using stochastic geometry. The seminal work by Gupta and Kumar [13] introduced key bounds and limits on the transport capacity of random wireless networks. Baccelli pioneered the use of stochastic geometry for ad hoc networks [14]. By using stochastic geometry, closed-formed expressions are derived for the SINR distribution of ad hoc networks; this analysis technique

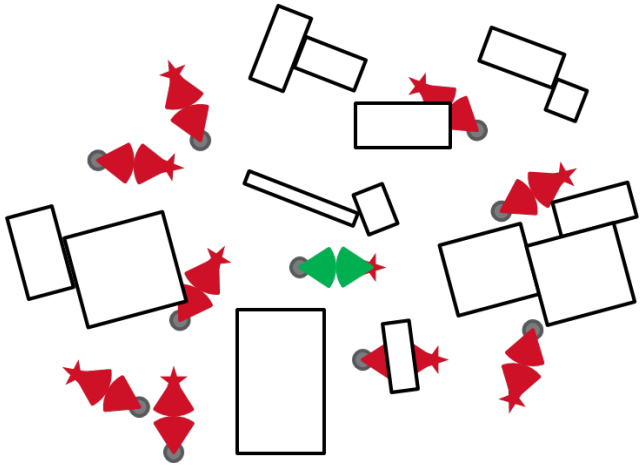

Figure 1.2: In a mmWave ad hoc network, the transmitter and receiver use antenna arrays to direct the RF energy towards each other. The interference caused to neighboring users in the sidelobe is lessened as compared to omni-directional transmission. Building blockage also limits signal strength as mmWave propagation is heavily attenuated by building materials and diffraction around buildings is not a strong phenomenon.

has proved to be extremely popular tool to analyze wireless networks [3,15–22].

In the second and third contribution of this dissertation, I address important aspects of mmWave antenna array system design: beam alignment error and training overhead. A key enabling technology for using mmWave frequencies is active steerable beam pointing [12, 23, 24]. By coupling the energy better in the channel, the transmitter and receiver achieve beamforming gain to provide sufficient signal-to-noise (SNR) at the receiver. The key idea is that the transmitter and receiver sequentially try different beam pairs to find the pair with the largest effective received power [25, 26]. Due to mobility between users, within a user, or in the environment, the beam must constantly be realigned. This incurs a high cost as the time to test all the pair combinations

grows with the square of the number of pairs.

Together, the contributions of this dissertation demonstrate the capability of mmWave ad hoc networks communicate in an outdoor, mobile environment. I illustrate that mmWave ad hoc networks can communicate over long distances and remain less susceptible to interference than low-frequency ad hoc networks. I argue that mmWave networks do not need to cooperate in a clustered environment due to the directional antenna arrays. Lastly, I show that while overhead in training mmWave antenna array increases latency and reduces rate, high data rates are possible given the proper optimizing of the network parameters.

1.4 Summary of Contributions

This section summarizes the contributions of my PhD dissertation.

1. Chapter 2: Signal to Interference Plus Noise Ratio in mmWave Ad Hoc Networks

   In this chapter, I formulate the performance of mmWave ad hoc networks in a stochastic geometry framework. I incorporate random factors of a mmWave ad hoc network such as building blockage, antenna alignment, interferer position, and user position. Using a similar framework, I compare and contrast the performance against a lower frequency UHF ad hoc network. The main contributions of the chapter can be summarized as follows:

(a) I compute a bound for mmWave ad hoc network signal-to-interference-and-noise (SINR) complimentary cumulative distribution function (CCDF). Using the SINR CCDF, a Taylor approximation is used to compute the transmission capacity and area spectral efficiency of the network. I argue for LOS-aware protocols due to the large performance increase from LOS communication at mmWave. Lastly, I calculate the effect of random receiver location on performance.

(b) I derive the interference-to-noise ratio (INR). I include discussion of the INR when a network is operating at the transmission capacity.

(c) I characterize the effect of two-way communication on the transmission capacity and area spectral efficiency. I show that optimal bandwidth allocation leads to large gains in both performance metrics.

2. Chapter 3: Ergodic Rate in Random mmWave Ad Hoc Networks

   In this chapter, I characterize the ergodic rate of mmWave ad hoc networks for two different spatial distributions of transmitters. I leverage stochastic geometry to model mmWave ad hoc networks as uniform networks (e.g. a Poisson point process) and a LOS cluster process (e.g. Poisson cluster process). The main contributions of the chapter are summarized as follows:

   (a) I derive the ergodic rate of a uniform mmWave ad hoc network assuming LOS communication, directional antennas, building block-

age, and Gamma fading. An antenna scaling trend, as transmitter density increases, of uniform mmWave ad hoc networks is derived. The result indicates that the number of antennas can scale sub-linearly with transmitter density.

(b) I compute the ergodic rate of a clustered mmWave ad hoc network assuming LOS communication, directional antennas, building blockage, and Gamma fading. An antenna scaling trend of clustered ad hoc networks is proposed as a heuristic using the ergodic rate theorem which indicates that antenna arrays must scale linearly with user density. I define and develop a relationship between the SINR for communication within a cluster (intra-cluster) and between clusters (inter-cluster) which gives the proximity of the nearest cluster while maintaining rate requirements within a cluster.

(c) I characterize of the effect of random beam misalignment between the desired user pairs. I present results for two antenna models: sectored and Gaussian. The loss in rate per user is shown to be proportional to alignment error variance; a rate loss of up to 45% occurs if the alignment error standard deviation is 10°.

3. Chapter 4: Beam Training in Random mmWave Ad Hoc Networks

In this chapter, I characterize the overhead cost of beam alignment in terms of latency and rate reduction. I use stochastic geometry to model the user pair locations, the antenna array as a sectored antenna array,

and line-of-sight (LOS) ball blockage model. I derive analytic expressions and bounds to be derived for the data transmission delay and the user perceived rate. The main contributions of the chapter are summarized as follows:

(a) I compute the relative strength of the interfering users in a mmWave ad hoc network. The results show that despite the decreasing probability of a mainlobe collision between a user and interferer as the antenna array grows, the interferers with colliding mainlobes remain the dominant and thus the limiting source of an interference-limited scenario. In LOS and non-line-of-sight (NLOS) scenarios, mainlobe collisions are stronger by a factor that is proportional to the array size given a sectored antenna model. I present results that show the increase in synchronization time due to a blockage event at the transmitter as well as a complete blockage event at the receiver. I show that blockage events at the transmitter are essentially nonrecoverable due to the degradation of signal power for fast training techniques while blockage events at the receiver may allow successful communication.

(b) I derive of the expected data transmission delay of three different beamforming strategies as a function of transmission probability and antenna array size. I show that using omni-directional reception is optimal for mmWave ad hoc networks if the transmission probability is sufficiently low or if the antenna array size and train-

ing length is sufficiently large. In particular, I give expressions for the optimal transmission probability for minimizing the delay as well as well as the region where omni-directional reception is optimal.

(c) I characterize of the user-perceived ergodic rate when using each of the synchronization methods. The results indicate that the optimal transmission probability for ergodic rate is typically larger than the optimal point for delay within a fixed transmission block; a similar conclusion holds for the array size. In the high mobility case where overhead is most costly, if the underlying user density is too high, the users must back off the channel too frequently for successful training to complete and data transmission to begin.

1.5 Organization

The rest of the dissertation is organized as follows. Chapter 2 introduces the SINR and INR of mmWave ad hoc networks, as well as the transmission capacity. Chapter 3 presents the ergodic rate for clustered and uniform mmWave ad hoc networks including the capacity scaling and capacity loss regarding antenna arrays. Chapter 4 determines the potential overhead for beam sweeping for mmWave ad hoc networks. The dissertation is concluded in Chapter 5 with parting thoughts and avenues of future work.

Chapter 2

Signal to Interference Plus Noise Ratio in Random mmWave Ad Hoc Networks

In this chapter[1], I derive the SINR CCDF of outdoor mmWave ad hoc networks with LOS and NLOS communication. I first give a overview of prior stochastic geometry results pertinent to mmWave and ad hoc networks in Section 2.1. Next, I introduce the system model and relevant metrics in Section 2.3. In Section 2.4, I detail the derivation of the one-way SINR CCDF which is followed by the two-way SINR CCDF in Section 2.5. The results are presented in Section 2.6, and the chapter is concluded in Section 2.7.

2.1 Introduction

Prior work has leveraged stochastic geometry to calculate the performance of ad hoc networks [20]. The transmission capacity is the maximum spatial density (users per m^2) of transmitters given an outage constraint and is well studied, see [3,15,16,19,20,27], and references therein. A related metric

[1]This chapter is based on the work that will appear in the journal paper: A. Thornburg, T. Bai and R. W. Heath Jr., "Performance Analysis of Outdoor mmWave Ad Hoc Networks," in IEEE Transactions on Signal Processing, vol. 64, no. 15, pp. 4065-4079, Aug.1, 1 2016. This work was supervised by Prof. Robert Heath. Dr. Tianyang Bai provided insights in the stochastic geometry modeling of mmWave wireless networks.

is the area spectral efficiency which yields the $b/s/Hz/m^2$ of a network [28]. Both metrics are widely used to compare and contrast transmission techniques and network architectures.

Beamforming has been analyzed with stochastic geometry and other methods in ad hoc networks under the term *smart antennas*, phased arrays, or adaptive antennas. Prior work on ad hoc networks considered smart antennas and other directional antennas [16, 29–32]. The transmission capacity of ad hoc networks with directional antennas was computed in [16] assuming small-scale Rayleigh fading. A directional MAC testbed was benchmarked in [29]. In [30], the analyses and performance of the system assumes Rayleigh fading. The optimization of the MAC for directional antennas was discussed in [31,32]. While the results are frequency agnostic, the results are built around channel models that reasonably apply only for sub-mmWave systems.

Blockage is an important impairment in mmWave ad hoc systems. Work in [12, 33, 34] showed that the path-loss models were different between line-of-sight (LOS) and non-line-of-signt (NLOS) due to building blockage. This was the basis of the stochastic geometry analysis in [1] which was applied to cellular systems. The exclusion zone of the cellular system model in [1] is not applicable to ad hoc networks. In the cellular model, the users fall in the Voronoi cell of the base station. The strongest interferer due to the Voronoi structure must lie outside a ball centered at the receiver. While in an Aloha ad hoc network, an interfering transmitter can be arbitrary close [35]. In [36], blockage results from small-scale fading. At mmWave frequencies,

blockages are due to obstacles like buildings which heavily attenuate mmWave signals [37]. The effect of blockage is developed in [1] for mmWave cellular networks; rate trends for cellular are captured with real-world building footprints in [38]. A LOS-ball approach is taken in [39] for backhaul networks which is validated using real-world building data. Wearable networks which quantified the effect of human blockage was considered in [40]. No consideration has been made in the literature, however, to the effect of blockage on outdoor mmWave ad hoc networks.

2.2 Contributions

In this chapter, I formulate the performance of mmWave ad hoc networks in a stochastic geometry framework. I incorporate random factors of a mmWave ad hoc network such as building blockage, antenna alignment, interferer position, and user position. Using a similar framework, I compare and contrast the performance against a lower frequency UHF ad hoc network. The main contributions of the chapter can be summarized as follows:

- Derivation of a bound for mmWave ad hoc network signal-to-interference-and-noise (SINR) complimentary cumulative distribution function (CCDF). Using the SINR CCDF, a Taylor approximation is used to compute the transmission capacity and area spectral efficiency of the network. I argue for LOS-aware protocols due to the large performance increase from LOS communication at mmWave. Lastly, I calculate the effect of random receiver location on performance.

- Computation of the interference-to-noise ratio (INR). I include discussion of the INR when a network is operating at the transmission capacity.
- Characterizing the effect of two-way communication on the transmission capacity and area spectral efficiency. I show that optimal bandwidth allocation leads to large gains in both performance metrics.

The rest of the chapter is organized as follows. Section 2.3 provides the system model and assumptions used in the chapter. Section 2.4 derives the SINR distribution, transmission capacity, ASE, and INR distribution for the one-way network. Section 2.5 quantifies the transmission capacity and ASE for two-way networks. I present the results in Section 2.6 and conclude the chapter in Section 2.7. Throughout the chapter, $\mathbb{P}[X]$ is the probability of event X and $\mathbb{E}$ is the expectation operator. A summary of the commonly used variables is in Table 2.1.

2.3 System Model

2.3.1 Network Model

Consider an ad hoc network where users act as transmitter or receiver. I use the dipole model of [35] where each transmitter in the network has a corresponding receiver at distance r_o. The transmitters operate at constant power with no power control. The location of the transmitting users within the network are points from a homogeneous Poisson point process (PPP) Φ on the Euclidean plane $\mathbb{R}^2$ with intensity λ_{u}, which is standard for evaluating the

Φ	homogeneous Poisson point process (PPP)
λ_{u}	intensity of the PPP
ζ	transmission probability
λ	effective transmitter density
r_o	communication distance
SINR	signal-to-noise ratio
Γ	SINR threshold for success comm
$p(x)$	blockage probability function
β	blockage building density
a_i	path loss exponent
N	number of antennas
$G_{\mathrm{ml}}, G_{\mathrm{sl}}$	mainlobe,sidelobe antenna gain
κ	system antenna gain
λ_ϵ	transmission capacity

Table 2.1: System variables for Chapter 2

transmission capacity of ad hoc networks, see [20] and the references therein. I analyze performance at the *typical* dipole pair at the origin. The performance of the typical dipole characterizes the network performance thanks to Slivnyak's Theorem [35]. The channel is accessed using a synchronized slotted Aloha-type protocol with parameter ζ. During each block, a user transmits with probability ζ or remains silent with probability $(1-\zeta)$. I condition on a fully outdoor network. I define the effective transmitting user density, used throughout the rest of the chapter, as

$$\lambda = \zeta p_{\mathrm{out}} \lambda_{\mathrm{u}}, \tag{2.1}$$

where p_{out} is the probability a user is outdoors. A homogeneous PPP is perhaps overly simplistic, but I leave the investigation of mmWave ad hoc networks modeled with non-homogeneous PPPs to future work. I leave the optimization

of p_{tx} to future work, but provide a framework to find the solution in Section 2.5. The analysis of [37] shows how to compute p_{out} using stochastic geometry.

2.3.2 Use of Beamforming

Now I explain the role of beamforming in the mmWave signal model. The natural approach to combat increased omni-directional path-loss of mmWave is to use a large antenna aperture, which is achieved using multiple antennas [12, 41, 42]. The resulting array gain overcomes the frequency dependence on the path-loss and allows mmWave systems to provide reasonable link margin. I denote the path-loss intercept as $A = 20\log_{10}\left(\frac{2\pi d_{\text{ref}}}{\lambda_{\text{ref}}}\right)$ with $d_{\text{ref}} = 1m$ [34] and λ_{ref} as the carrier wavelength.

I assume that adaptive directional beamforming is implemented at both the transmitter and receiver where a main lobe is directed towards the dominate propagation path while smaller sidelobes direct energy in other directions. No attempt is made to direct nulls in the pattern to other receivers [43]; this is an interesting problem for future work. To facilitate the analysis, I approximate the actual beam pattern using a sectored model, as in [16]. The beam pattern is parameterized by three values: main lobe beamwidth (θ_{ant}), main lobe gain (G_{ml}), and back lobe gain (G_{sl}). Such an antenna is shown in Fig. 2.1 where the mainlobe is 90°, 30°, or 9° with gain of 3dB, 10dB, or 15dB, respectively. The interferers are also equipped with directional antennas. Because the underlying PPP is isotropic in $\mathbb{R}^2$, I model the beam-direction of the typical node and each interfering node as a uniform random variable on

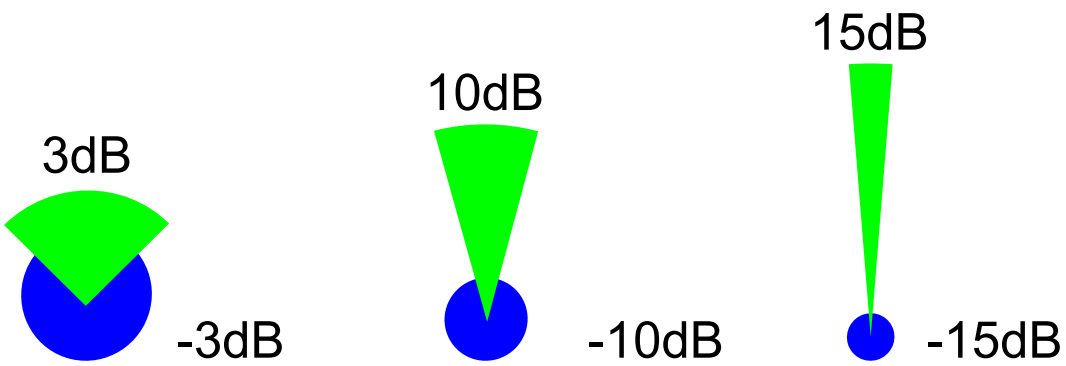

Figure 2.1: An illustration of the sectored antenna model I use. Beamwidths are 90°, 30°, and 9°, respectively.

$[0, 2\pi]$. Thus, the effective system antenna gain of the interference seen by the typical node is a discrete random variable described by

$$\kappa_i = \begin{cases} G_{\text{ml}}G_{\text{ml}} & \text{w.p. } \rho_{\text{ml,ml}} = (\frac{\theta_{\text{ant}}}{\pi})^2 \\ G_{\text{ml}}G_{\text{sl}} & \text{w.p. } \rho_{\text{ml,sl}} = 2\frac{\theta_{\text{ant}}}{\pi}\frac{\pi-\theta_{\text{ant}}}{\pi} \\ G_{\text{sl}}G_{\text{sl}} & \text{w.p. } \rho_{\text{sl,sl}} = (\frac{\pi-\theta_{\text{ant}}}{\pi})^2 \end{cases}. \tag{2.2}$$

The typical dipole performs perfect beam alignment and thus has an antenna gain of $G_{\text{ml}}G_{\text{ml}}$. I note that the sectored model is pessimistic with regards to side band power. A typical uniform linear array, for instance, will consist of a main-lobe and many less powerful side-lobes each separated by nulls. The sectored model takes the most powerful side-lobe as the entire side-lobe (i.e. on average, the sectored model provides higher side-lobe power). Other work ignores the side-lobe power [44].

2.3.3 Blockage Model

The signal path can be either unobstructed/LOS or blocked/NLOS, each with a different path-loss exponent. This distinction is supported by

empirical measurements conducted in Austin, Europe, and Manhattan [11, 12, 33, 34]. The measurements conducted by [34] include various vertical heights such as building (e.g. 17m) and closer-to-pedestrian (e.g. 7m). I believe the 7m measurements to be applicable to ad hoc networks. The measurements of [34], at 28, 38, 60, and 73GHz, show the path-loss difference of LOS/NLOS. Additionally, a European consortium, Miweba, has also conducted peer-to-peer urban canyon measurements made similar conclusions [33]. One reason for larger difference in LOS/ NLOS path losses is that diffraction becomes weaker in mmWave, as the carrier frequency goes high [33]. Besides, the Fresnel zone, whose size is proportional to the square of the wavelength, becomes smaller at mmWave. Therefore, the mmWave signals will be less likely affected by objects in the LOS links, and transmit as in free space [33]. The work of [37] assumes no particular architecture for the 2-dimensional stochastic geometry derivation. The work captures the distribution and placement of buildings with potential applications to cellular networks and ad hoc networks.

The blockages are modeled as another Poisson point process of buildings independent of the communication network. Each point of the building PPP is independently marked with a random width, length, and orientation. Under such a scenario, it was shown that by using a random shape model of buildings to model blockage [37, 45], the probability that a communication link of outdoor users is LOS is $\mathbb{P}[\text{LOS}] = e^{-\beta d}$,where d is the link length and

$$\beta = \frac{2\lambda_{\text{b}}(\mathbb{E}[W] + \mathbb{E}[L])}{\pi}, \tag{2.3}$$

with λ_{b} as the building PPP density, $\mathbb{E}[W]$ and $\mathbb{E}[L]$ are the average width and length, respectively, of the buildings. I note that the work of [37] includes a parameter to capture the setting where transmitters are indoors, but this is not required in the model as I analyze outdoor networks and therefore condition on outdoor transmitters. A different analysis would be required for indoor networks. This is reasonable because because mmWave signals are heavily attenuated by many common building materials [12]. For example, brick exhibits losses of 30dB at 28 GHz. While the leakage of indoor mmWave signals might be possible through open windows, I ignore the potential interference from indoors and focus solely on the outdoor setting.

The path-loss exponent on each interfering link is a discrete random variable described by

$$\alpha_i = \begin{cases} \alpha_{\mathrm{L}} & \text{w.p. } p(x) \\ \alpha_{\mathrm{N}} & \text{w.p. } 1 - p(x) \end{cases}, \tag{2.4}$$

where α_{L} and α_{N} are the LOS and NLOS path-loss exponents and $p(x)$ is the probability a link of length x is LOS. Fig. 2.2 shows an example realization of the ad hoc network. The density and mean building size are modeled to match The University of Texas at Austin [37]. I ignore correlations between blockages, as in [37]; the blockage on each link is determined independently. While the correlations might affect the tail behavior of the SINR distribution [46], it was shown that the difference in the practical operating SINR range is small when ignoring the correlation [45]. Moreover, simulations that use real geographical data [39, 47] match analytic expressions ignoring blockage correlation.

2.3.4 SINR

To help with the analytic tractability, I model the fading as a Nakagami random variable with parameter N_{h}. Consequently, the received signal power, h, can be modeled as a gamma random variable, $h \sim \Gamma(N_{\mathrm{h}}, 1/N_{\mathrm{h}})$. As $N_{\mathrm{h}} \to \infty$, the fading becomes a deterministic value centered on the mean, whereas $N_{\mathrm{h}} = 1$ corresponds to Rayleigh fading.

The SINR is the basis of the performance metrics in this chapter. P_{t} is the transmit power of each dipole, κ_o is the antenna gain corresponding to both main beams aligned, h_o is the fading power at the dipole of interest, A_{m} is the path-loss intercept, r_o is the fixed dipole link length, α_o is the path-loss exponent, and N_o^{m} is the noise power. The interference term for each interfering dipole transmitter is indexed with i: d_i is used to represent the distance from the interferer to receiver of interest, h_i is each interference fading power distributed IID according to a gamma distribution, and κ_i is the discrete random antenna gain distributed IID according to (2.2). The SINR is defined as [35]

$$\mathrm{SINR} = \frac{P_{\mathrm{t}}\kappa_o h_o A_{\mathrm{m}} r_o^{-\alpha_o}}{N_o^{\mathrm{m}} + \sum_{i\in\Phi} P_{\mathrm{t}}\kappa_i h_i A_{\mathrm{m}} d_i^{-\alpha_i}}. \tag{2.5}$$

2.4 One-Way Ad Hoc Communication

In this section, I derive the SINR distribution for one-way transmission in the ad hoc network described in Section 2.3. I first characterize the *overall* SINR complimentary cumulative distribution function (CCDF) by analyzing

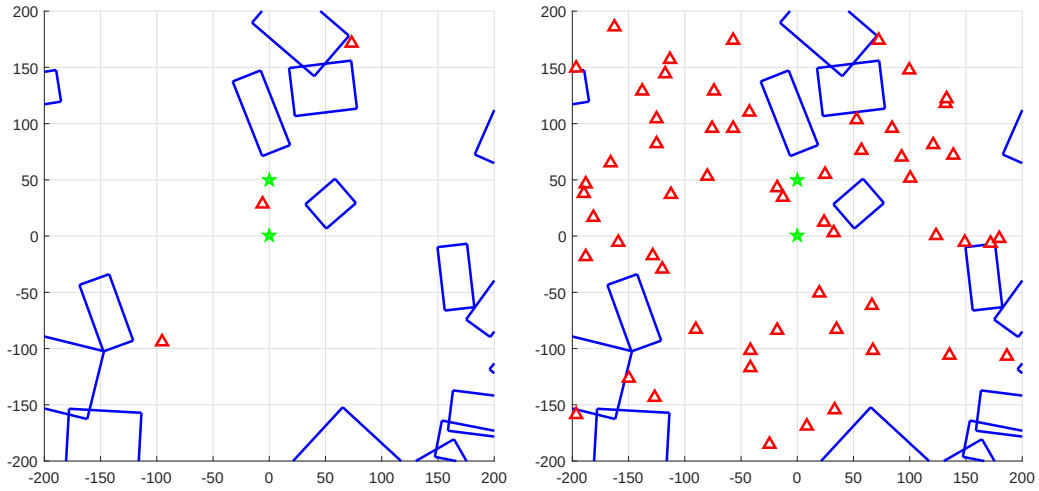

Figure 2.2: Example realizations of the random network with blockage. The blue rectangles are random boolean buildings which attenuate the signal. The red triangles are the Poisson point process of interferers. The green star represents the *typical node*. The user densities are what I call *sparse* (a) and *dense* (b) when discussing the results.

the network when the desired link is either LOS and NLOS. Next, I define the *protocol-gain* by limiting communication to LOS links and argue why this is a useful concept. I quantify the effect of random receiver distance. I show that neglecting noise and NLOS interference does not change the SINR distribution, suggesting that mmWave ad hoc networks are *LOS interference limited* in dense networks. This is reinforced by the derivation of the INR cumulative distribution function CDF. Lastly, the performance metrics, transmission capacity and area spectral efficiency, are computed using a bound of the SINR CCDF.

2.4.1 SINR Distribution

I define the CCDF of the SINR as

$$P_{\mathrm{c}}(\Gamma) = \mathbb{P}[\mathrm{SINR} \geq \Gamma], \tag{2.6}$$

where Γ is target SINR. In other work, (2.6) is referred to as the *coverage probability* [16, 20, 35]. I can use the law of total probability to expand the SINR CCDF as [1]

$$P_{\mathrm{c}}(\Gamma) = P_{\mathrm{c}}^{\mathrm{L}}(\Gamma)\mathbb{P}[\mathrm{LOS}] + P_{\mathrm{c}}^{\mathrm{N}}(\Gamma)\mathbb{P}[\mathrm{NLOS}], \tag{2.7}$$

where $P_{\mathrm{c}}^{\mathrm{L}}$ and $P_{\mathrm{c}}^{\mathrm{N}}$ are the conditional CCDFs on the event that the main link is LOS and NLOS, respectively. The SINR CCDF conditioned on the link being LOS is [1]

$$P_{\mathrm{c}}^{\mathrm{L}}(\Gamma) = \mathbb{P}[\mathrm{SINR} \geq \Gamma | \mathrm{LOS}]. \tag{2.8}$$

Going forward, for brevity, I will drop the conditional notation when using P_c^{L}. Using (2.5),

$$P_{\mathrm{c}}^{\mathrm{L}}(\Gamma) = \mathbb{P}\left[\frac{P_{\mathrm{t}}\kappa_o h_o A_{\mathrm{m}} r_o^{-\alpha_{\mathrm{L}}}}{N_o^{\mathrm{m}} + \sum_{i\in\Phi} P_{\mathrm{t}}\kappa_i h_i A_{\mathrm{m}} d_i^{-\alpha_i}} \geq \Gamma\right] \tag{2.9}$$

$$= \mathbb{P}\left[h_o \geq \frac{\Gamma r_o^{\alpha_{\mathrm{L}}}}{P_{\mathrm{t}}\kappa_o A_{\mathrm{m}}}\left(N_o^{\mathrm{m}} + \sum_{i\in\Phi}\frac{P_{\mathrm{t}}\kappa_i h_i A_{\mathrm{m}}}{d_i^{\alpha_i}}\right)\right] \tag{2.10}$$

$$= \mathbb{P}\left[h_o \geq \frac{\Gamma r_o^{\alpha_{\mathrm{L}}}}{P_{\mathrm{t}}\kappa_o A_{\mathrm{m}}}(N_o^{\mathrm{m}} + I_\Phi)\right] \tag{2.11}$$

$$= 1 - \mathbb{P}\left[h_o < \frac{\Gamma r_o^{\alpha_{\mathrm{L}}}}{P_{\mathrm{t}}\kappa_o A_{\mathrm{m}}}(N_o^{\mathrm{m}} + I_\Phi)\right] \tag{2.12}$$

$$= 1 - \int_0^\infty \mathbb{P}\left[h_o < \frac{\Gamma r_o^{\alpha_{\mathrm{L}}}}{P_{\mathrm{t}}\kappa_o A_{\mathrm{m}}}(N_o^{\mathrm{m}} + x)|I_\Phi = x\right] p_\Phi(x)dx, \tag{2.13}$$

where I_Φ is the aggregate interference due to the PPP and p_Φ is the probability distribution function of the PPP. I introduce the following Lemma to aid the analysis.

Lemma 2.4.1. *The cumulative distribution function of a normalized gamma random variable with integer parameter k, $y \sim \Gamma(k, 1/k)$, can be tightly lower bounded as*

$$\left[1 - e^{-az}\right]^k < \mathbb{P}\left[y < z\right]$$

with $a = k(k!)^{-1/k}$.

Proof. See Appendix 2.8.1. □

Now I can bound (2.13) as

$$P_{\mathrm{c}}^{\mathrm{L}}(\Gamma) < 1 - \int_0^\infty \left[\left(1 - e^{-a \frac{\Gamma r_o^{\alpha_{\mathrm{L}}}}{P_{\mathrm{t}} \kappa_o A_{\mathrm{m}}} (N_o^{\mathrm{m}} + x)} \right)^{N_{\mathrm{h}}} \right] p_\Phi(x) dx \tag{2.14}$$

$$= 1 - \mathbb{E}_\Phi \left[\left(1 - e^{-a \frac{\Gamma r_o^{\alpha_{\mathrm{L}}}}{P_{\mathrm{t}} \kappa_o A_{\mathrm{m}}} (N_o^{\mathrm{m}} + I_\Phi)} \right)^{N_{\mathrm{h}}} \right] \tag{2.15}$$

$$= \sum_{n=1}^{N_{\mathrm{h}}} \binom{N_{\mathrm{h}}}{n} (-1)^{n+1} \mathbb{E}_\Phi \left[e^{-an \frac{\Gamma r_o^{\alpha_{\mathrm{L}}}}{P_{\mathrm{t}} \kappa_o A_{\mathrm{m}}} (N_o^{\mathrm{m}} + I_\Phi)} \right], \tag{2.16}$$

where (2.16) is from the Binomial Theorem [1].

Because the correlation between each random blockage is ignored, each point in the building blockage PPP is independent which permits the use of the thinning theorem from stochastic geometry [21]. I further thin Φ based on the random antenna gain. Essentially, I can now view the interference as 6 independent PPPs such that

$$I_\Phi = I_{\Phi_{\mathrm{LOS}}}^{G_{\mathrm{ml}} G_{\mathrm{ml}}} + I_{\Phi_{\mathrm{LOS}}}^{G_{\mathrm{ml}} G_{\mathrm{sl}}} + I_{\Phi_{\mathrm{LOS}}}^{G_{\mathrm{sl}} G_{\mathrm{sl}}} + I_{\Phi_{\mathrm{NLOS}}}^{G_{\mathrm{ml}} G_{\mathrm{ml}}} + I_{\Phi_{\mathrm{NLOS}}}^{G_{\mathrm{ml}} G_{\mathrm{sl}}} + I_{\Phi_{\mathrm{NLOS}}}^{G_{\mathrm{sl}} G_{\mathrm{sl}}}, \tag{2.17}$$

with the superscripts representing the discrete random antenna gain defined in (2.2) and each interfering node either a LOS transmitter or NLOS transmitter. I can distribute the expectation in (2.16) as

$$P_{\mathrm{c}}^{\mathrm{L}} < \sum_{n=1}^{N_{\mathrm{h}}} (-1)^{n+1} \binom{N_{\mathrm{h}}}{n} e^{-nK_{\mathrm{L}} \Gamma N_o^{\mathrm{m}}} \prod_i \prod_j \mathbb{E}_{I_{\Phi_j^i}} \left[e^{-nK_{\mathrm{L}} \Gamma I_{\Phi_j^i}} \right] \tag{2.18}$$

with $i \in \{(\mathrm{ml}, \mathrm{ml}), (\mathrm{ml}, \mathrm{sl}), (\mathrm{sl}, \mathrm{sl})\}$, $j \in \{\mathrm{LOS}, \mathrm{NLOS}\}$, and $K_{\mathrm{L}} = \frac{a r_o^{\alpha_{\mathrm{L}}}}{P_{\mathrm{t}} \kappa_o A_{\mathrm{m}}}$. In (2.18), i and j index each interference sub-PPP. In essence, each expectation is the Laplace transform of the associated sub-PPP, and each of these Laplace transforms are multiplied together.

Using stochastic geometry, I can analytically represent the first Laplace expectation term as

$$\mathbb{E}\left[e^{-nK_{\mathrm{L}}\Gamma I_{\Phi_{\mathrm{LOS}}}^{G_{\mathrm{ml}}G_{\mathrm{ml}}}}\right] = e^{-2\pi\lambda p_{\mathrm{GG}}\int_0^\infty\left(1-\mathbb{E}_h\left[e^{-\frac{nK_{\mathrm{L}}\Gamma P_{\mathrm{t}}A_{\mathrm{m}}GGh}{x^{\alpha_{\mathrm{L}}}}}\right]\right)p(x)x\mathrm{d}x}, \tag{2.19}$$

where $\rho_{G_{\mathrm{ml}}G_{\mathrm{ml}}}$ and $p(x)$, capture the thinning of the PPP for the first sub-PPP in (2.17). Notice that $\mathbb{E}_h[e^{\eta h}]$ corresponds to the moment-generating function (MGF) of the random variable h (e.g. gamma). A similar approach was taken in [1] for the analysis of mmWave cellular networks. The final Laplace transform of the PPP is given as

$$\mathcal{L}_{I_{\Phi_{\mathrm{LOS}}}^{G_{\mathrm{ml}}G_{\mathrm{ml}}}} = e^{-2\pi\lambda\rho_{G_{\mathrm{ml}}G_{\mathrm{ml}}}\int_0^\infty\left(1-1/(1+\frac{nQ_{\mathrm{L}}\Gamma}{x^{\alpha_{\mathrm{L}}}N_{\mathrm{h}}})^{N_{\mathrm{h}}}\right)p(x)x\mathrm{d}x}. \tag{2.20}$$

with $Q_{\mathrm{L}} = K_{\mathrm{L}}P_{\mathrm{t}}G_{\mathrm{ml}}G_{\mathrm{ml}}A_{\mathrm{m}} = \frac{ar_o^{\alpha_{\mathrm{L}}}G_{\mathrm{ml}}G_{\mathrm{ml}}}{\kappa_o}$. Each other Laplace transform is computed similarly, but noting that $\rho_{G_{\mathrm{ml}}G_{\mathrm{ml}}}$, $p(x)$, and $x^{\alpha_{\mathrm{L}}}$ will change depending on the antenna gain of the sub-PPP and if the sub-PPP is LOS or NLOS. I can summarize the results in the following theorem

Theorem 2.4.1. *The SINR distribution of an outdoor mmWave ad hoc network can be tightly upper bounded by*

$$\begin{aligned} P_{\mathrm{c}}(\Gamma) < &\sum_{n=1}^{N_{\mathrm{h}}}\binom{N_{\mathrm{h}}}{n}(-1)^{n+1}e^{-nK_{\mathrm{L}}\Gamma N_o^{\mathrm{m}}}e^{-2\pi\lambda(\omega_{\mathrm{L}}+\omega_{\mathrm{N}})}p(r) \\ &+\sum_{n=1}^{N_{\mathrm{h}}}\binom{N_{\mathrm{h}}}{n}(-1)^{n+1}e^{-nK_{\mathrm{N}}\Gamma N_o^{\mathrm{m}}}e^{-2\pi\lambda(\xi_{\mathrm{L}}+\xi_{\mathrm{N}})}\Big(1-p(r)\Big) \end{aligned} \tag{2.21}$$

where

$$\omega_{\mathrm{L}} = \sum_i \rho_i \int_0^\infty \left[1 - 1/\left(1 + \frac{nQ_{\mathrm{L}}\Gamma}{x^{\alpha_{\mathrm{L}}} N_{\mathrm{h}}}\right)^{N_{\mathrm{h}}}\right] p(x) x \mathrm{d}x \tag{2.22}$$

$$\omega_{\mathrm{N}} = \sum_i \rho_i \int_0^\infty \left[1 - 1/\left(1 + \frac{nQ_{\mathrm{L}}\Gamma}{x^{\alpha_{\mathrm{L}}} N_{\mathrm{h}}}\right)^{N_{\mathrm{h}}}\right] \big(1 - p(x)\big) x \mathrm{d}x \tag{2.23}$$

$$\xi_{\mathrm{L}} = \sum_i \rho_i \int_0^\infty \left[1 - 1/\left(1 + \frac{nQ_{\mathrm{N}}\Gamma}{x^{\alpha_{\mathrm{N}}} N_{\mathrm{h}}}\right)^{N_{\mathrm{h}}}\right] p(x) x \mathrm{d}x \tag{2.24}$$

$$\xi_{\mathrm{N}} = \sum_i \rho_i \int_0^\infty \left[1 - 1/\left(1 + \frac{nQ_{\mathrm{N}}\Gamma}{x^{\alpha_{\mathrm{N}}} N_{\mathrm{h}}}\right)^{N_{\mathrm{h}}}\right] \big(1 - p(x)\big) x \mathrm{d}x \tag{2.25}$$

with $K_{\mathrm{L}} = \frac{a r_o^{\alpha_{\mathrm{L}}}}{P_{\mathrm{t}} \kappa_o A_{\mathrm{m}}}$, $K_{\mathrm{N}} = \frac{a r_o^{\alpha_{\mathrm{N}}}}{P_{\mathrm{t}} \kappa_o A_{\mathrm{m}}}$, $i \in \{(\mathrm{ml}, \mathrm{ml}), (\mathrm{ml}, \mathrm{sl}), (\mathrm{sl}, \mathrm{sl})\}$, $Q_{\mathrm{L}} = \frac{a r_o^{\alpha_{\mathrm{L}}} \kappa_i}{\kappa_o}$, *and* $Q_{\mathrm{N}} = \frac{a r_o^{\alpha_{\mathrm{N}}} \kappa_i}{\kappa_o}$.

Proof. Substituting each Laplace transform (2.20) into (2.18) for the conditional $P_{\mathrm{c}}^{\mathrm{L}}$ yields the first summation in Theorem 2.4.1. The same process is done for the Laplace transforms corresponding to $P_{\mathrm{c}}^{\mathrm{N}}$. These summations are then multiplied by $\mathbb{P}[\mathrm{LOS}]$ and $\mathbb{P}[\mathrm{NLOS}]$, respectively, to give the full CCDF of (2.7). □

In Theorem 2.4.1, ω_{L} and ω_{N} correspond to the LOS and NLOS interference, respectively, when the desired signal is LOS while ξ_{L} and ξ_{N} correspond to the LOS and NLOS interference, respectively, when the desired signal is NLOS. While Theorem 2.4.1 may appear unwieldy, the decomposition of the terms illustrates the insight that can be gained from the Theorem. In the first summation, there are exponential terms that correspond to noise, LOS interference (i.e. ω_{L}), and NLOS interference (i.e. ω_{N}). Further, both ω_{L} and

Parameter	Value
λ	5×10^{-5}, 5×10^{-4} (m^{-2})
r	25, 50, 75 (m)
β, α_{LOS}, α_{NLOS}	0.008, 2, 4
N_o^{m}	-117 dB
h_i, N_{h}	Gamma, 7
θ_{ant}, G_{ml}, G_{sl}	$\frac{\pi}{6}$, 10, 0.1
P_{t}	1W (30dBm)

Table 2.2: Parameters of results.

ω_{N} (and similarly ξ_{L} and ξ_{N}) can be decomposed based on each antenna gain. It is possible to compare relative contributions to the total SINR CCDF. For example, by computing ω_{N}, I was able to see that $\omega_{\text{L}} \gg \omega_{\text{N}}$ for many different system parameters of interest. Therefore, $e^{-2\pi\lambda(\omega_{\text{L}}+\omega_{\text{N}})} \approx e^{-2\pi\lambda\omega_{\text{L}}}$ which means NLOS interference has relatively no effect on the SINR distribution. I use this insight in Section 2.4.5 to conclude that mmWave ad hoc networks are *LOS interference limited*.

2.4.2 Validation of the Model

Before proceeding, I verify the tightness of the bound in Theorem 2.4.1. Table 2.2 shows the values used throughout the section. The parameters of (2.7) are simulated through Monte Carlo, while Theorem 2.4.1 is used for the analytic model. For the simulation, a PPP was generated over an area of 4km^2. The building model of [48] is used to generate the building blockage for the simulation. This includes correlation between the points. An underlying building density of $\lambda_{\text{b}} = 9.3 \times 10^{-5}$ is used with a expected width and length

of the buildings as $\mathbb{E}[L] = 64$ and $\mathbb{E}[W] = 70$. This yields $\beta = 0.008$. The thermal noise power of 500MHz bandwidth at room temperature is -117dB. I used $N_{\mathrm{h}} = 3$ when computing the analytic expressions. I chose $N_{\mathrm{h}} = 3$ because measurement campaigns have shown that small-scale fading is more deterministic at mmWave [34]. In the measurements of [12, 49], small-scale fading is not very significant. Because of the directional antennas and sparse channel characteristics, the uniform scattering assumption for Rayleigh fading is not valid at mmWave frequencies. I chose a 30° beamwidth. Additionally, 10dB gain corresponds to the theoretical gain of a 10 element uniform linear array unit gain antennas.

Fig. 2.3a compares the analytic SINR distribution with the empirical given a $\lambda = 5 \times 10^{-5}\mathrm{m}^{-2}$ or an average of 50 users/km^2. This can be attributed to the directional antennas limiting the interference seen by the typical node. The analytic expression in Theorem 2.4.1 of the mmWave ad hoc network matches extremely well to the simulations. For all three link lengths, the SINR of the users is greater than 0dB a majority of the time.

Fig. 2.3b compares the SINR distribution results for a much denser network, $\lambda = 5 \times 10^{-4}\mathrm{m}^{-2}$ which corresponds to an average of 500 users/km^2. Again, Theorem 2.4.1 matches the simulation well. For the larger link distances, I see bi-modal behavior of the CCDF with the plateaus around -10dB.

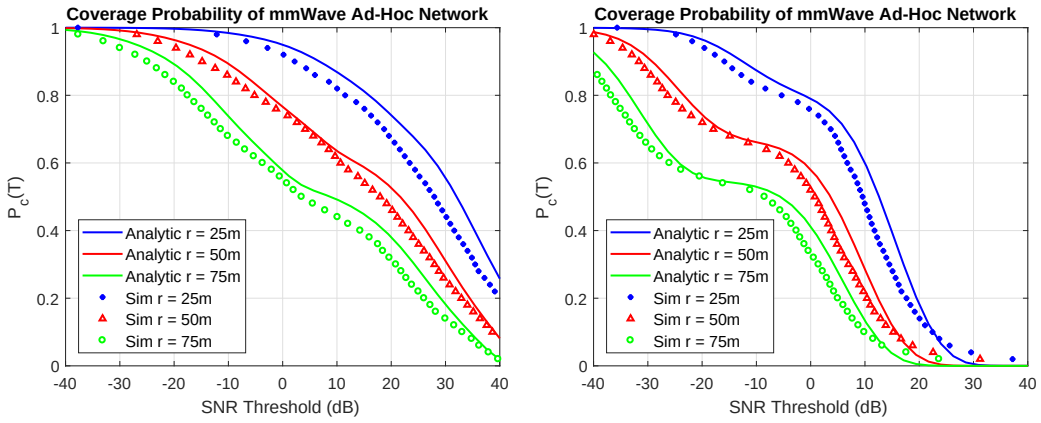

(a) (b)

Figure 2.3: The SINR distribution of mmWave ad hoc networks with $\lambda = 5 \times 10^{-5}$ (a) and $\lambda = 5 \times 10^{-4}$ (b).

2.4.3 LOS Protocol-Gain

In this section, I define and discuss the *LOS protocol-gain*. I can view $P_{\mathrm{c}}(\Gamma)$ as a mixture of $P_{\mathrm{c}}^{\mathrm{L}}(\Gamma)$ and $P_{\mathrm{c}}^{\mathrm{N}}(\Gamma)$. In Fig. 2.3b, the interference causes most of the density of $P_{\mathrm{c}}^{\mathrm{N}}(\Gamma)$ to shift to very low SINR. The plateaus in the CCDF of Fig. 2.3b illustrate this separation. Unless the SINR threshold is very low (e.g. below -20dB), these links will not be able to communicate without LOS communication. This motivates the need for a protocol to ensure LOS communication (e.g. using a LOS relay to multi-hop around a building). If LOS communication is assumed, the SINR distribution in the LOS regime will be equal to $P_{\mathrm{c}}^{\mathrm{L}}(\Gamma)$ (i.e. set $\mathbb{P}[\mathrm{LOS}] = 1$). With many users nearby, the network will have multiple users that could potentially be a LOS receiver.

Fig. 2.4 shows the SINR distribution of a mmWave ad hoc network if the desired link is LOS. The improvement is quite large. The 90% coverage

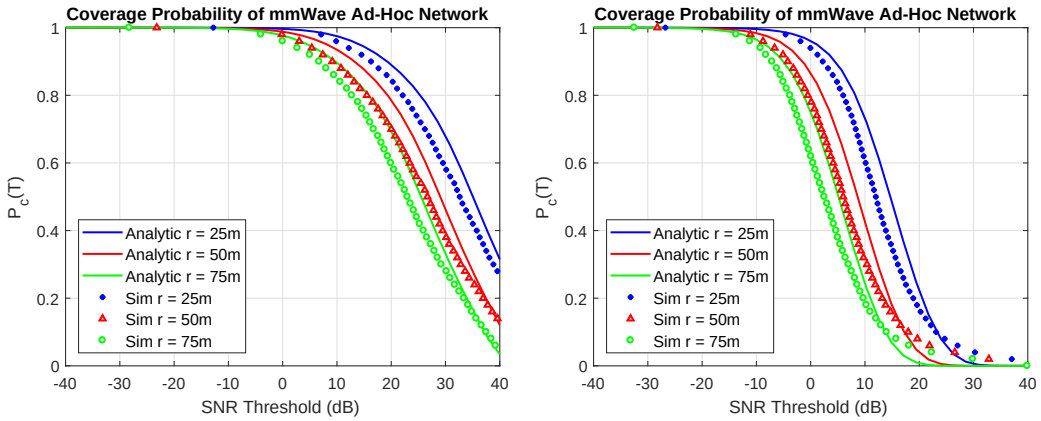

(a) (b)

Figure 2.4: The SINR distribution of mmWave ad hoc networks with $\lambda = 5 \times 10^{-5}$ (a) and $\lambda = 5 \times 10^{-4}$ (b). If the desired link is LOS, significant improvement to the SINR distribution is realized. I term this the *LOS protocol-gain*.

point in Fig. 2.4a is improved by 10dB for 25m, 20dB for 50m, and 30dB for 75m, compared to the same network in 2.3a. The improvement in Fig. 2.4b is even more drastic. For the 25m link, 20dB improvement is seen. This knowledge should influence MAC design, which is why I call it *protocol-gain*.

2.4.4 Distributions of r

One of the limitations of the dipole model is the fixed length of the communication link. This model is used for its analytic tractability but is not a realistic expectation. In a D2D gaming scenario, for example, the distance between the receiver and transmitter will vary as the two users walk around. To quantify this, I can integrate Theorem 2.4.1 against a receiver location density function. The SINR distribution accounting for different receiver geometries

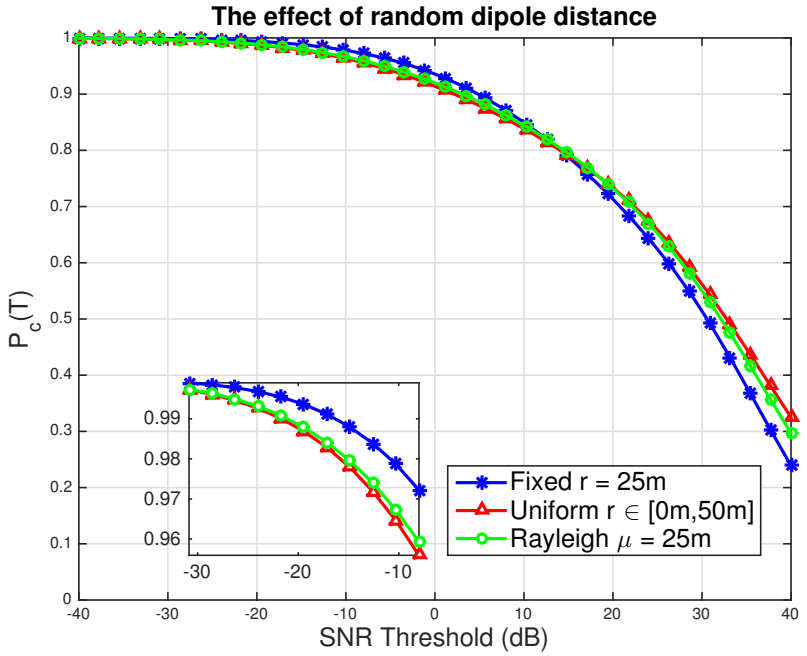

Figure 2.5: The effect of receiver distribution is quantified for the overall (LOS/NLOS) SINR distribution (a) and LOS-only SINR distribution (b). Each link, on average, is 25m.

is

$$P_{\mathrm{c}}^{r}(\Gamma) = \int_{S} P_{\mathrm{c}}(r,\Gamma) f_R(r) dr \tag{2.26}$$

where S is the support of the location density distribution and f_R is the density and $P_{\mathrm{c}}(r,\Gamma)$ is Theorem 2.4.1, but I allow varying receiver distances. I compare two different distributions against the fixed dipole assumption.

As shown in Fig. 2.5, I use two receiver geometries to compare against, the uniform and Rayleigh [18]. For larger SINR thresholds, including a random receiver distance improves performance. This is due to the positive effect of having the receiver closer some of the time. As shown in Fig. 2.3, communi-

cation when NLOS generally has poor SINR. The random shorter link means LOS communication is more likely. Conversely, the random receiver locations hurt performance for lower SINR thresholds. If assuming random receiver locations, both distributions give similar results despite the Rayleigh distribution having unbounded support. Surprisingly, the results indicate that simply knowing the mean of the distribution captures much of the SINR distribution.

2.4.5 LOS Interference Limited Networks

Interference is a key design limitation for ad hoc networks. Cellular network analysis has shown that mmWave cellular networks can be modeled as noise-limited with inter-site-distances of 200m [1, 12, 38, 39]. This network topology, however, is different from an ad hoc network as cellular users associate with a fixed base station. I now characterize the transition from noise-limited to interference-limited operation as a function of user density, building density, antenna pattern, and transmission distance. I achieve this by using the interference-to-noise ratio (INR) cumulative distribution function (CDF)

$$P^{\mathrm{NL}}(\Gamma) = \mathbb{P}[\mathrm{INR} \leq \Gamma]. \tag{2.27}$$

I leave the threshold value up to system designers to determine what value of Γ is appropriate for defining noise limited. A natural choice may be 1 (0dB)

or 10 (10dB). The INR CDF can be written as

$$
\begin{aligned}
P^{\mathrm{NL}}(\Gamma) &= \mathbb{P}\left[\frac{\sum_{\mathrm{i}\in\Phi} P_{\mathrm{t}}\kappa_{\mathrm{i}}h_{\mathrm{i}}A_{\mathrm{m}}r_{\mathrm{i}}^{-\alpha_{\mathrm{i}}}}{N_o^{\mathrm{m}}} \leq \Gamma\right] && (2.28)\\
&= \mathbb{P}\left[1 \geq \frac{\sum_{\mathrm{i}\in\Phi} P_{\mathrm{t}}\kappa_{\mathrm{i}}h_{\mathrm{i}}A_{\mathrm{m}}r_{\mathrm{i}}^{-\alpha_{\mathrm{i}}}}{\Gamma N_o^{\mathrm{m}}}\right] && (2.29)\\
&= \mathbb{P}\left[1 \geq \frac{I_\Phi}{\Gamma N_o^{\mathrm{m}}}\right] && (2.30)\\
&= 1 - \mathbb{P}\left[1 < \frac{I_\Phi}{\Gamma N_o^{\mathrm{m}}}\right]. && (2.31)
\end{aligned}
$$

To analytically evaluate $\mathbb{P}\left[1 < \frac{I_\Phi}{\Gamma N_0}\right]$, I replace 1 with a random variable, C, with low variance. I let $C \sim \Gamma(N_{\mathrm{C}}, 1/N_{\mathrm{C}})$. If I examine the probability density function (PDF) of C,

$$
f_C(x) = \frac{N_{\mathrm{C}}^{N_{\mathrm{C}}} x^{N_{\mathrm{C}}-1} e^{-N_{\mathrm{C}}x}}{\Gamma(N_{\mathrm{C}})}, \tag{2.32}
$$

the $\lim_{N_{\mathrm{C}}\to\infty} f_C(x) = \delta(x-1)$. Further, I leverage Lemma 2.4.1 again. The INR distribution can then be bounded as

$$
\begin{aligned}
P^{\mathrm{NL}} &= 1 - \mathbb{P}\left[C < \frac{I_\Phi}{\Gamma N_0}\right] && (2.33)\\
&< 1 - \mathbb{E}_\Phi\left[\left(1 - e^{-a\frac{I_\Phi}{\Gamma N_o^{\mathrm{m}}}}\right)^{N_{\mathrm{C}}}\right] && (2.34)\\
&= \sum_{n=1}^{N_{\mathrm{C}}} \binom{N_{\mathrm{C}}}{n} (-1)^{n+1} \mathbb{E}_\Phi\left[e^{-an\frac{I_\Phi}{\Gamma N_o^{\mathrm{m}}}}\right], && (2.35)
\end{aligned}
$$

where (2.34) is from the law of total probability and gamma CDF approximation while (2.35) is from the Binomial Theorem. The transmitters, again, are six independent PPPs as explained in (2.17). Because each sub-process is independent, I re-write (2.35) as a product of expectations. The analytic expression of the first Laplace expectation term is

$$\mathbb{E}\left[e^{-\frac{an}{N_o^{\mathrm{m}}\Gamma}I_{\Phi_{\mathrm{LOS}}}^{G_{\mathrm{ml}}G_{\mathrm{ml}}}}\right] = e^{-2\pi\lambda\rho_{G_{\mathrm{ml}}G_{\mathrm{ml}}}\int_0^\infty\left(1-\mathbb{E}_h\left[e^{-\frac{anP_{\mathrm{t}}A_{\mathrm{m}}G_{\mathrm{ml}}G_{\mathrm{ml}}h}{x^\alpha N_o^{\mathrm{m}}\Gamma}}\right]\right)p(x)x\mathrm{d}x}. \tag{2.36}$$

I invoke the MGF of a gamma random variable to yield the final Laplace transform of the PPP as

$$\mathcal{L}_{I_{\Phi_{\mathrm{LOS}}}^{G_{\mathrm{ml}}G_{\mathrm{ml}}}} = e^{-2\pi\lambda\rho_{G_{\mathrm{ml}}G_{\mathrm{ml}}}\int_0^\infty\left(1-1/(1+\frac{anP_{\mathrm{t}}A_{\mathrm{m}}G_{\mathrm{ml}}G_{\mathrm{ml}}}{x^\alpha N_o^{\mathrm{m}}\Gamma N_{\mathrm{h}}})^{N_{\mathrm{h}}}\right)p(x)x\mathrm{d}x}. \tag{2.37}$$

Each other Laplace transform is computed similarly but $\rho_{G_{\mathrm{ml}}G_{\mathrm{ml}}}$ will correspond to the probability of the antenna gain $\{(\mathrm{ml},\mathrm{ml}),(\mathrm{ml},\mathrm{sl}),(\mathrm{sl},\mathrm{sl})\}$ and the NLOS probability is $1-p_{\mathrm{LOS}}$. I summarize the results in the following theorem.

Theorem 2.4.2. *The INR distribution of a mmWave ad hoc network can be tightly bounded by*

$$P^{\mathrm{NL}}(\Gamma) < \sum_{n=1}^{N_{\mathrm{C}}}\binom{N_{\mathrm{C}}}{n}(-1)^{n+1}e^{-2\pi\lambda(\upsilon_{\mathrm{L}}+\upsilon_{\mathrm{N}})} \tag{2.38}$$

where

$$\upsilon_{\mathrm{L}} = \sum_i \rho_i\int_0^\infty\left(1-1/\big(1+\frac{anP_{\mathrm{t}}A_{\mathrm{m}}\kappa_i}{x_{\mathrm{L}}^\alpha N_o^{\mathrm{m}}\Gamma N_{\mathrm{h}}}\big)^{N_{\mathrm{h}}}\right)p(x)x\mathrm{d}x \tag{2.39}$$

$$\upsilon_{\mathrm{N}} = \sum_i \rho_i\int_0^\infty\left(1-1/\big(1+\frac{anP_{\mathrm{t}}A_{\mathrm{m}}\kappa_i}{x_{\mathrm{N}}^\alpha N_o^{\mathrm{m}}\Gamma N_{\mathrm{h}}}\big)^{N_{\mathrm{h}}}\right)\big(1-p(x)\big)x\mathrm{d}x \tag{2.40}$$

with $i\in\{(\mathrm{ml},\mathrm{ml}),(\mathrm{ml},\mathrm{sl}),(\mathrm{sl},\mathrm{sl})\}$.

Proof. Substituting the Laplace transform (2.37) into (2.35) yields the result. □

While I focus on investigating the impact of the node density and beamwidth of directional beamforming in this chapter, the INR distribution also depends on other system parameters, such as transmission power. It should be noted that the INR in (2.27) scales with the transmit power; interesting future work is discovering a transmission power control scheme to optimize the INR. Such a scheme could limit the transmit power based on the proximity of the nearest interferer.

2.4.6 One-Way Performance Analysis

Now, using Theorem 2.4.1, I characterize the transmission capacity, λ_ϵ. This is the largest λ the network can support given an SINR threshold, Γ and outage ϵ. More simply, $1-\epsilon = P_{\mathrm{c}}(\Gamma)$ of users will have an SINR larger than Γ. The transmission capacity can also be defined as the number of successful transmissions per unit area, which is directly connected to the number of users supported by the network. To do this, I approximate the exponential terms of Theorem 2.4.1 as

$$P_{\mathrm{c}}^{\mathrm{L}} < \sum_{n=1}^{N_{\mathrm{h}}} (-1)^{n+1} \binom{N_{\mathrm{h}}}{n} e^{-nK_{\mathrm{L}}\Gamma N_o^{\mathrm{m}}} \left(1 - 2\pi\lambda_\epsilon \Theta + 2\pi\lambda_\epsilon^2 \Theta^2\right) \tag{2.41}$$

where $\Theta = \omega_{\mathrm{L}} + \omega_{\mathrm{N}}$. I leverage the bound, $e^{-x} \leq (1 - x + x^2/2)$ for $x \in \mathbb{R}^+$, for the Laplace functional term. This bound is tight for small x. I am interested in analyzing the optimal λ for P_{c} near 1. As a result, the Laplace functional will be close to 1; the argument will be close to 0. A similar bound is done for the NLOS term in Theorem 2.4.1. I combine (2.41) and the NLOS approximation

to form

$$1-\epsilon < \sum_{n=1}^{N_{\mathrm{h}}} (-1)^{n+1} \binom{N_{\mathrm{h}}}{n} e^{-nK_{\mathrm{L}}\Gamma N_o^{\mathrm{m}}} \times \left(1 - 2\pi\lambda_\epsilon\Theta + 2\pi\lambda_\epsilon^2\Theta^2\right) + \sum_{n=1}^{N_{\mathrm{h}}} (-1)^{n+1} \binom{N_{\mathrm{h}}}{n} \times e^{-nK_{\mathrm{N}}\Gamma N_o^{\mathrm{m}}} \left(1 - 2\pi\lambda_\epsilon\Psi + 2\pi\lambda_\epsilon^2\Psi^2\right) \tag{2.42}$$

with $\Psi = \xi_{\mathrm{L}} + \xi_{\mathrm{N}}$. Because of this bound, P_{c} is now a quadratic equation in λ which can be solved in closed-form. The exact solution depends on N_{h}. Symbolic tools, such as *Mathematica*, can factor and solve (2.42) such that

$$\lambda_\epsilon = f(\Gamma, \epsilon). \tag{2.43}$$

Area spectral efficiency is a useful metric because it can characterize the network performance, rather than just a single link, as SINR does [28]. I define area spectral efficiency as

$$\mathrm{ASE} := \underbrace{\lambda_\epsilon}_{\frac{\text{users}}{\text{area}}} \underbrace{\log_2(1+\Gamma)}_{\text{efficiency}} \underbrace{(1-\epsilon)}_{\%\text{ofthetime}}. \tag{2.44}$$

Substituting (2.43) into (2.44) yields a function of just Γ and ϵ. The ASE yields a result in terms of bits/sec/Hz/m^2.

2.5 Two-way Ad Hoc Communication

The derivations from the Section 2.4 are for *one-way* communication. There is no consideration for the reverse link (i.e. receiver to transmitter). In real systems, however, successful transmission usually relies on a two-way

communication stack. The two-way transmission capacity quantifies the maximum density of users a network can support while *both* the forward and reverse link are subject to outage constraint, ϵ [27].

The *forward* link is defined as the transmitter to receiver link (i.e. what was discussed in Section 2.4), while the *reverse* link is the receiver to transmitter control link. Frequency division duplexing (FDD) is used between the forward and reverse links, as is done in [27]. Each link operates concurrently with differing rate requirements. Consider the bandwidth from Section 2.4 split among the forward and reverse links. Hence, B_{total} is the bandwidth available to the system. The forward link is allocated B_{F}, while the reverse link is allocated $B_{\text{R}} = B_{\text{total}} - B_{\text{F}}$. The SINR is similarly defined as SINR_{F} and SINR_{R}. Correspondingly, from Shannon's equation, the links achieve rates, R_{F} and R_{R}. A user with rate requirement R_{F} would then have an SINR threshold of $\Gamma_{\text{F}} = 2^{R_{\text{F}}/B_{\text{F}}} - 1$. It should be noted that time division duplexing can similarly be used with the threshold of $\Gamma_{\text{F}} = 2^{\frac{R_{\text{F}}}{\tau_{\text{F}} B_{\text{total}}}} - 1$ with τ_{F} being the fraction of time for the forward link. The reverse link thresholds are similarly defined. I consider only FDD for the remainder of the analysis.

2.5.1 Two-way SINR Analysis

The two-way SINR probability is the probability that the forward link *and* reverse link exceed an SINR threshold. More precisely,

$$P_{\text{c}}^{\text{tw}} = \mathbb{P}[\text{SINR}_{\text{F}} > \Gamma_{\text{F}}, \text{SINR}_{\text{R}} > \Gamma_{\text{R}}]. \tag{2.45}$$

I assume that the forward and reverse link do not have the same SINR threshold because the reverse control link is generally low-rate compared to the forward link. To analyze this probability, I leverage the following definitions and lemma.

Definition 1 [27]: A random variable X defined on $(\Omega, \mathcal{F}, \mathbb{P})$ is increasing if $X(\omega) \leq X(\omega')$ for a partial ordering on ω, ω'. X is decreasing if $-X$ is increasing.

The SINR is a random variable defined on the probability space which is determined by how the interferers are placed on the plane. Let ω be a set of active interferers from the PPP. Then, $\omega' \geq \omega$ if ω' is a superset of ω. The SINR (2.5) decreases if another interferer is added: $\text{SINR}(\omega) \geq \text{SINR}(\omega')$. Therefore, SINR is a decreasing random variable.

Definition 2 [27]: An event A from $\mathcal{F}$ is increasing if $\mathbb{I}_A(\omega) \leq \mathbb{I}_A(\omega')$ when $\omega \leq \omega'$ where $\mathbb{I}_A$ is the indicator function. The event is decreasing if A^c is increasing.

The SINR probability event, $\{\text{SINR} > \Gamma\}$ is a decreasing event. If another interfering user is added to ω, the probability of successful transmission decreases. Now, I can leverage the Fortuin, Kastelyn, Ginibre (FKG) inequality [50].

Lemma 2 [50]: If both $A, B \in \mathcal{F}$ are increasing or decreasing events then $P(AB) \geq P(A)P(B)$.

The FKG inequality can give a bound on the two-way SINR prob-

ability. The bound is only tight when the forward and reverse channels are independent; the dependence, however, can be low in ad hoc network as shown in [1,27]. In [27], this was shown to be a tight lower bound. Using FKG, I can define the two-way SINR probability as

$$P_{\mathrm{c}}^{\mathrm{tw}} \geq \mathbb{P}[\mathrm{SINR}_{\mathrm{F}} > \Gamma_{\mathrm{F}}]\mathbb{P}[\mathrm{SINR}_{\mathrm{R}} > \Gamma_{\mathrm{R}}]. \tag{2.46}$$

Therefore, the two-way SINR probability can be lower-bounded as

$$\begin{aligned} P_{\mathrm{c}}^{\mathrm{tw}} \geq & \left[\sum_{n=1}^{N_{\mathrm{h}}}(-1)^{n+1}\binom{N_{\mathrm{h}}}{n}e^{-2\pi\lambda\left[\omega_{\mathrm{L}}(\Gamma_{\mathrm{F}})+\omega_{\mathrm{N}}(\Gamma_{\mathrm{F}})\right]}\right] \\ & \left[\sum_{n=1}^{N_{\mathrm{h}}}(-1)^{n+1}\binom{N_{\mathrm{h}}}{n}e^{-2\pi\lambda\left[\omega_{\mathrm{L}}(\Gamma_{\mathrm{R}})+\omega_{\mathrm{N}}(\Gamma_{\mathrm{R}})\right]}\right]. \end{aligned} \tag{2.47}$$

2.5.2 Two-Way Performance Analysis

Now I compute the two-way transmission capacity, $\lambda_{\epsilon}^{\mathrm{tw}}$. Because of the constraint that both transmitter and receiver must succeed in transmission, I can argue $\lambda_{\epsilon}^{\mathrm{tw}} \leq \lambda_{\epsilon}$. It is unclear, however, if the gap is large in a mmWave network. Using the transmission capacity framework can quantify how many users must be removed from the network to support the reverse link. Using a similar approach as with the *one-way* transmission capacity, I use a Taylor expansion of the exponential function to yield

$$\begin{aligned} P_{\mathrm{c}}^{\mathrm{tw}} \approx & \left[\sum_{n=1}^{N_{\mathrm{h}}}(-1)^{n+1}\tbinom{N_{\mathrm{h}}}{n}\left(1-2\pi\lambda_{\epsilon}^{\mathrm{tw}}\Theta(T_{\mathrm{F}})+2\pi(\lambda_{\epsilon}^{\mathrm{tw}})^2\Theta^2(\Gamma_{\mathrm{F}})\right)\right] \\ & \left[\sum_{n=1}^{N_{\mathrm{h}}}(-1)^{n+1}\tbinom{N_{\mathrm{h}}}{n}\left(1-2\pi\lambda_{\epsilon}^{\mathrm{tw}}\Theta(\Gamma_{\mathrm{R}})+2\pi(\lambda_{\epsilon}^{\mathrm{tw}})^2\Theta^2(\Gamma_{\mathrm{R}})\right)\right]. \end{aligned} \tag{2.48}$$

The result is a quartic equation in $\lambda_\epsilon^{\text{tw}}$ which has an analytic expression. The general solution, however, is quite messy, and the equation is a page long, so it is omitted here. An analytical solver, such as *Mathematica*, can factor the coefficients of (2.48) which can be input into a polynomial root solver to yield the solution. The two-way area spectral efficiency can be defined as [19]

$$\text{ASE}_\epsilon^{\text{tw}} := \lambda_\epsilon \left(\frac{R_{\text{F}} + R_{\text{R}}}{B_{\text{total}}} \right) (1 - \epsilon). \tag{2.49}$$

Given rate requirements R_{F} and R_{R}, what is the allocation of bandwidth that maximizes (2.49)? I explore this trade-off in Section 2.6.

2.6 Performance Results

In this section, I evaluate the performance metrics to obtain the transmission capacity, λ_ϵ. Further, I compute the area spectral efficiency to define the *best* λ, given by $\lambda^\star$. I compare the achievable rates for mmWave networks with classic results for lower frequency ad hoc networks. The section is concluded with an investigation into two-way communication.

Throughout the section, I compare the mmWave results to UHF ad hoc networks (e.g. 2.4 GHz). For the UHF network, I adjust the model parameters to fit UHF networks. I maintain a constant antenna *aperature* between models which keeps the relative physical size of the devices constant. For an antenna, the gain is computed using $G = \frac{A_{\text{eff}}}{\lambda^2/4\pi}$ where A_{eff} is the aperature of the antenna. By increasing the frequency ten-fold (e.g. 2.4GHz to 28GHz), the gain of the resulting mmWave antenna is 100 (20dB); this matches the 20dB

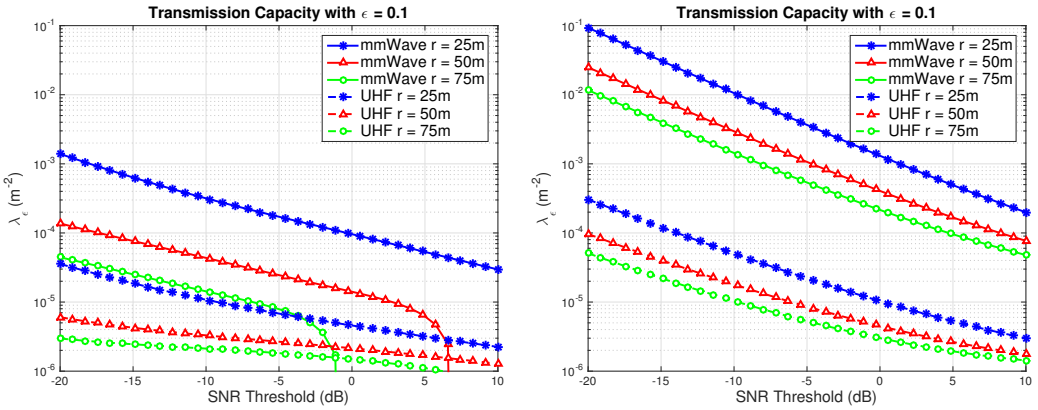

(a) (b)

Figure 2.6: The largest λ for a 10% outage at various SINR thresholds and dipole distances for NLOS/LOS communication (a) and LOS-only communication (b).

total gain for both transmitter and receiver (i.e. 10dB for each transmitter and receiver). I maintain 1W (0dB) of transmit power for UHF. To capture the effect of LOS/NLOS communication, I use $\alpha_{\mathrm{L}} = 2.09$ and $\alpha_{\mathrm{N}} = 3.75$ as shown in [51] which are taken from 3GPP LTE measurements. I use the same blockage model as mmWave. I use a path-loss intercept of 40.4dB and a noise power of -127dB (e.g noise power for 50MHz). For the rate calculations, I use a bandwidth of 50MHz.

2.6.1 Transmission Capacity

Fig. 2.6 shows the transmission capacity for mmWave and lower frequency networks with a 10% outage. Fig. 2.6 shows the relationship between providing a higher SINR (and thus rate) to users while maintaining a constant outage constraint. As expected, the shortest dipole length can support

the highest density of users. A linear increase in SINR (in dB) results in an exponential decrease in the density of users in the network.

In Fig. 2.6a, both LOS and NLOS communication is allowed. If the dipole length is 25m, mmWave networks can allow a larger density. If the dipole length is 50m or 75m, however, lower-frequency networks can permit higher densities when the communication threshold is higher. This is because the mmWave network begins to be noise limited. Essentially, the blockage probability is larger than ϵ; because of the longer link length (and increased path-loss exponent for NLOS communcation), there is no density that will meet the threshold requirements and the transmission capacity is 0. For the UHF network, the lower path-loss exponent and noise power permit a positive transmission capacity. Fig. 2.6b shows the improvement if communication is kept to LOS links. Because the communication is always LOS, the longer links can now support a positive transmission capacity for higher SINR thresholds.

2.6.2 Area Spectral Efficiency

Similar trends are evident in Fig. 2.7. The mmWave network has a $10\times$ efficiency gain compared to UHF networks when the transmission capacity is non-zero. This gain is realized through the interference reduction in the directional antenna array and the increased path-loss exponent for NLOS links. Because buildings do not attenuate UHF as much, even the NLOS interference in a UHF network limits performance.

The shape of the curves suggests an optimal density with respect to

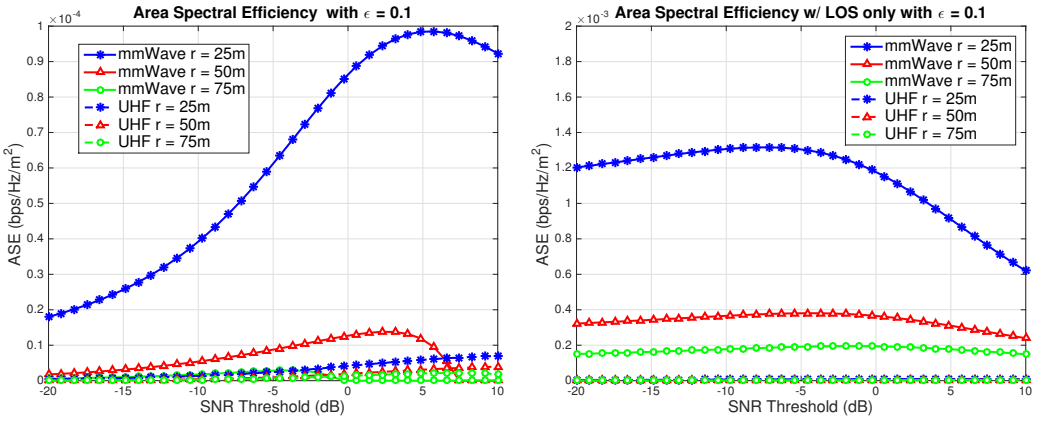

(a) (b)

Figure 2.7: Area spectral efficiency of network with 10% outage. If the dipole link is restricted to LOS (b), an order-of-magnitude improvement is shown over NLOS/LOS dipole links (a). Note the different y-axis scales.

ASE. This leads to the optimization problem

$$\lambda^\star = \underset{\lambda_\epsilon}{\operatorname{argmax}} \ \lambda_\epsilon \log_2(1+\Gamma)(1-\epsilon). \tag{2.50}$$

The numerical solution to this problem is the density corresponding to the largest ASE from Fig. 2.7. I leave the exploration of analytical solutions to (2.50) for future work. Fig. 2.8 shows the numerically obtained $\lambda^\star$ from Fig. 2.7b. The optimal density is exponentially decreasing in r. The optimal density, $\lambda^\star$, corresponds to an average neighbor distance 1/2 the link distance in the LOS-only (*protocol gain*) case. **MmWave ad hoc networks can not only support high density, but this density is best for overall network efficiency**. This is due to both the directional antennas and blockage. The blockage thins the interference PPP as shown in Section 2.4.5. The remaining LOS interferers are effectively *pushed away*. The interference power from a

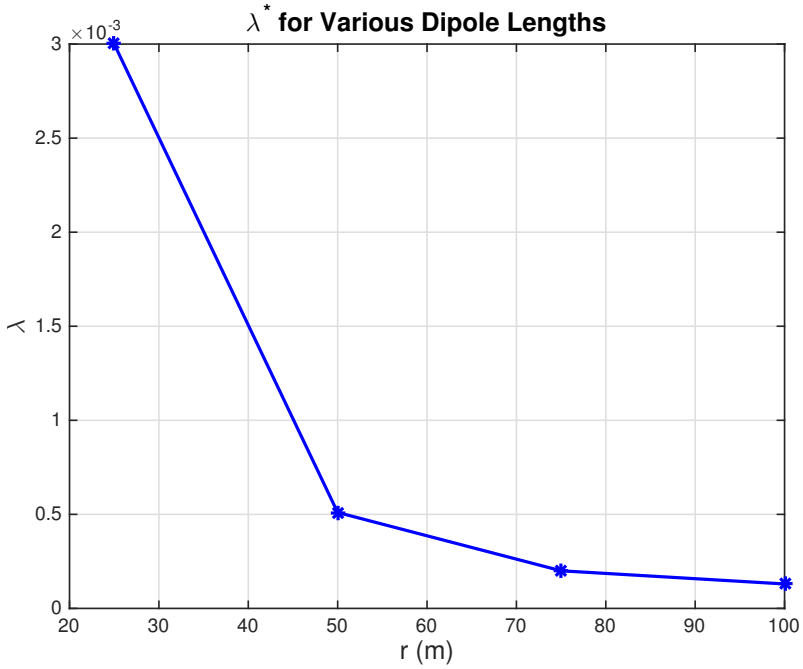

Figure 2.8: Optimal network density for various dipole lengths, subject to 10% outage.

close neighbor into the side-lobe (i.e. the power is heavily attenuated) is the same as that interferer being further away but using omni-directional antennas. Of course, if an interferer is in the main-lobe of the antenna, this phenomenon works against the receiver, but more often, it helps.

2.6.3 Rate Analysis

Fig. 2.9 shows the rate coverage probability, where $R = W\log_2(1+\Gamma)$, and W is the system bandwidth. From Theorem 2.4.1, a user will achieve SINR $> \Gamma$ with some probability as shown in Fig. 2.3a and Fig. 2.3b which leads to an achievable rate probability. For example, according to Fig. 2.4a, a

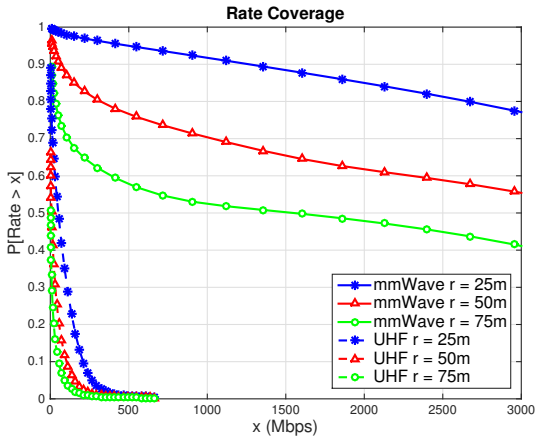

Figure 2.9: MmWave ad hoc networks provide significant increase in rate coverage over lower frequency networks.

LOS mmWave communication link of 50m will have an SINR of at least 10dB 95% of the time which, assuming Gaussian signaling, leads to a rate according to Shannon's equation. In Fig. 2.9 I consider networks with both LOS and NLOS communication.

The system bandwidth used in Fig. 2.9 is 500MHz for the mmWave and 50MHz for the lower frequency system. While the bandwidth is only a 10× increase, I see orders-of-magnitude increase in the rate coverage for mmWave networks. All link lengths of the mmWave network support over 1Gbps a majority of the time.

2.6.4 INR Distribution

Figs. 2.10, 2.11, and 2.12 show the INR CDF for three values of λ for each of the beam patterns in Fig. 2.1. Indeed, in all antenna patterns, the sparsest network exhibits noise limited behavior. For example, the $\mathbb{P}[\text{INR} <$

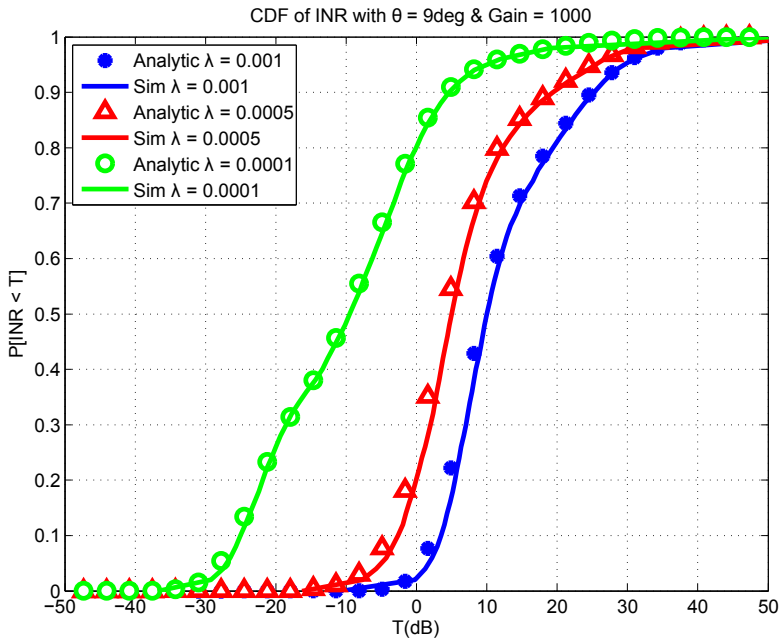

Figure 2.10: The INR CDF for $\theta_{\text{ant}} = 9°$. With extreme beamforming, the network remains interference limited in all but the sparest network.

0dB] = 0.4 for 30° antennas in the sparest network. Yet, these results show compelling evidence that a mmWave ad hoc network can still be considered interference limited. In dense networks (22m and 70m spacing), in all but the very narrow beam case, the network exhibits strong interference. Because of this, I urge caution when considering mmWave networks to be noise limited.

Fig 2.13 shows the INR distribution if I ignore NLOS interference for when $\theta_{\text{ant}} = 30°$. It shows that for many mmWave networks the interference is largely driven by the LOS interference in the two denser networks. The CDF of the two denser networks in Fig. 2.13 is nearly identical to Fig. 2.11 which indicates that NLOS interference plays no role at those densities. I believe this

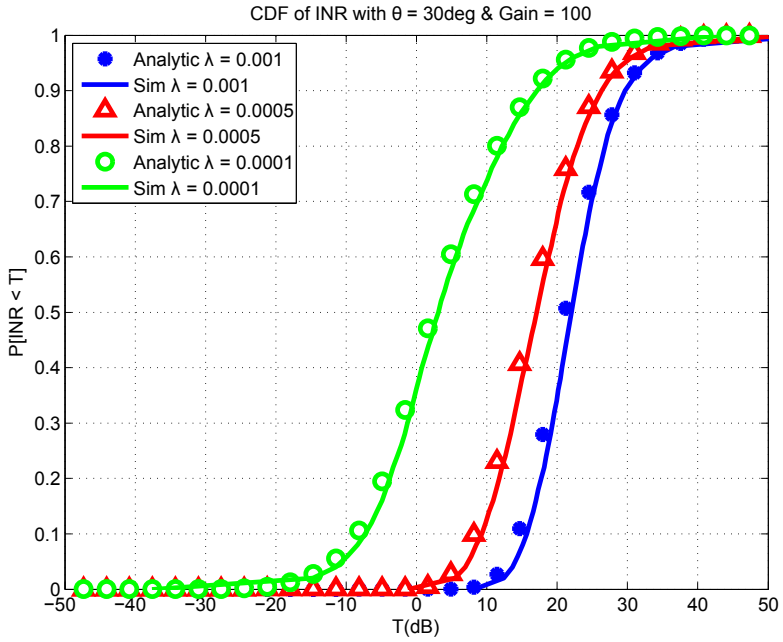

Figure 2.11: The INR CDF for $\theta_{\text{ant}} = 30°$. In the sparsest network, the interference power is more dominant than the noise power (i.e. $\mathbb{P}[\text{INR} < 0\text{dB}] = 0.4$ for the green circle network), but the red triangle curve shows that the more dense network is always interference limited.

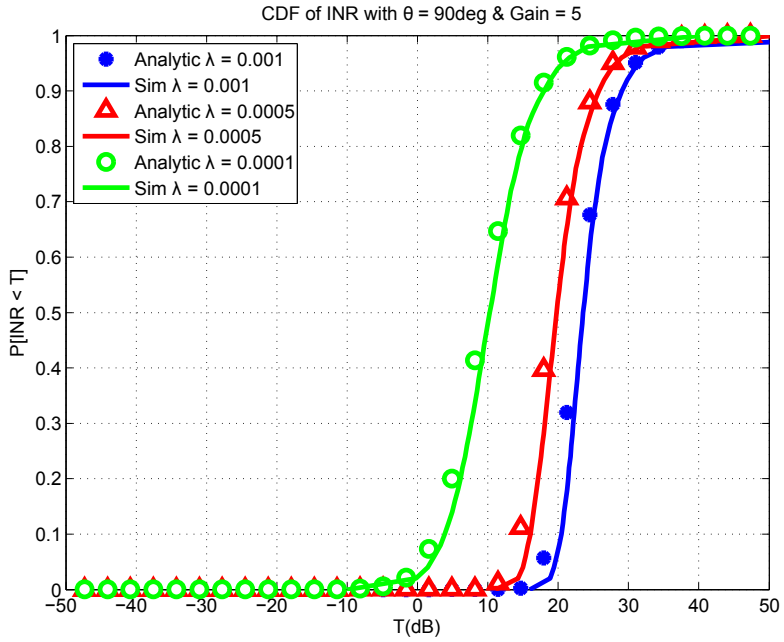

Figure 2.12: The INR CDF for $\theta_{\text{ant}} = 90°$. In all networks, the interference power is nearly always more dominant than the noise power (i.e. $\mathbb{P}[\text{INR} < 0\text{dB}] = 0.05$ for the green circle network).

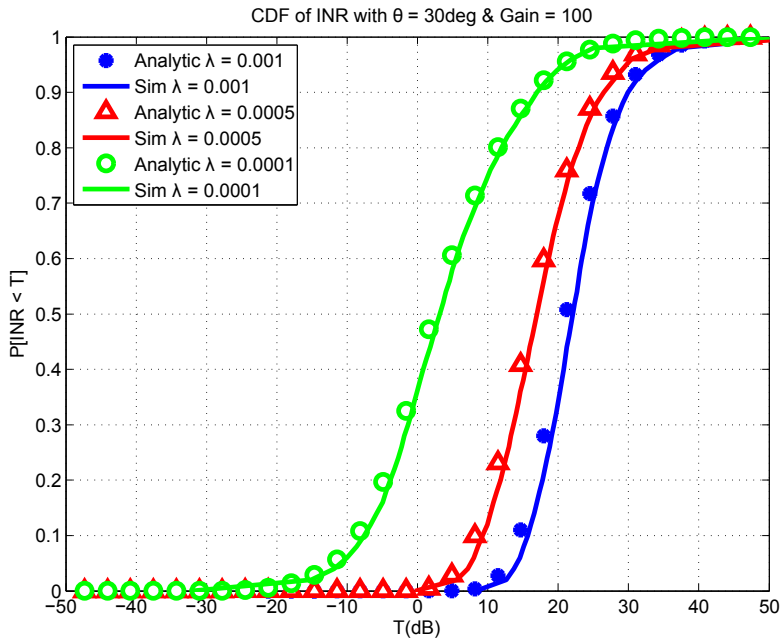

Figure 2.13: The INR CDF for $\lambda = 5 \times 10^{-5}$ and $\theta_{\text{ant}} = 30°$ with only LOS interference. Compare to Fig. 2.11, I find that the shape of INR distributions is largely determined by the LOS interference when the network is dense.

shows compelling evidence that interference cancellation may be useful, even at mmWave frequencies. In particular, eliminating LOS interference is most important.

In Fig. 2.14, the INR is shown for the transmission capacity of the networks from Figs. 2.6a & 2.6b. If conditioned on LOS communication (i.e. *LOS protocol-gain*), the networks support very dense deployments. As such, the INR is nearly always $>$ 0dB as shown in Fig. 2.14. If the network does not enforce a LOS-only transmission scheme, the transmission capacity is less. The interference, however, is not negligible for networks of 25m and 50m. If

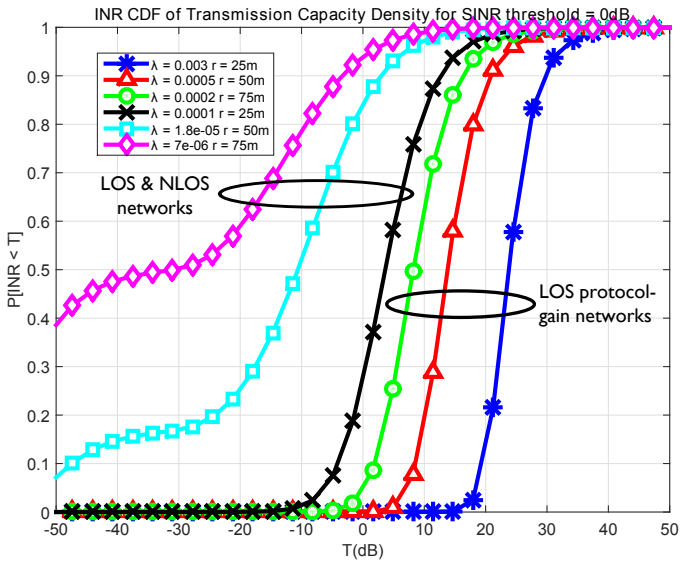

Figure 2.14: The densities correspond to the transmission capacity from Figs. 2.6a & 2.6b for SINR threshold on 0dB.

the communication link is 25m, the INR is $>$ 0dB 70% of the time; if the link is 50m, the INR is less but still > -10dB roughly half the time.

2.6.5 Two-Way Communication Results

The results presented in this section consider a two-way system using bandwidth allocation to split resources. I show that, in asymmetric traffic, the transmission capacity of a two-way network can be vastly improved compared to equal bandwidth allocation or rate-proportional allocation. The two-way area spectral efficiency is compared to one-way area spectral efficiency. I show that 75% of the one-way efficiency can be achieved for outage of 10% which is a 100% increase over the baseline equal allocation. In all the results, the

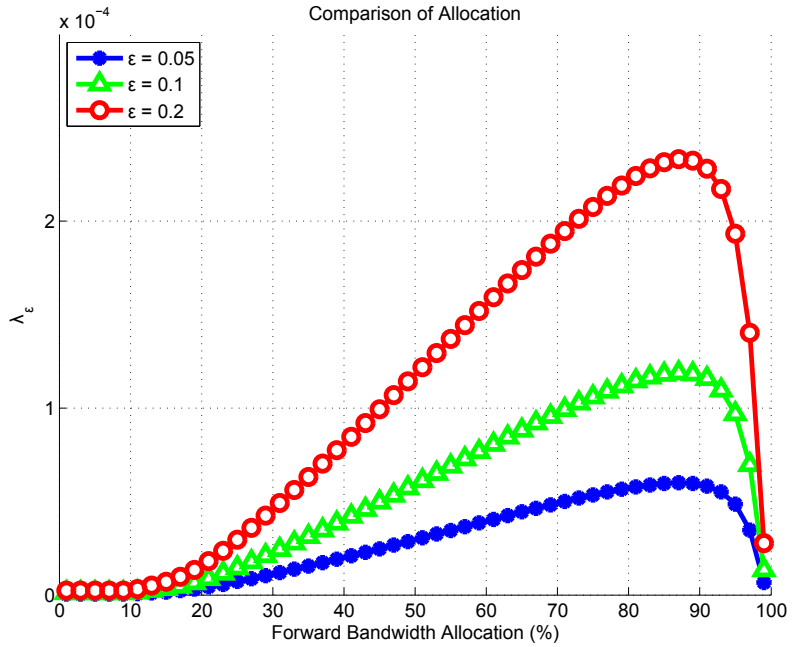

Figure 2.15: The transmission capacity of a two-way network can be improved by allocating bandwidth in an optimal way.

dipole link length is 50m.

I consider asymmetric traffic. For example, in TCP assuming 1000 byte data packets, the receiver must reply with 40 byte ACK packets [52]. Hence, the rate asymmetry in TCP is 1/25. The following results consider a system bandwidth of 100MHz, a forward rate requirement of 200Mbps, and a reverse link rate requirement of 8Mbps.

Fig. 2.15 shows the transmission capacity as a function of forward bandwidth allocation. As more bandwidth is added to the forward link, the required $\mathrm{SINR_F}$ decreases to meet the rate requirement. Because the reverse link rate requirement is quite small, the increase in $\mathrm{SINR_R}$ does not change the

SINR probability much (i.e. I am operating at very low SINR_R which is where the SINR probability plateaus to 1). Fig. 2.15 shows the naivet of simply splitting the bandwidth in half. A nearly 2x improvement in transmission capacity is achieved by going from 50% to the optimal allocation of 90%. What is somewhat more surprising is that a 96% split (i.e. splitting according to the rate requirement) results in nearly the same performance as a naive 50% allocation. Lastly, Fig. 2.15 shows that this allocation is invariant to outage constraint.

Fig 2.16 shows the performance gains in terms of area spectral efficiency that can be achieved by various bandwidth allocations. In all curves, the sum rate of the system is 208Mbps. As expected from Fig. 2.15, the area spectral efficiency is the worst in the naive 50/50 bandwidth allocation. The rate based (96%/4%) allocation performs better, but additional gains can be made by further optimizing the allocation. With the optimal allocation, the two-way system can achieve 75% the area spectral efficiency of the one-way system. Because the one-way and two-way area spectral efficiency is linear in λ_ϵ and $\lambda_\epsilon^{\text{tw}}$, respectively, I can see the effect two-way communication has on the transmission capacity. If the users split the resources equally, considering the two-way constraint reduces the density by nearly a factor of 3. If the resources are split optimally, the network can support $2\times$ the number of users from the equal split. This density is roughly 75% of one-way density.

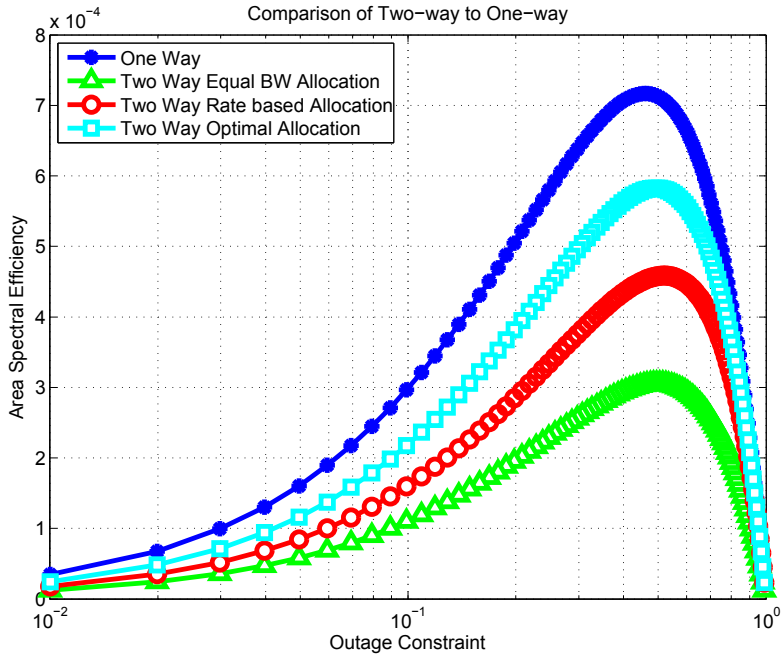

Figure 2.16: Significant ASE gains can be achieved by intelligently allocating bandwidth.

2.7 Conclusions

I presented an analysis that characterized the performance of mmWave ad hoc networks for both one-way and two-way communication. I showed that mmWave networks can improve on the performance and efficiency of UHF networks when considering both LOS and NLOS communication. Massive improvements in transmission capacity and area spectral efficiency (e.g. 10-100×) are possible when only communicating over LOS links which motivates LOS aware protocols. Further, I showed the NLOS interference is negligible and LOS interference can still be the limiting factor for a mmWave ad hoc network. This also motivates the need for LOS interference mitigation strategies. Lastly, by, understanding the requirements of the reverse link in the mmWave network for two way traffic, 75% of the one-way capacity can be achieved which is twice as efficient as an equal allocation of resources.

2.8 Appendix

2.8.1 Proof of Lemma 2.4.1

From [53] Theorem 1,

$$\left[1 - e^{-\beta x^p}\right]^{1/p} < \frac{\int_0^x e^{-t^p} dt}{\Gamma(1 + 1/p)} \tag{2.51}$$

with $\beta = [\Gamma(1 + 1/p)]^{-p}$ and $p \in (0, 1)$. It is shown in [53] that

$$\int_0^x e^{-t^p} dt = \frac{1}{p} \gamma\left(\frac{1}{p}, x^p\right) \tag{2.52}$$

where $\gamma(\cdot, \cdot)$ is the lower incomplete gamma function. A normalized gamma random, $y \sim \Gamma(k, \theta)$, variable is such that the shape, k, and scale, θ, are

inverses of each other so that $\mathbb{E}[y] = 1$ (i.e $\theta = 1/k$). If I let $k = 1/p$ and $x^p = kz$, I have

$$\begin{aligned}
\left[1 - e^{-\beta x^p}\right]^{1/p} &< \frac{1}{p}\frac{\gamma\left(\frac{1}{p}, x^p\right)}{\Gamma(1+1/p)} \\
\left[1 - e^{-\beta kz}\right]^{k} &< \frac{k\gamma\left(k, kz\right)}{\Gamma(1+k)} \\
\left[1 - e^{-az}\right]^{k} &< \frac{\gamma\left(k, kz\right)}{\Gamma(k)} \\
&= \mathbb{P}[y < z]
\end{aligned} \tag{2.53}$$

with $a = k\left[\Gamma(1+k)\right]^{-1/k} = k(k!)^{-1/k}$. □

Chapter 3

Ergodic Rate in Random mmWave Ad Hoc Networks

In Chapter 2, I derived the SINR distribution of a spatially uniform mmWave ad hoc network. While the PPP model is useful in many network scenarios, other spatial deployments are of interest as well. In this chapter[1], I extend the work from the previous chapter to include when users are *clustered* spatially. Additionally, the analysis extends to the evaluation of the ergodic rate of mmWave ad hoc networks. I derive antenna array scaling trends which shows how the array size must scale as users density increases to keep ergodic rate constant. Lastly, this contribution ends with quantifying the lost rate when mmWave antenna beams are not aligned.

3.1 Introduction

The ergodic rate is a useful metric because it quantifies the average rate that is attainable by the users in the network. The ergodic rate has been explored via stochastic geometry in several chapters on low frequency

[1]This chapter is based on the work published in the journal paper: A. Thornburg and R. W. Heath, "Ergodic Rate of mmWave Ad Hoc Networks," to appear in IEEE Transactions on Wireless Communications, 2017. This work was supervised by Prof. Robert Heath.

networks, see e.g. [17, 54] and references therein. MmWave ad hoc networks have also been studied in the past using different metrics. Finite mmWave wearable networks were investigated in [40]. Prior work in [55–57] considered only the coverage of homogeneous networks, while the work in [40] considers a finite enclosed network such as a train car for wearables.

Because ad hoc networks are limited by nearby interference, accurately modeling the spatial characteristics of the transmitters is needed. In the case of military squads or consumer cliques, users may be clustered together either around a squad leader or a WiFi hotspot, for example. In this chapter, the clustering is considered an inherent property of the network; the clustering is not due to a MAC protocol which is considered in [58–60]. Prior work has considered clustered lower frequency ad hoc networks [61, 62]. In [61], several interference properties and the coverage of a clustered Neyman-Scott process was derived; results for spread-spectrum communication to deal with the intra-cluster interference were presented. The performance of clustered interference alignment (IA) networks was developed in [62], and it was shown that IA can effectively deal with intra-cluster interference for certain cluster sizes as IA outperformed TDMA for larger cluster sizes. The previous work showed that mmWave ad hoc networks are line-of-sight (LOS) interference limited [56]. Because of this, I am motivated to analyze the ergodic rate spatially uniform mmWave ad hoc networks as well as clustered mmWave ad hoc networks, which has not been investigated previously.

The number of elements within an array is a new design parameter

as mmWave arrays allow many elements within a small physical footprint [23]. Antenna arrays with many elements to beam steer energy are used in mobile systems to fulfill the mmWave link budget [1, 55, 63]. Using ergodic rate as a base metric, antenna scaling trends of ad hoc networks were derived in [17, 54]. The antenna scaling trend shows how many antennas are needed to keep ergodic rate per user constant as users are added to the network (i.e. the marginal gain of adding an antenna to the array in terms of extra users). Both [17, 54] also quantify the scaling of rate in ad hoc networks. In [17], the authors exploit channel state information (CSI) to develop scaling laws for SIMO networks, while in [54], the authors extend [17] to MIMO ad hoc networks using zero-forcing and successive-interference-cancellation. The scaling of low frequency multi-antenna ad hoc networks with Rayleigh fading was derived in [17]. In order to fully utilize the gain from antenna arrays, the alignment of the antenna beams must be accurate. Others have characterized the effect of beam alignment in wireless networks [64–66]. In [64], stochastic geometry was used to analyze the effect of misalignment. It was shown that performance can be affected by the misalignment of directional antenna beams. It does not include mmWave phenomenon such as blockage and analyzes the performance in terms of transmission rate, as do [65, 66]. I compute the ergodic rate scaling as the user density and antenna array size increases and derive effect of imperfect beam alignment on ergodic rate for mmWave ad hoc networks which has not previously been done in the literature.

3.2 Contributions

In this chapter, I characterize the ergodic rate of mmWave ad hoc networks for two different spatial distributions of transmitters. I leverage stochastic geometry to model mmWave ad hoc networks as uniform networks (e.g. a Poisson point process) and a LOS cluster process (e.g. Poisson cluster process). The main contributions of the chapter are summarized as follows:

- Derivation of the ergodic rate of a uniform mmWave ad hoc network assuming LOS communication, directional antennas, building blockage, and Gamma fading. An antenna scaling trend, as transmitter density increases, of uniform mmWave ad hoc networks is derived. The result indicates that the number of antennas can scale sub-linearly with transmitter density.

- Computation of the ergodic rate of a clustered mmWave ad hoc network assuming LOS communication, directional antennas, building blockage, and Gamma fading. An antennna scaling trend of clustered ad hoc networks is proposed as a heuristic using the ergodic rate theorem which indicates that antenna arrays must scale linearly with user density. I define and develop a relationship between the SINR for communication within a cluster (intra-cluster) and between clusters (inter-cluster) which gives the proximity of the nearest cluster while maintaining rate requirements within a cluster.

- Characterization of the effect of random beam misalignment between the desired user pairs. I present results for two antenna models: sectored and Gaussian. The loss in rate per user is shown to be proportional to alignment error variance; a rate loss of up to 45% occurs if the alignment error standard deviation is 10°.

The rest of the chapter is organized as follows. Section 3.3 provides the system model and assumptions used in the chapter. Section 3.4.1 derives the ergodic rate and scaling of the uniform mmWave ad hoc network. Section 3.4.2 develops the ergodic rate, scaling, and inter-cluster coverage of clustered mmWave ad hoc networks. Section 3.5 discusses the rate loss due to antenna misalignment on the signal of interest. I present the numerical results in Section 3.6 and conclude the chapter in Section 3.7. A summary of the commonly used variables is in Table 3.1.

3.3 System Model

In this section, I establish the two different network architectures: the uniform model and clustered model. I present the signal model which includes the path-loss, building blockage model, and antenna model. Next, I define the key metric of the work, the ergodic rate. Finally, I show several mathematical preliminaries that will aid the subsequent sections.

Φ_{p}	parent point process
Φ_{c}	cluster point process
Φ	homogeneous Poisson point process (PPP)
N^x	finite cluster point process centered on x
λ_{p}	intensity of parent point process
λ_{u}	intensity of the PPP
R_c	cluster radius
r_o	intra-cluster communication distance
r_{e}	inter-cluster communication distance
I_{a}	intra-cluster interference
I_{e}	inter-cluster interference
$\mathrm{SINR}_{\mathrm{u}}$	SINR with PPP
$\mathrm{SINR}_{\mathrm{a}}$	intra-cluster SINR
$\mathrm{SINR}_{\mathrm{e}}$	inter-cluster SINR
$p(x)$	blockage probability function
α_{m}	path loss exponent
N	number of antennas
$\mathcal{L}(z)$	Laplace functional of point process
$\mathcal{G}(v)$	generating functional of point process

Table 3.1: System variables for Chapter 3

3.3.1 Network Topologies and Access Schemes

The network topology determines the interference characteristics. I analyze two different network topologies for user locations: *uniform* and *clustered*. These topologies have noticeably different spatial characteristic as shown in Fig. 3.1. If the distances between transmitters is invariant to geographic location (e.g. mesh network), I model the transmitter locations as uniform; if transmitters tend to gather around certain geographic locations, a clustered model is appropriate (e.g. a device-to-device VR monster app).

I build the transmitter models from the standard homogeneous Poisson point process (PPP) [3,21,55]. I denote the collection of transmitter locations on $\mathbb{R}^2$ formed by the PPP Φ as the *uniform* network. I denote the intensity of Φ as $\lambda_{\mathrm{u}} = \zeta\lambda$ where ζ is the transmission probability and λ is the intensity of all potential transmitters.

Given a finite area of $\mathbb{R}^2$, the transmitters will be randomly uniformly placed within the area. To account for geographic clustering, I also use a general Poisson cluster point process Φ_{c}. The cluster process is formed by randomly placing c transmitters in a ball of radius R_c centered at the points of a parent Poisson point process Φ_{p}. Specifically,

$$\Phi_{\mathrm{c}} = \bigcup_{y \in \Phi_{\mathrm{p}}} N^y, \tag{3.1}$$

where each $N^y \in \mathcal{B}(y, R_c)$ is a finite point process of c points centered on y. For simplicity, I assume all users in the finite point process cluster N^y experience the same LOS or NLOS distinction as clustered users are likely to

be affected by the same spatial blockage if R_c is smaller than the average LOS distance. I consider the distinction between LOS and NLOS parent points as an independent mark. Each parent point is therefore LOS and NLOS as a result of the Thinning theorem. The cluster parent process Φ_{p} is an Poisson point process with intensity measure given as

$$\Lambda(B) = \underbrace{\int_B \lambda_{\mathrm{p}}(x)p(x)dx}_{\text{LOS clusters}} + \underbrace{\int_B \lambda_{\mathrm{p}}(x)\left(1-p\left(x\right)\right)dx}_{\text{NLOS clusters}} \tag{3.2}$$

for all Borel sets B of $\mathbb{R}^2$ where λ_{p} is the intensity of the generative cluster Poisson point process and $p(x)$ is the probability a link of length $|x|$ is LOS. I call the cluster density λ_{p}. Without loss of generality, due to Slivnyak's theorem, I consider a typical cluster located at the origin N^o by conditioning on the event that a point at the origin exists in Φ_{p}.

For this work, I consider a random *symmetric* ad hoc network such as a device-to-device (D2D) or tactical military network. Each transmitter in both the uniform and clustered network has the same hardware and/or capabilities (e.g. antenna number, processing capability, beam alignment scheme). I consider a symmetric network due to tractability, and practical relevance for peer-to-peer applications. Each transmitter has a receiver located at a fixed distance r_o away with the orientation distributed uniformly in $[0, 2\pi]$ [21]; these receiver points are not part of Φ_{p} nor Φ_{c}. Fig. 3.1 shows an example realization of the network PPP with the associated receivers.

I consider two MAC protocols: uncoordinated channel access (UCA) and time-division multiple-access (TDMA). For the uniform network under

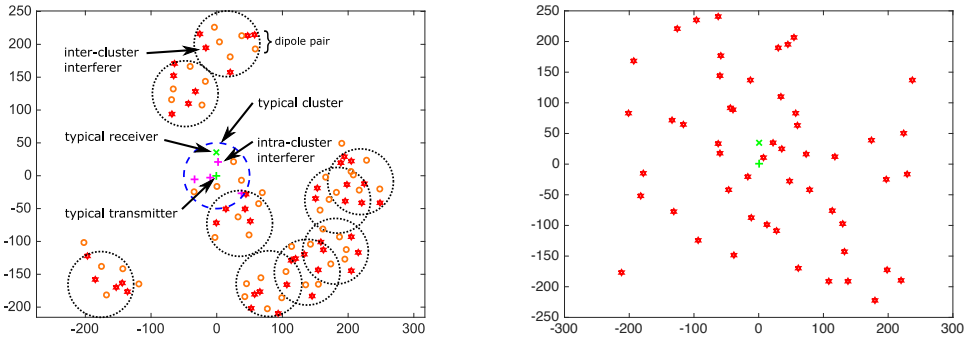

(a) (b)

Figure 3.1: An example realization of the LOS clustered network (a) compared to LOS PPP (b). The interfering clusters shown are all LOS from the perspective of the typical cluster at the origin. The dashed blue circle is the boundary for the typical cluster while the black dotted circle is the boundary for the other clusters. The clustered point process exhibits much different spatial properties than the LOS PPP.

UCA, all the transmitters access the channel within each channel time slot as determined by ζ. For the clustered network under UCA, all c transmitters in a cluster access the channel with each time slot as determined by ζ. In TDMA, only one transmitter from each cluster accesses the channel with each time slot. I do not consider TDMA for the uniform network; because I consider single-hop networks, each transmitter-receiver pair is geographically isolated with no coordination between transmitters. In other stochastic geometry work, the UCA is considered as ALOHA, but the randomness of the ALOHA channel access would make the number of active transmitters per cluster random; this added randomness reduces the tractability of the analysis. TDMA is widely used in mmWave standards such as IEEE 802.11ad [67].

Each cluster communicates with the same frequency resources.

3.3.2 Channel and Antenna Models

I use the standard unbounded path loss model

$$\ell(x) = \frac{A_{\mathrm{m}}}{|x|^{\alpha_{\mathrm{m}}}} \tag{3.3}$$

where α_{m} is the path loss exponent (PLE) and A_{m} is the path loss intercept. This model is valid for far-field communication and if the interference is greater than 1m away. Measurements show a lower PLE for line-of-sight (LOS) versus non-line-of-sight (NLOS) signals [34]. This discrepancy is largely caused by building blockage. I use a distance-dependent LOS blockage function $p(r)$. In general, the work is agnostic to the choice of a proper p; I, however, model the blockage as in [48, 56, 68]. As shown in [48] using random shape theory, the probability a link is LOS is given by $p(r) = \exp(-\beta r)$ where β is a function of the average building perimeter and area. For simplicity, I ignore correlation of LOS probabilities among links, as in [48]. It was shown that the difference in the performance analysis is small for sparse to moderately dense outdoor environments when ignoring the correlation [48]. The previous work [57] showed that mmWave networks are LOS-interference limited; I ignore the contribution of NLOS users in the analytical expressions throughout the chapter. The cluster process Φ_{c}, therefore, effectively represents the clustered LOS transmitters seen from the typical cluster at the origin while the uniform process Φ is the LOS user process. For LOS signals, α_{m} is typically between 2 and 2.5.

I assume the transmitter and receiver are able to beam steer towards the desired angle of departure and arrival. In the previous chapter, I used the sectored antenna model [56, 57, 68]. I model the antenna array with a sectored antenna model

$$G^{\text{tx/rx}}(\theta) = \begin{cases} N & \theta \in [-\nu\theta_{3dB}, \nu\theta_{3dB}] \\ \frac{1}{N} & \text{otherwise} \end{cases}, \tag{3.4}$$

where N is the number of antennas at each transmitter and receiver and the mainlobe beamwidth factor ν is 2. I relax the sectored assumption in Section 3.5. The 3dB beamwidth of a ULA is approximately $\frac{\delta'}{2N}$ where $\delta' = \frac{102\pi}{180}$. The mainlobe of the sectored antenna is then $\frac{\delta'}{N}$. The resultant *system* gain $G^{\text{rx}}G^{\text{tx}}$ is modeled as a discrete random variable κ such that

$$\kappa = \begin{cases} N^2 & \text{w.p. } p_1 = \frac{\delta^2}{N^2} \\ 1 & \text{w.p. } p_2 = 2\left(1 - \frac{\delta}{N}\right)\frac{\delta}{N} \\ N^{-2} & \text{w.p. } p_3 = \left(1 - \frac{\delta}{N}\right)^2, \end{cases} \tag{3.5}$$

where $\delta = \frac{\delta'}{2\pi}$. When beamforming with the sectored antenna, the channel power is $h = N^2|\gamma|^2$ where $|\gamma|^2$ corresponds to Gamma fading with mean 1 and parameters $(N_h, \frac{1}{N_h})$. For $N_h = 1$, this corresponds to Rayleigh fading, while as $N_h \to \infty$ the fading becomes deterministic. I use a Gamma random power term for each signal to capture both the minimal small-scale fading and any other random attenuation effects. At mmWave frequencies, small-scale fading is not a strong phenomenon as shown in [11, 68]. Additionally, it is unlikely the power transfer of the channel is perfect. For example, the scattering and reflection of the mmWave may not transfer 100% of the power; in [12], this is modeled as an exponential random variable, which is a special case of Gamma.

3.3.3 Signal Metrics

The received signal for the user at the origin for both uniform and clustered networks is

$$y_o = \sqrt{\ell(r_o)h_o\kappa_o A_{\mathrm{m}}}s_o + \sum_{i\in\Phi_{\mathrm{c}}} \sqrt{\ell(x_i - r_o)h_i\kappa_i A_{\mathrm{m}}}s_i + v, \tag{3.6}$$

where $s_o, s_i \sim \mathcal{N}_{\mathrm{C}}(0, P_t)$, P_t is the signal power, $v \sim \mathcal{N}_{\mathrm{C}}(0, N_o^{\mathrm{m}})$, N_o^{m} is the noise power, κ_o, κ_i is the antenna gain as defined in (3.5), $h_i \sim \Gamma(N_h, \frac{1}{N_h})$, and x_i is the random location of each point of point process to the typical receiver r_o. Ignoring misalignment, I assume that the desired signal performs perfect beamforming such that $\kappa_o = N^2$. The received SINR of the uniform network is

$$\mathrm{SINR}_{\mathrm{u}} = \frac{P_t A_{\mathrm{m}} N^2 \ell(r_o) h_o}{N_o^{\mathrm{m}} + \sum_{i\in\Phi} P_t A_{\mathrm{m}} \ell(x_i - r_o) h_i \kappa_i}, \tag{3.7}$$

where the interference is from transmitters in Φ. Additionally, I wish to note the use of intr*a*-cluster $\mathrm{SINR}_{\mathrm{a}}$. For the clustered network, the $\mathrm{SINR}_{\mathrm{a}}$ is the same as $\mathrm{SINR}_{\mathrm{u}}$, but the interference is summed over the clustered point process Φ_{c}. I note that the signal terms are identical between the two networks which is to be expected. Each network models the signal as an user pair transmitting and receiving at a fixed distance. This is the SINR of the user pair within a cluster. I introduce the int*e*r-cluster $\mathrm{SINR}_{\mathrm{e}}$ later in the chapter as a means to quantify the communication between clusters.

I am interested in analyzing the ergodic rate which is the expected sum

rate of the network, expressed in terms of $b/s/Hz$. I define this as

$$R^{\Sigma} = \mathbb{E}_{\mathcal{P},h,\kappa}\left[\sum_{i\in\mathcal{P}} \log_2\left(1+\mathrm{SINR}_i\right)\right], \tag{3.8}$$

for some point process of transmitters $\mathcal{P}$. This is the average sum rate assumming Gaussian signaling and is a lower bound on the unknown sum capacity. The ergodic rate as defined in (3.8) captures the dynamics of the channel and network. As nearby users begin or cease transmitting, the SINR varies over time slots. The fixed-rate approach of the previous work and others does not consider rate-adaption techniques to take advantage of different fading and point process realizations [1, 56]. Previous work considers a success probability based on a fixed SINR threshold. By adapting the rate and coding scheme over different realizations, the ergodic rate quantifies the contribution from good and bad channels. For the network topologies considered in this chapter, I leverage the properties of point processes to simplify (3.8). In the case of the uniform network with a homogeneous PPP, I can use Slivynak's Theorem such that

$$R_{\mathrm{u}}^{\Sigma} = \lambda_{\mathrm{u}}|A|\mathbb{E}^{o}_{\Phi,h,\kappa}\left[\log_2\left(1+\mathrm{SINR}_{\mathrm{u}}\right)\right], \tag{3.9}$$

where A is the area of interest for the network [17] Each transmitter/receiver pair experiences the same SINR on average as the typical pair at the origin [21]. Similarly, I can simplify the clustered network metric as

$$R_{\mathrm{c}}^{\Sigma} = \lambda_{\mathrm{p}}c|A|\mathbb{E}^{o}_{\Phi_{\mathrm{c}},h,\kappa}\left[\log_2\left(1+\mathrm{SINR}_{\mathrm{a}}\right)\right], \tag{3.10}$$

where all clusters in the network experience the same signal to interference and noise ratio (SINR) statistics as the *typical* cluster located at the origin [61]. The sum rate, therefore, is the expected rate at the origin multiplied by the cluster density c. I present results in terms of the sum ergodic rate (e.g. R_{u}^{Σ} and R_{c}^{Σ}) as well as the ergodic rate of each user ($b/s/Hz/\text{user}$). These quantities are defined as $R_{\mathrm{u}} = \frac{R_{\mathrm{u}}^{\Sigma}}{\lambda_{\mathrm{u}}|A|}$ and $R_{\mathrm{c}} = \frac{R_{\mathrm{c}}^{\Sigma}}{\lambda_{\mathrm{p}} c|A|}$.

3.3.4 Mathematical Preliminaries

The following technical details will aid the development of the results in the next sections.

Lemma 3.3.1. *Let $X > 0$ and $Y > 0$ be non-negative and independent random variables. Then, for any $a > 0$,*

$$\mathbb{E}\left[\ln\left(1+\frac{X}{a+Y}\right)\right] = \int_0^{\infty} \frac{e^{-az}}{z}\left(1-\mathbb{E}\left[e^{-zX}\right]\right)\mathbb{E}\left[e^{-zY}\right]dz.$$

Proof. See [17, Lemma 2] and references therein. □

To evaluate the scaling trends on the rate of the networks, I also use the following lemma

Lemma 3.3.2.

$$\log_2\left(1+\frac{e^{\mathbb{E}[\log(X)]}}{\mathbb{E}[Y]}\right) \leq \mathbb{E}\left[\log_2\left(1+\frac{X}{Y}\right)\right] \leq \log_2\left(1+\mathbb{E}[X]\mathbb{E}\left[\frac{1}{Y}\right]\right).$$

Proof. See [17, Lemma 2] and references therein. □

I denote $\mathcal{G}$, $\mathcal{G}_{\mathrm{p}}$, $\mathcal{G}_{\mathrm{c}}$ as the generating functionals of a point process, the parent process, and cluster process, respectively,

$$\mathcal{G}(v) \overset{(a)}{=} \mathcal{G}_{\mathrm{p}}\left(\mathcal{G}_{(\cdot)}(v)\right) \tag{3.11}$$

$$\overset{(b)}{=} \mathcal{G}_{\mathrm{p}}\left(\mathcal{G}_{(y)}(v)\right) \tag{3.12}$$

$$\overset{(c)}{=} \mathcal{G}_{\mathrm{p}}\left(\mathcal{G}_{\mathrm{c}}\left(v\left(y+\cdot\right)\right)\right) \tag{3.13}$$

$$\overset{(d)}{=} \exp\left(-\int_{\mathbb{R}^2}\left(1-\mathcal{G}_{\mathrm{c}}\left(v\left(y+\cdot\right)\right)\right)\Lambda(dy)\right) \tag{3.14}$$

$$\overset{(e)}{=} \exp\left(-\lambda_{\mathrm{p}}\int_{\mathbb{R}^2}\left(1-\mathcal{G}_{\mathrm{c}}\left(v\left(y+\cdot\right)\right)\right)p\left(y\right)dy\right), \tag{3.15}$$

where (a)-(c) is due to [69, eqs. 5.15 & 5.16], (d) is due to the generating functional for any Poisson point process, and (e) is due to (3.2). I note that the generating functional of the cluster $\mathcal{G}_{\mathrm{c}}$ is

$$\mathcal{G}_{\mathrm{c}}\left(v\left(y+\cdot\right)\right) = \mathbb{E}\left[\prod_{x\in N_o} v(y+x)\right] \tag{3.16}$$

$$= \left(\frac{1}{\pi R_c^2}\int_{\mathcal{B}(0,R_c)} v(y+x)dx\right)^c, \tag{3.17}$$

where c is the fixed number of points in the cluster.

3.4 Ergodic Rate in Outdoor mmWave Ad Hoc Networks

In this section, I develop the theorems that characterize the ergodic rate of outdoor mmWave ad hoc networks in both uniform and clustered networks.

3.4.1 Uniform Network

To analyze the ergodic rate, I start by rearranging (3.7) so that

$$\mathrm{SINR_u} = \frac{h_o \ell(r_o)}{\frac{N_o^{\mathrm{m}}}{N^2 P_t A_{\mathrm{m}}} + \sum_{i \in \Phi} \ell(x_i - r_o) h_i \kappa_i'}, \tag{3.18}$$

where $\kappa_i' = \frac{\kappa_i}{N^2}$ and κ_i is each unnormalized sectored antenna gain. Because the gain κ_i from each interfering transmitter is an independent random variable, the thinning theorem is used to split the interference into three separate PPPs. The interference in $\mathrm{SINR_u}$ is decomposed such that

$$I_{\mathrm{p}} = \sum_n I_{\mathrm{u}}^n, \tag{3.19}$$

where $I_{\mathrm{u}}^n = \sum_{i \in \Phi | \kappa_i' = n} \ell(x_i - r_o) h_i \kappa_i'$ is the interference with antenna gain $n \in \{1, N^{-2}, N^{-4}\}$. With this decomposition in mind, I can state the main result of the section.

Theorem 3.4.1. *The ergodic rate per unit area (b/s/Hz/*user*) of a uniform outdoor mmWave network is*

$$R_{\mathrm{u}} = \frac{1}{\log(2)} \int_0^\infty \frac{e^{-z\theta}}{z} \left[1 - \left(1 + \frac{z \ell(r_o)}{N_h} \right)^{-N_h} \right] \mathcal{L}_{\mathrm{p}}(z) dz \tag{3.20}$$

with

$$\theta = \frac{N_o^{\mathrm{m}}}{N^2 P_t A_{\mathrm{m}}} \tag{3.21}$$

and

$$\mathcal{L}_{\mathrm{p}}(z) = \exp\left(-2\pi \lambda_{\mathrm{u}} \sum_n p_n \int_0^\infty \left[1 - \left(1 + \frac{z \ell(r) \kappa_n'}{N_h} \right)^{-N_h} \right] p(r) dr \right). \tag{3.22}$$

Proof. The proof is presented in Appendix 3.8.1. □

3.4.1.1 Scaling of Uniform Networks

In this section, I establish how the antenna array must grow to accommodate new users (i.e. as λ_{u} grows) with the goal of keeping the *per user* ergodic rate constant. Because λ_{u} grows large, and thus noise becomes negligible, I switch my focus to the $\mathrm{SIR}_{\mathrm{p}}$, which is defined as

$$\mathrm{SIR}_{\mathrm{p}} = \frac{h_0}{r_o^{\alpha_{\mathrm{m}}} \sum_{i \in \Phi} d_i^{-\alpha_{\mathrm{m}}} h_i \kappa_i'}. \tag{3.23}$$

Additionally, for this section, I ignore the blockage as λ_{u} increases because as the network density increases the blockage of users nearby diminishes. The following theorem specifies the scaling rate of antennas as the user density increases.

Theorem 3.4.2. *Assume the number of antennas at each user N scales such that $N^2 = t\lambda_{\mathrm{u}}$ for $\alpha_{\mathrm{m}} \in (2, 4]$. Then the rate scales such that*

$$\frac{R_{\mathrm{u}}^{\Sigma}}{\lambda_{\mathrm{u}}} = \Theta\left(\log_2(1 + t^{\frac{-\alpha_{\mathrm{m}}}{2}})\right) \tag{3.24}$$

as $\lambda_{\mathrm{u}} \to \infty$.

Proof. The proof is presented in Appendix 3.8.2. □

Comment: Somewhat surprisingly for $\alpha_{\mathrm{m}} \in (2, 4]$, the number of antennas scales independently of the PLE and simply scales with $\Theta(\sqrt{\lambda_{\mathrm{u}}})$. This follows other scaling trends for ad hoc networks [13, 17]. In previous rate scaling results, [17] showed that the link distance r_o must scale with $\Theta(\sqrt{\lambda_{\mathrm{u}}})$ to match the interference scaling. The result shows that the same scaling can

be achieved by increasing the antenna array. It is important to note that the upper bound arises from only a single interferer. As the network becomes dense, the closest transmitter to the receiver that is accidentally aligned in the antenna beam pattern essentially limits the overall performance of the system. Practically, the asymptotics of antennas and user density is not seen in a real system (i.e infinite antennas). I have seen that for $\alpha_{\mathrm{m}} \in (2, 4]$ and $N < 10$ the number of antennas can scale as $\lambda_{\mathrm{u}}^{\frac{1}{4/\alpha_{\mathrm{m}}+1}}$. I will discuss this further in the results.

3.4.2 Clustered Network

In this section, I derive the ergodic rate of a clustered mmWave network under two channel access assumptions. To begin, I re-arrange the $\mathrm{SINR}_{\mathrm{a}}$ such that

$$\mathrm{SINR}_{\mathrm{a}} = \frac{h_o \ell(r_o)}{\frac{N_o^{\mathrm{m}}}{N^2 P_t A_{\mathrm{m}}} + \sum_{i \in \Phi_{\mathrm{c}}} \ell(x_i - r_o) h_i \kappa_i'}, \tag{3.25}$$

where $\kappa_i' = \frac{\kappa_i}{N^2}$. Similar to the uniform case, I define the interference term to be $I_{\mathrm{c}} = I_{\mathrm{a}} + I_{\mathrm{e}}$ where I_{a} is the intra-cluster interference and I_{e} is the inter-cluster interference. Each interference term can be further decomposed in three sub-PPPs depending on the gain of the interference as before.

Theorem 3.4.3. *The ergodic rate per user ($b/s/Hz/$user) of an outdoor clustered mmWave network with directional antennas and uncoordinated channel access is*

$$R_{\mathrm{c}}^{\mathrm{UCA}} = \frac{1}{\log(2)} \int_o^{\infty} \frac{e^{-z\theta}}{z} \left[1 - \left(1 + \frac{z\ell(r_o)}{N_h} \right)^{-N_h} \right] \mathcal{L}_{\mathrm{a}}(z) \mathcal{L}_{\mathrm{e}}(z) dz \tag{3.26}$$

with

$$\theta = \frac{N_o^{\mathrm{m}}}{N^2 P_t A_{\mathrm{m}}}, \tag{3.27}$$

$$\mathcal{L}_{\mathrm{a}}(z) = \left(g(r_o, z)\right)^{c-1}, \tag{3.28}$$

$$\mathcal{L}_{\mathrm{e}}(z) = \exp\left(-2\pi\lambda_{\mathrm{p}} \int_o^{\infty} \left(1 - g(r,z)^c\right) rp(r) dr\right), \tag{3.29}$$

and

$$g(r,z) = \sum_n \frac{p_n}{\pi R_c^2} \int_{\mathcal{B}(0,R_c)} \left(1 + \frac{z\ell\left(u - r\right)\kappa_n'}{N_h}\right)^{-N_h} du. \tag{3.30}$$

Proof. The proof is presented in Appendix 3.8.3. □

Comment: I note the inclusion of $g(r,z)$ (i.e. averaging of the interference signal over the clusters) in (3.76) and (3.84) which is typical of clustered point process [61,62]. Essentially, (3.76) averages over the typical cluster which is offset by r_o whereas (3.84) averages over the interference clusters which are offset by r. While a closed form expression, Theorem 3.4.3 requires several numerical integrations which can take some time. In particular, the integral over the ball in $g(r,z)$ cannot be reduced by converting to polar coordinates because of the offset of r. It is possible, however, to view the integral as the expectation of the random distance from a given point r to a random point in the ball $\mathcal{B}(0,R_c)$. The distribution of this random distance can be derived to simplify $g(r,z)$ to a single integration.

Next, I specialize the results to TDMA channel access.

Corollary 3.4.4. *The ergodic rate per user ($b/s/Hz/$user) of an outdoor clustered mmWave network with directional antennas and TDMA channel access is*

$$R_{\mathrm{c}}^{\mathrm{TDMA}} = \frac{1}{\log(2)} \int_o^{\infty} \frac{e^{-z\theta}}{z} \left[1 - \left(1 + \frac{z\ell(r_o)}{N_h} \right)^{-N_h} \right] \mathcal{L}_{\mathrm{e}}(z) dz \tag{3.31}$$

with

$$\theta = \frac{N_o^{\mathrm{m}}}{N^2 P_t A_{\mathrm{m}}} \tag{3.32}$$

and

$$\mathcal{L}_{\mathrm{e}}(z) = \exp\left(-2\pi\lambda_{\mathrm{p}} \int_o^{\infty} \left(1 - g(r,z)\right) rp(r) dr \right). \tag{3.33}$$

Proof. This is a simplification of Theorem 3.4.3 noting that there is no intra-cluster interference and only one interfering transmitter per cluster. □

3.4.2.1 Scaling of Cluster mmWave Ad Hoc Networks

In this section, I investigate the scaling properties of clustered mmWave ad hoc networks as $c \to \infty$. I scale the number of users in the cluster c rather than the cluster density λ_{p} because as the inter-cluster distance grows small, the spatial characteristics of the interference approach the uniform network case. Again, I am interested in keeping the *per user* ergodic rate constant as c grows large. Because I am letting c grow large, I switch the focus to the $\mathrm{SIR}_{\mathrm{c}}$ which is defined as

$$\mathrm{SIR}_{\mathrm{c}} = \frac{h_0}{r_o^{\alpha_{\mathrm{m}}} \sum_{i \in \Phi_{\mathrm{c}}} d_i^{-\alpha_{\mathrm{m}}} h_i \kappa_i'}. \tag{3.34}$$

I only present a claim in this section as the scaling of the network with c appears intractable.

Claim 1. *Assume the number of antennas at each user N scales such that $N = tc$. Then the rate scales such that*

$$\frac{R_{\mathrm{c}}^{\Sigma}}{c\lambda_{\mathrm{p}}} = \Theta\left(\log_2(1 + t^{\frac{-\alpha_{\mathrm{m}}}{2}})\right) \tag{3.35}$$

as $c \to \infty$.

Proof. The claim is based on an numerical evaluation of Theorem 3.4.3. The numerical results are presented in Section 3.6. □

3.4.2.2 Coverage in Clustered mmWave Ad Hoc Networks

I consider two coverage metrics in the clustered case: *intra-cluster* coverage and *inter-cluster* coverage. I say users are covered if $\mathbb{P}[\mathrm{SINR} > \Gamma] \geq 1 - \epsilon$. This ensures that users can support a data rate $R = \log_2(1 + \Gamma)$ at least $(1 - \epsilon)\%$ of the time. I denote the intra and inter-cluster coverage by $\mathrm{P}_{\mathrm{a}}(\Gamma) = \mathbb{P}[\mathrm{SINR}_{\mathrm{a}} > \Gamma]$ and $\mathrm{P}_{\mathrm{e}}(\Gamma) = \mathbb{P}[\mathrm{SINR}_{\mathrm{e}} > \Gamma]$. The intra-cluster coverage is the coverage between a receiver and transmitter operating within the same cluster head. This is useful for peer-to-peer gaming applications or soldiers of the same squad sharing data. The inter-cluster coverage is the coverage between the cluster heads. This characterizes data propagation throughout the network; if clusters are isolated (e.g poor inter-cluster coverage), the data between squads will not propagate.

For inter-cluster communication, I define another SINR as

$$\mathrm{SINR_e} = \frac{P_t A_\mathrm{m} N^2 r_\mathrm{e}^{-\alpha_\mathrm{m}} h_o}{N_o^\mathrm{m} + \sum_{i \in \Phi_\mathrm{c}} P_t A_\mathrm{m} \ell(x_i - r_o) h_i \kappa_i}, \tag{3.36}$$

where r_e is the random distance to the nearest cluster center. For simplicity, I consider this point rather than a point randomly located in the cluster. The distribution of this random distance is $f_{r_\mathrm{e}}(r)$ given in [48, Corollary 10.1].

In this section, for clarity and brevity, I consider $N_h = 1$ as it simplifies the expressions. The previous work considered coverage and transmission rate of mmWave ad hoc networks for $N_h > 1$. To see a derivation with the added complexity, see [56]. I am interested in the balance between the inter and intra cluster coverage. To begin, I define the transmission rate of the intra-cluster communication to be

$$q(\epsilon, \Gamma) = \arg\max_{\lambda_\mathrm{p}} \text{ s.t. } \mathrm{P_a}(\Gamma) \geq 1 - \epsilon, \tag{3.37}$$

which is the largest cluster density while maintaining the intra-cluster coverage requirement. Because $\mathrm{P_a}(\Gamma)$ is a decreasing function with λ_p, it suffices to solve $\mathrm{P_a}(\Gamma) = 1 - \epsilon$ for λ_p. Given this cluster density, I can evaluate $\mathrm{P_e}(\Gamma)$. I define a metric to quantify this as the intra-ϵ inter-cluster coverage. Specifically, I define it as

$$P(\epsilon, \Gamma) = \mathbb{P}[\mathrm{SINR_e} > \Gamma | \lambda_\mathrm{p} = q(\epsilon, \Gamma)]. \tag{3.38}$$

This metric quantifies the probability that an inter-cluster link is covered while ensuring that each intra-cluster link is covered at least $(1 - \epsilon)\%$ of the time.

As the cluster density increases, r_{e} decreases, but the communication within the cluster must deal with more interference.

Corollary 3.4.5. *The intra-ϵ inter-cluster coverage of an outdoor clustered mmWave ad hoc network is*

$$P(\epsilon,\Gamma)=\int_{o}^{\infty} e^{-r_{\mathrm{e}}^{\alpha_{\mathrm{m}}}\theta\Gamma}\mathcal{L}_{\mathrm{a}}(r_{\mathrm{e}}^{\alpha_{\mathrm{m}}}\Gamma)\mathcal{L}_{\mathrm{e}}(r_{\mathrm{e}}^{\alpha_{\mathrm{m}}}\Gamma)f_{r_{\mathrm{e}}}(r)dr, \tag{3.39}$$

with θ, $\mathcal{L}_{\mathrm{a}}$, and $\mathcal{L}_{\mathrm{e}}$ defined as in Theorem 3.4.3 and the cluster density λ_{p} in $\mathcal{L}_{\mathrm{e}}$ equal to

$$q(\epsilon,\Gamma)=\frac{-\log\left(\frac{1-\epsilon}{\exp(-r_{o}^{\alpha_{\mathrm{m}}}\theta\Gamma)\mathcal{L}_{\mathrm{a}}(r_{o}^{\alpha_{\mathrm{m}}}\Gamma)}\right)}{2\pi W(r_{o}^{\alpha_{\mathrm{m}}}\Gamma)}, \tag{3.40}$$

with

$$W(r_{o}^{\alpha_{\mathrm{m}}}\Gamma)=\int_{o}^{\infty}\left(1-\left(g(r,r_{o}^{\alpha_{\mathrm{m}}}\Gamma)\right)^{c}\right)rp\left(r\right)dr. \tag{3.41}$$

Proof. The proof is presented in Appendix 3.8.4. □

Comment: I define Corollary 3.4.5 such that the SINR threshold is the same for intra-cluster and inter-cluster communication. Having a different SINR threshold would give different guaranteed rates for intra-cluster versus inter-cluster communication. This could cause data bottlenecks if the goal of the network was to allow data to propagate both within the cluster and between the clusters. While I consider the same rate requirements, Corollary 3.4.5 can be modified to allow for different rate requirements (e.g. $\Gamma_{\mathrm{a}},\Gamma_{\mathrm{e}}$).

3.5 Imperfect Beam Alignment

The beam alignment algorithm for a mmWave device will inevitably introduce error into the pointing of the mainlobe of the antenna beam [64, 70, 71]. As such, the misaligned beam will not achieve the maximum gain (e.g. N^2) as noted in Section 3.3. As the signal term of the the uniform and clustered network are the same, the results presented in this section apply for both the uniform and clustered networks.

In this section, I quantify the drop in the ergodic rate due to the misalignment. First, I introduce the error model. Second, I derive the loss in rate when sectored antennas are misaligned. Lastly, I comment on why the sectored model is lacking, introduce the Gaussian antenna model, and compute the loss in rate for Gaussian antennas.

I model the beam alignment error as $\epsilon \sim \mathcal{N}_T(0, \sigma^2)$ where $\mathcal{N}_T$ is the truncated Gaussian distribution and σ^2 is the variance of the error. As a baseline, these values are taken from the Cramer-Rao bound of common beam alignment algorithms [70, 71]. Because I consider an ad hoc network, each communicating link will have a misaligned beam. Due to the uncoordinated nature of the ad hoc network, I propose the following.

Lemma 3.5.1. *The statistics of the interference in an outdoor mmWave network are invariant to antenna beam misalignment.*

Proof. The desired pointing angle of an interferer's antenna is uniformly distributed from $[0, 2\pi]$ because the associated receiver is also distributed uni-

formly from $[0, 2\pi]$. Similarly, the pointing angle of the typical receiver is uniform over $[0, 2\pi]$. Because the pointing angles wrap around with any perturbation of the angle, the distribution will remain uniform over $[0, 2\pi]$. The resultant angle between the interferer and the typical receiver remains the product of two uniform random variables. □

3.5.1 Sectored Antenna

Because of the symmetry in the sectored antenna, I directly calculate the probability of the error changing the gain of the antenna. With the truncated error model, the probability that the antenna gain, $G^{\text{tx/rx}}$, remains in the mainlobe is the probability the absolute value of the error is less than the 3dB beamwidth, $\mathbb{P}[|\epsilon| \leq \theta_{3dB}]$. More precisely,

$$p_G(\sigma) = \int_{-\theta_{3dB}}^{\theta_{3dB}} f_{\mathcal{N}_T}(x)dx \tag{3.42}$$

$$= \frac{\text{Erf}\left(\theta_{3dB}/\sqrt{2\sigma^2}\right)}{\text{Erf}\left(\pi/\sqrt{2\sigma^2}\right)}, \tag{3.43}$$

where $f_{\mathcal{N}_T}(x)$ is the PDF of the truncated normal distribution and Erf is the error function. Essentially, each receiver/transmitter gain is now a discrete random variable described as

$$G^{\text{tx/rx}} = \begin{cases} N & \text{w.p. } p_G(\sigma) \\ \frac{1}{N} & \text{w.p. } 1 - p_G(\sigma) \end{cases}. \tag{3.44}$$

With this, I now define the resulting *system* gain (i.e. $G^{\text{tx}}G^{\text{rx}}$) as

$$G^{\text{tx}}G^{\text{rx}} = \begin{cases} N^2 & \text{w.p. } p_G(\sigma)^2 \\ 1 & \text{w.p. } 2p_G(\sigma)\left(1 - p_G(\sigma)\right) \\ \frac{1}{N} & \text{w.p. } \left(1 - p_G(\sigma)\right)^2 \end{cases}. \tag{3.45}$$

I now use this to quantify the loss in rate due to antenna misalignment with sectored antennas.

Lemma 3.5.2. *The loss in ergodic rate per user in a mmWave ad hoc network due to beam alignment error with sectored antennas is*

$$\Delta R = \log_2(N^2) 2 p_G(\sigma) \left(1 - p_G(\sigma)\right) + \log_2(N^4) \left(1 - p_G(\sigma)\right)^2 + \mathcal{O}\left(\frac{1}{\text{SINR}}\right). \tag{3.46}$$

Proof. The proof is presented in Appendix 3.8.5. □

The final step in Lemma 3.5.2 makes intuitive sense as there should be no loss in rate due to errors that keep the mainlobes aligned. I note that Lemma 3.5.2 gives the loss in rate *per user* because I have not accounted for the density of users. Simply multiply by λ_{u} to obtain the results in terms of $(b/s/Hz/m^2)$. While the loss in rate per user is invariant to user density by Lemma 3.5.2, the overall sum network rate is not. I will show in the results that the high SINR approximation is quite accurate for various system parameters.

3.5.2 Gaussian Antenna

Most prior stochastic geometry work with mmWaves considers a sectored antenna with an ideal gain pattern. I consider a second antenna model Gaussian [33, 68]. The sectored antenna is slightly unrealistic as real antenna patterns have roll-off; the Gaussian antenna model captures this effect while remaining tractable [33]. It is similar to the sectored model used in [56, 57, 68],

but with a smoother roll-off. It is defined as

$$G_i^{\text{tx/rx}} = \left(N - \frac{1}{N}\right) e^{-\eta\theta^2} + \frac{1}{N} \tag{3.47}$$

where G is the maximum gain which occurs as $\theta = 0$ and η is a parameter that controls the 3dB beamwidth. For example, to set η for a specific beamwidth

$$G_i^{\text{tx/rx}} = \left(N - \frac{1}{N}\right) e^{-\eta\theta_{3dB}^2} + \frac{1}{N} \tag{3.48}$$

$$\frac{1}{2}N = \left(N - \frac{1}{N}\right) e^{-\eta\theta_{3dB}^2} + \frac{1}{N} \tag{3.49}$$

$$\eta = \frac{\log\left(\frac{N-\frac{1}{N}}{1/2N-\frac{1}{N}}\right)}{\theta_{3dB}^2}. \tag{3.50}$$

If I consider the resulting *system* antenna gain

$$G^{\text{tx}}G^{\text{rx}} = \left(Ge^{-\eta\epsilon_{tx}^2} + g\right)\left(Ge^{-\eta\epsilon_{rx}^2} + g\right), \tag{3.51}$$

with the sidelobe gain g, I see that because of the error in alignment at both the receiver and transmitter the system gain will get some fractional portion of mainlobe gain due to the exponential term involving the error. I quantify this fractional portion as a random variable, ζ. I derive the CDF as

$$\mathbb{P}[\zeta \leq x] = \mathbb{P}[e^{-\eta\epsilon^2} \leq x] \tag{3.52}$$

$$= \mathbb{P}[-\eta\epsilon^2 \leq \log(x)] \tag{3.53}$$

$$= \mathbb{P}\left[\epsilon \geq \pm\sqrt{-\log(x)/\eta}\right] \tag{3.54}$$

$$= 1 - \frac{\text{Erf}\left(\sqrt{\frac{-\log(x)}{2\eta\sigma^2}}\right)}{\text{Erf}\left(\frac{\pi}{\sqrt{2\sigma^2}}\right)} \quad x \in [G_{\min}, 1], \tag{3.55}$$

where

$$G_{\min} = e^{-\eta\pi^2}. \tag{3.56}$$

The PDF of ζ is the derivative of (3.55)

$$f_\zeta(x) = \frac{x^{\frac{1}{2\eta\sigma^2}-1}}{\sigma \mathrm{Erf}\left(\frac{\pi}{\sqrt{2}\sigma}\right)\sqrt{-2\pi\eta\log(x)}} \quad x \in [G_{\min}, 1]. \tag{3.57}$$

The PDF in (3.57) captures the randomness at either the transmitter or receiver, but not both. I must define a new random variable $K = \zeta_{\mathrm{rx}}\zeta_{\mathrm{tx}}$ as the product of each end of the communication link. If I expand (3.51), there are extra terms that represent one end of the link completely misaligned and operating out of the sidelobe. In this work, however, I am interested in quantifying the effect of *relatively small* antenna alignment errors. I am interested in error regimes when the mainlobes are still mostly aligned. Because of this, I will ignore the sidelobe power such that $G^{\mathrm{rx}}G^{\mathrm{tx}} \approx Ne^{-\eta\epsilon_{\mathrm{rx}}^2}Ne^{-\eta\epsilon_{\mathrm{tx}}^2} = N^2K$. Because of this simplification the PDF of K and therefore the system gain computable. The product distribution of the antenna gain loss described in (3.57) yields the PDF of K as

$$f_K(z) = \int_{-\infty}^{\infty} f_{\zeta_{tx}}(x) f_{\zeta_{rx}}(z/x)\frac{1}{|x|}dx \tag{3.58}$$

$$= \int_z^1 \frac{x^{\frac{1}{2\eta\sigma^2}-1}}{\sigma\sqrt{-2\pi\eta\log(x)}}\frac{(z/x)^{\frac{1}{2\eta\sigma^2}-1}}{\sigma\sqrt{-2\pi\eta\log(z/x)}}\frac{1}{x}dx \tag{3.59}$$

$$= \frac{z^{\frac{1}{2\eta\sigma^2}-1}}{2\eta\sigma^2\mathrm{Erf}\left(\frac{\pi}{\sqrt{2}\sigma}\right)^2} \quad z \in [G_{\min}^2, 1], \tag{3.60}$$

where the bounds of integration go from z to 1 because z/x cannot be greater than 1 and $G_{\min}^2 = e^{-2\eta\pi^2}$. Note that (3.60) is for a symmetric network, e.g.

each handset has similar hardware and thus η and σ are the same for each. I have found that the product distribution to be intractable if $\eta_{\text{rx}} \neq \eta_{\text{tx}}$ and $\sigma_{\text{rx}} \neq \sigma_{\text{tx}}$. This assumption is reasonable for an ad hoc network or D2D network.

Using (3.60), I summarize the loss similarly as with the sectored antenna with the following Lemma.

Lemma 3.5.3. *The loss in ergodic rate per user in a mmWave ad hoc network due to beam alignment error with Gaussian antennas are approximated as*

$$\Delta R = \frac{4\eta\sigma^2 - 2e^{-\pi^2/\sigma^2}\left(2\eta\sigma^2 + 2\eta\pi^2\right)}{\text{Erf}\left(\frac{\pi}{\sqrt{2}\sigma}\right)^2 \log(4)} + \mathcal{O}\left(\frac{1}{\text{SINR}}\right). \tag{3.61}$$

Proof. I proceed as with Lemma 3.5.2. Let G_ϵ be the reduction in the gain from perfect antenna gain $G_p = N^2$. I begin with the final step of Lemma 3.5.2.

$$\Delta R \approx \mathbb{E}[\log_2(\frac{G_p}{G_\epsilon})] \tag{3.62}$$

$$\stackrel{a}{=} -\mathbb{E}[\log_2(K)] \tag{3.63}$$

$$= -\int_{G_{\min}^2}^{1} \log_2(z) f_K(z) dz \tag{3.64}$$

where (a) is due to the assumption that $G_\epsilon = N^2 K$. Evaluating the integral yields the result. □

Note that the second term in the numerator is due to the lower bound of the integral in (3.5.3) which is nearly zero for large ratios of π^2/σ^2; this also

means that $\text{Erf}\left(\frac{\pi}{\sqrt{2}\sigma}\right) \approx 1$. Thus, the loss in rate is mostly determined by $4\eta\sigma^2/\log(4)$.

Comment: These results are valid for both uniform and clustered networks as the error in beam misalignment only affects the signal term. As stated earlier, the signal terms for clustered and uniform networks are the same. The scaling results, however, are affected for a fixed σ. For a fixed misalignment error, the antenna array will eventually become impossible to align as the beamwidth shrinks. I plan to consider this tradeoff in future work.

3.6 Numerical Results

In this section, I compare the analytical results from the previous sections with numerical simulations. First, I analyze the general ergodic rate of a uniform mmWave ad hoc network with perfect beam alignment (e.g. Theorem 3.4.1). Second, I calculate the results for clustered ad hoc networks with both UCA and TDMA. I also show the trade-off between inter and intra cluster coverage. Then, I present the results for the scaling of both clustered and uniform ad hoc networks. Finally, I look at the impact of beam misalignment with sectored antennas and Gaussian antennas.

In Fig. 3.2, I plot the ergodic rate for an aligned uniform mmWave ad hoc network with $N = 10$. The user densities of the networks vary from $\lambda_{\text{u}} = 10^{-6}$ to 10^{-3} which correspond to an average of 1 to 1000 users per

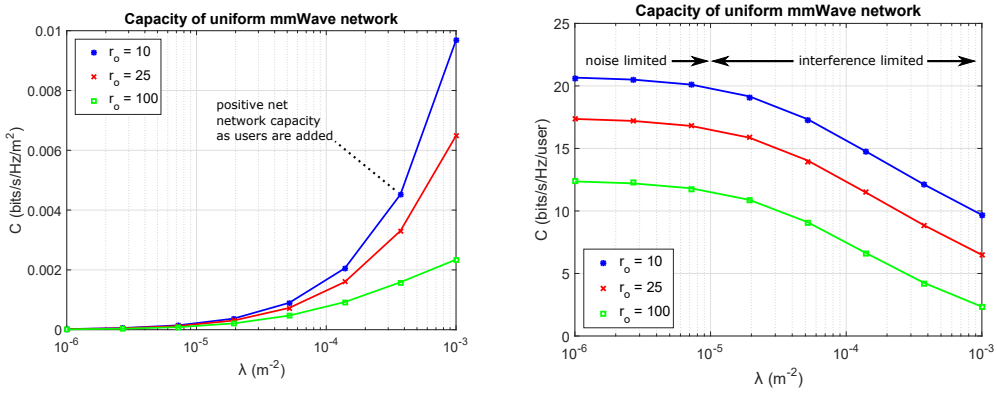

Figure 3.2: The solid line in each plot is obtained by evaluating Theorem 3.4.1 while the markers correspond to numerical simulation. The network-centric view is shown in (a) where the ergodic rate per unit area is shown. The per-user ergodic rate is shown in (b).

1km^2, respectively. The dipole communication length varies $r = 10, 25, 100m$. The noise power is set to -100dB (-70dBm). The path loss intercept is 60dB which matches the measurements from [12]. The path loss exponent is set to $\alpha_{\mathrm{m}} = 2.5$. The random Gamma power variable parameter is set to $N_h = 1$ as in [56]. The transmit power is normalized to 1. I plot the results in terms of both $(b/s/Hz/m^2)$ and $(b/s/Hz/\text{user})$. I see that Theorem 3.4.1 is an accurate representation of the ergodic rate as it matches the simulations. Intuitively, I see in Fig. 3.2b that the per user ergodic rate decreases as the density (and therefore interference) increases. The overall net network rate, however, is positive as shown in Fig. 3.2a by the positive slope of the curves; Theorem 3.4.1 provides a method to balance the needs the users versus the needs of the network. Lastly, in the previous work [57], I argue that mmWave networks are

still interference limited. The per-user ergodic rate in Fig. 3.2b shows that for network densities greater than 10^{-5} the communication links are very much interference limited as the rate drops significantly per user.

In Fig. 3.3, I show the results of Theorem 3.4.3 compared with simulation. For the simulation, the building model of [48] is used to generate the building blockage. This includes correlation between the points and eliminates the LOS cluster requirement. An underlying building density of $\lambda_{\mathrm{b}} = 9.3\times10^{-5}$ is used with a expected width and length of the buildings as $\mathbb{E}[L] = 64$ and $\mathbb{E}[W] = 70$. This yields $\beta = 0.008$. I consider two cluster sizes and two communication distances over a range of cluster densities. I set $\alpha_{\mathrm{m}} = 2.5$, $N_o^{\mathrm{m}} = -100\mathrm{dB}$, $A_{\mathrm{m}} = -60\mathrm{dB}$, and $N = 10$. Fig. 3.3 shows that, for large communication distances, the size of the cluster leaves a constant performance gap with the larger cluster performing better as the probability that the interfering transmitters are far away increases. For short communication distances, the small cluster size severely limits the performance even at low cluster densities.

Fig. 3.4 shows the comparison of TDMA with UCA using numerical simulation and the analytic expressions from Section 3.4.2. The parameters are the same in Fig. 3.3, but with the cluster size fixed at $R_c = 25$ and $r_o = 10$ and varying numbers of antennas. For $N = 1$, I see that TDMA is the best choice for total cluster rate as the directional antennas do not attenuate any of the intra-cluster interference at low cluster density or inter-cluster interference at high cluster densities. With only three antennas, however, simply having

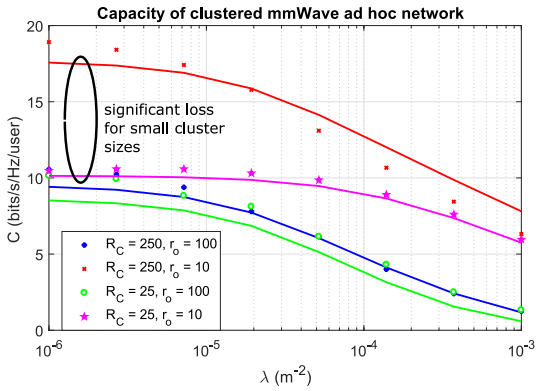

Figure 3.3: A verification plot of Theorem 3.4.3 that shows a match between the analytical expressions and simulation. The solid curves are the analytical expressions while the markers are simulation results. The cluster size is given by R_c, and the communication distance is r_o.

uncoordinated communication in the cluster is optimal for many cluster densities. At high cluster densities, by restricting the transmission to one user per cluster, TDMA gives a larger per cluster rate. I can see the same trend for $N = 6$, but the transition is an even higher cluster density.

Fig. 3.5 shows the evaluation of (3.39) with $N = 10$ and various cluster sizes and intra-cluster communication distances. I see that for small cluster sizes of $R_c = 25$ the inter-cluster coverage is invariant to the intra-cluster communication distance. The optimal cluster density for the intra-cluster communication to maintain the SINR_a requirement with small cluster sizes does not vary with the communication distance. If the cluster size is $R_c = 250$, the transmitters are spread out more which allows a higher cluster density which improves the inter-cluster coverage. If the communication link is longer, I see that the inter-cluster coverage goes to zero for high SINR_a requirements.

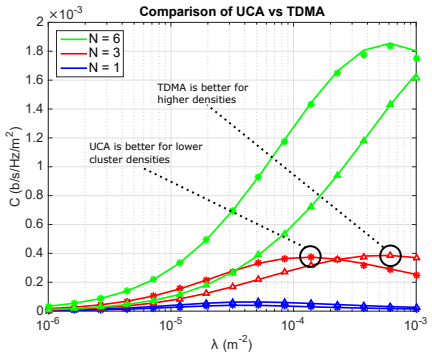

Figure 3.4: A comparison of uncoordinated channel access (UCA) with TDMA in a mmWave clustered network. The triangle marker corresponds to TDMA simulation while the star marker is UCA simulation. The solid curves are the analytical expressions from Theorem 3.4.3 and Corollary 3.4.4.

In Fig. 3.6a, I plot the ergodic rate of a uniform mmWave ad hoc network over a wide range of user densities and PLEs. The rate is evaluated according to Theorem 3.4.1. For each user density, I scale the number of antennas according to the rules developed in Theorem 3.4.2. The plot shows that the scaling trends developed are precise. For the $\alpha_{\mathrm{m}} = \{2.1, 3, 4\}$, I see a constant rate achieved for the solid lines as λ_{u} grows large when $N = \sqrt{\lambda_{\mathrm{u}}}$. Conversely, when the scaling is $N < \sqrt{\lambda_{\mathrm{u}}}$, I see the rate go to zero asymptotically which means that the signal gain and interference reduction of the additional antennas *does not* preserve the SINR of the network. Eventually the receiver is overwhelmed by interference. Lastly, for small λ_{u} and N, Fig. 3.6a shows that scaling $N^{\frac{4}{\alpha_{\mathrm{m}}}+1} = \lambda_{\mathrm{u}}$ gives a constant rate for small N and λ_{u}. As users are added from $\lambda_{\mathrm{u}} = 10^{-5}$, the ergodic rate remains constant until $\lambda_{\mathrm{u}} = 10^{0}$ for $\alpha_{\mathrm{m}} = 3$ and $\lambda_{\mathrm{u}} = 10^{-2}$ for $\alpha_{\mathrm{m}} = 2.5$. If the number of users and

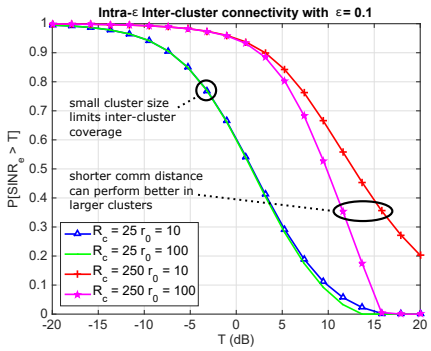

Figure 3.5: A plot showing the intra-ϵ inter-cluster coverage. The curves are generated by evaluating (3.39).

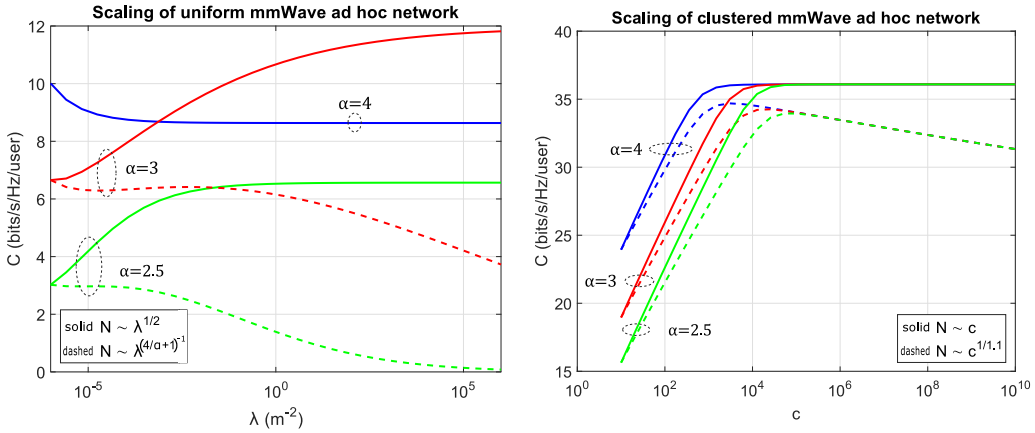

(a) (b)

Figure 3.6: In (a), rate scaling of a uniform mmWave ad hoc network where the rate is evaluated from Theorem 3.4.1 and the number of antennas scale according to Theorem 3.4.2. In (b), I evaluate Theorem 3.4.3 based on the scaling proposed by Proposition 1. The colors correspond to the PLEs used $\alpha_{\mathrm{m}} \in \{2.1, 3, 4\}$ as green, red, and blue, respectively.

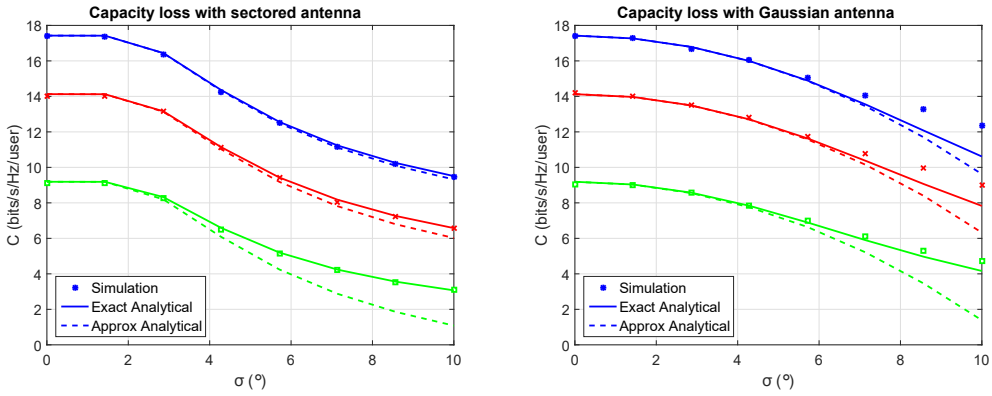

(a) (b)

Figure 3.7: The impact of antenna alignment depends on the antenna model used; (a) is a sectored antenna and (b) is a Gaussian antenna. The blue curve corresponds to $r_o = 10m$, the red curve corresponds to $r_o = 25m$, and the green curve corresponds to $r_o = 100m$. The analytical approximation curve uses Lemmas 3.5.2 and 3.5.3 while the exact analytical curve evaluates the expectation of Theorem 3.4.1 against the antenna error.

antennas is small, N can scale *slower* than $\sqrt{\lambda_u}$. In Fig. 3.6b, the number of antennas scales with the cluster user density c. The asymptotic result is obtained when N grows very large. At this N, the interference κ' is always $1/N^4$ because with so many antennas the main lobe beamwidth is extremely small. Even with this extreme interference reduction, the number of antennas must still scale linearly which is much faster than in the case of the uniform network.

In Fig. 3.7, I show the differences between Lemma 3.5.2 and Lemma 3.5.3 (both plots are on the same scale). For both plots in Fig. 3.7, $N = 10$ and I vary the communication distance. The user density is $\lambda_u = 10^{-5}$. In Fig. 3.7a, I see that for $\sigma = 4$ and $r_o = 100m$ the sectored antenna model

yields a rate of 7 $b/s/Hz$/user, but the Gaussian antenna indicates a rate of 8 $b/s/Hz$/user. This is a disagreement of roughly 15%. I see that the high SINR approximation is valid for small antenna errors or for small r_o. The results for the Gaussian antenna are less accurate for higher σ because I ignore the sidelobes as well for the Gaussian case when considering K. Both antenna results indicate that rate losses of 50% when $\sigma = 10$.

3.7 Conclusions

In this chapter, I presented a means to balance the ergodic rate requirements of the users with the efficiency needs of the overall network. Using tools from stochastic geometry, I derived exact expressions for the ergodic rate of clustered mmWave ad hoc network for uncoordinated channel access and TDMA. The results indicated that because mmWave utilizes directional beamforming uncoordinated channel access can be used to provide net cluster rate gains over TDMA as opposed to lower frequency communication. If the cluster density is large enough, however, the reduced interference from TDMA allowed for higher cluster rate. I introduced and developed the notion of *intra-ϵ inter-cluster* coverage. The results indicate that, for small cluster sizes, the clusters remain covered if the required data rate is small. Using the Theorems, I established scaling trends of both uniform and clustered mmWave ad hoc networks. The results showed that antenna arrays of uniform networks can scale sub-linearly while clustered network arrays must scale linearly as the user density increases. I characterized the performance loss of beam steering

misalignment using two different, popular antenna models. I showed that performance loss varies as much as 15% depending on the antenna model and system parameters. Further, I showed that antenna misalignment reduces ergodic rate *per user* by 45% if the error standard deviation is similar to the 3dB beamwidth of the array; in general, the loss in capacity is proportional to error variance σ^2 of beamforming.

3.8 Appendix

3.8.1 Proof of Theorem 3.4.1

I leverage Lemma 3.3.1 to expand the $\mathrm{SINR_u}$ term (3.7) in the rate equation (3.8). First, I note that $\mathbb{E}[e^{-zX}]$ from Lemma 3.3.1 corresponds the moment-generating function of the signal term; the random element of the signal is the Gamma random fading. Similarly, $\mathbb{E}[e^{-zY}]$ is the Laplace transform of the interference field generated by the PPP. To begin,

$$\mathcal{L}_{\mathrm{p}}(z) = \mathbb{E}\left[e^{-zI_{\mathrm{p}}}\right] \tag{3.65}$$

$$\overset{(a)}{=} \mathbb{E}\left[e^{-z\sum_n I_{\mathrm{p}}^n}\right] \tag{3.66}$$

$$= \prod_n \mathbb{E}\left[e^{-zI_{\mathrm{p}}^n}\right] \tag{3.67}$$

$$\overset{(b)}{=} \prod_n \mathbb{E}\left[\prod_{i\in\Phi}\left(1+\frac{z\ell\left(x_i-r_o\right)\kappa_n'}{N_h}\right)^{-N_h}\right] \tag{3.68}$$

$$\overset{(c)}{=} \prod_n \mathbb{E}\left[\prod_{i\in\Phi}\left(1+\frac{z\ell\left(x_i\right)\kappa_n'}{N_h}\right)^{-N_h}\right] \tag{3.69}$$

$$\overset{(d)}{=} \prod_n \exp\left(-p_n\lambda_{\mathrm{u}}\int_0^\infty\left[1-\left(1+\frac{z\ell\left(x\right)\kappa_n'}{N_h}\right)^{-N_h}\right]p(x)dx\right), \tag{3.70}$$

where (a) is due to the interference decomposition according to κ, (b) is from the evaluation of the moment generation function of the fading, (c) is because of the homogeneous nature PPP, and (d) due to the generation functional of the PPP. The intensity of each decomposed interference is $p_n\lambda_{\mathrm{u}}$. Converting the product to a sum and noting that the PPP is isotropic yields the result. $\square$

3.8.2 Proof of Theorem 3.4.2

I use Lemma 3.3.2 to derive upper and lower bounds on the rate exploiting the structure of the $\mathrm{SIR_p}$. To show that $R \geq \log_2(1+t^{\frac{-\alpha_{\mathrm{m}}}{2}})$, I begin noting that the rate decreases with N_h as the fading becomes more random because the mutual information between the receiver and transmitter decreases. I continue with $N_h = 1$ (e.g. Rayleigh fading) and Lemma 3.3.2 for the signal fading. I have

$$\begin{aligned}
R &\geq \mathbb{E}_{I_{\mathrm{m}}}\left[\log_2\left(1+\frac{e^{\mathbb{E}[\log h_0]}}{r_o^{\alpha_{\mathrm{m}}} I_{\mathrm{m}}}\right)\right] \\
&= \mathbb{E}_{I_{\mathrm{m}}}\left[\log_2\left(1+\frac{e^{-\gamma}}{r_o^{\alpha_{\mathrm{m}}} I_{\mathrm{m}}}\right)\right] \\
&= \frac{1}{\log(2)}\int_0^\infty \frac{1-e^{-\gamma z}}{z} e^{-z^{\frac{2}{\alpha_{\mathrm{m}}}}\pi\lambda_{\mathrm{u}} r_o^2 \frac{\sum_n p_n(\kappa_n')^{\frac{2}{\alpha_{\mathrm{m}}}}}{\mathrm{sinc}(2/\alpha_{\mathrm{m}})}} dz \\
&\overset{(a)}{\geq} \frac{2}{\alpha_{\mathrm{m}}}\log_2\left(1+\frac{\left(\mathrm{sinc}(\frac{2}{\alpha_{\mathrm{m}}})\right)^{\frac{\alpha_{\mathrm{m}}}{2}}}{\left(\pi r_o^2\lambda_{\mathrm{u}}\sum_n p_n\left(\kappa_n'\right)^{\frac{2}{\alpha_{\mathrm{m}}}}\right)^{\frac{\alpha_{\mathrm{m}}}{2}}}\right),
\end{aligned}$$

where $\gamma \approx 0.577$ is the Euler constant, (a) comes from the substitution $u = z^{\frac{2}{\alpha_{\mathrm{m}}}}\pi\lambda_{\mathrm{u}} R_d^2 \frac{\sum_n p_n(\kappa_n')^{\frac{2}{\alpha_{\mathrm{m}}}}}{\mathrm{sinc}(2/\alpha_{\mathrm{m}})}$ and (the fact that $e^{-u} \geq \frac{2}{\alpha_{\mathrm{m}}} e^{-u^{\frac{\alpha_{\mathrm{m}}}{2}}}$ for $\alpha_{\mathrm{m}} > 2$ [17]. The final step is simply a reversal of Lemma 3.3.1 without the expectation. I give

bounds on $\sum_n p_n(\kappa'_n)^{\frac{2}{\alpha_{\mathrm{m}}}}$. Using the values from (3.5), I have

$$\begin{aligned}\psi(N) &= \sum_n p_n(\kappa'_n)^{\frac{2}{\alpha_{\mathrm{m}}}} \\ &= \frac{\delta}{N^2} + 2\left(1-\frac{\delta}{N}\right)\frac{\delta}{N}\left(\frac{1}{N^2}\right)^{\frac{2}{\alpha_{\mathrm{m}}}} + \left(1-\frac{\delta}{N}\right)^2\left(\frac{1}{N^4}\right)^{\frac{2}{\alpha_{\mathrm{m}}}}.\end{aligned}$$

After expanding and combining terms, it can be seen that

$$\psi(N) = \frac{1}{N^2} + \frac{1}{N^{\frac{8}{\alpha_{\mathrm{m}}}}} + \mathcal{O}(N^{-\frac{4}{\alpha_{\mathrm{m}}}-1}).$$

Thus, for $\alpha_{\mathrm{m}} \in (2,4]$, the antenna factor term is dominated by N^{-2} as $N \to \infty$.

Next, for the upper bound, I note by a similar argument that R_{u} is bounded above by the rate of the network with no fading (e.g. $N_h = \infty$). Additionally, I can bound the rate from above by only considering the closest interferer from the sub-PPP with the highest gain (e.g. $\kappa = N^2$, $\kappa' = 1$). I have

$$\begin{aligned}R_{\mathrm{u}} &\leq \log_2\left(1+\ell(r_o)\mathbb{E}\left[\frac{1}{\min_{i\in\Phi}\{\ell(x_i-r_o)\}\kappa'_i}\right]\right) \\ &\overset{(a)}{=} \log_2\left(1+\ell(r_o)\mathbb{E}\left[\frac{r_{\mathrm{nn}}^{\alpha_{\mathrm{m}}}}{\kappa'}\right]\right) \\ &\overset{(b)}{=} \log_2\left(1+\ell(r_o)\int_0^\infty \frac{r_{\mathrm{nn}}^{\alpha_{\mathrm{m}}}}{\kappa'_m} 2\pi p_m \lambda_{\mathrm{u}} r_{\mathrm{nn}} e^{-\pi p_m \lambda_{\mathrm{u}} r_{\mathrm{nn}}^2} dr_{\mathrm{nn}}\right) \\ &\overset{(c)}{=} \log_2\left(1+\ell(r_o)\frac{\Gamma(1+\frac{\alpha_{\mathrm{m}}}{2})}{(\lambda_{\mathrm{u}}p_m)^{\frac{\alpha_{\mathrm{m}}}{2}}\kappa'_m}\right) \\ &= \log_2\left(1+\ell(r_o)\frac{\Gamma(1+\frac{\alpha_{\mathrm{m}}}{2})}{\left(\lambda_{\mathrm{u}}\frac{\delta^2}{N^2}\right)^{\frac{\alpha_{\mathrm{m}}}{2}}}\right)\end{aligned}$$

where (a) is due to the nearest-neighbor (closest interferer) r_{nn} of the sub-PPP, κ'_m is the max gain of the system, and p_m is its corresponding probability, (b)-(c) is the evaluation of the expectation over the nearest-neighbor distribution.

Combining the upper and lower bounds and noting that $N^{-2} \leq \psi(N) \leq MN^{-2}$ for $\alpha_{\mathrm{m}} \in (2,4]$, I arrive at the final bounds as

$$\log_2\left(1+\frac{a}{t^{\frac{\alpha_{\mathrm{m}}}{2}}}\right) \leq R_{\mathrm{u}} \leq \log_2\left(1+\frac{b}{t^{\frac{\alpha_{\mathrm{m}}}{2}}}\right). \quad \square$$

3.8.3 Proof of Theorem 3.4.3

The first term of (3.26) is a direct application of Lemma 3.3.1. The second term is obtained after taking the MGF of the signal fading. The Laplace transform of the intra-cluster interference is given as

$$\begin{aligned}
\mathcal{L}_{\mathrm{a}}(z) &= \mathbb{E}\left[e^{-zI_{\mathrm{a}}}\right] && (3.71)\\
&= \mathbb{E}\left[e^{-z\sum_{i\in N^o}\ell(x_i-r_o)h_i\kappa_i'}\right] && (3.72)\\
&\overset{(a)}{=} \mathbb{E}\left[\prod_{i\in N^o}\left(1+\frac{z\ell(x_i-r_o)\kappa_i'}{N_h}\right)^{-N_h}\right] && (3.73)\\
&\overset{(b)}{=} \left(\mathbb{E}\left[\left(1+\frac{z\ell(x-r_o)\kappa_i'}{N_h}\right)^{-N_h}\right]\right)^{c-1} && (3.74)\\
&= \left(\sum_n p_n \mathbb{E}_x\left[\left(1+\frac{z\ell(x_i-r_o)\kappa_i'}{N_h}\right)^{-N_h}\right]\right)^{c-1} && (3.75)\\
&\overset{(c)}{=} \left(\sum_n \frac{p_n}{\pi R_c^2}\int_{\mathcal{B}(0,R_c)}\left(1+\frac{z\ell(x_i-r_o)\kappa_i'}{N_h}\right)^{-N_h} dx\right)^{c-1}, && (3.76)
\end{aligned}$$

where (a) is the MGF of an exponential random variable, (b) is due to independence and the $c-1$ other transmitters in the cluster, and (c) is a substitution due to (3.17).

The Laplace transform of the inter-cluster interference is given as

$$\mathcal{L}_{\mathrm{e}}(z) = \mathbb{E}\left[e^{-zI_{\mathrm{e}}}\right] \tag{3.77}$$

$$= \mathbb{E}\left[e^{-z\sum_{i\in\Phi_{\mathrm{c}}}\ell(x_i-r_o)h_i\kappa_i'}\right] \tag{3.78}$$

$$= \mathbb{E}\left[\prod_{i\in\Phi_{\mathrm{c}}}\left(1+\frac{z\ell(x_i-r_o)\kappa_i'}{N_h}\right)^{-N_h}\right] \tag{3.79}$$

$$= \mathbb{E}\left[\prod_{y\in\Phi_{\mathrm{p}}}\prod_{x\in N^y}\left(1+\frac{z\ell(y-x-r_o)\kappa'}{N_h}\right)^{-N_h}\right] \tag{3.80}$$

$$= \mathbb{E}_{\Phi_{\mathrm{p}}}\left[\prod_{y\in\Phi_{\mathrm{p}}}\mathbb{E}_{N^y}\left[\prod_{x\in N^y}\left(1+\frac{z\ell(y-x-r_o)\kappa'}{N_h}\right)^{-N_h}\right]\right] \tag{3.81}$$

$$\overset{(a)}{=} \mathcal{G}\left(\left(1+\frac{z\ell(y-x-r_o)\kappa'}{N_h}\right)^{-N_h}\right) \tag{3.82}$$

$$\overset{(b)}{=} \exp\left(-\lambda_{\mathrm{p}}\int_{\mathbb{R}^2}\left(1-g\left(y,z\right)^c\right)p\left(y\right)dy\right) \tag{3.83}$$

$$\overset{(c)}{=} \exp\left(-2\pi\lambda_{\mathrm{p}}\int_o^\infty\left(1-g\left(r,z\right)^c\right)rp\left(r\right)dr\right), \tag{3.84}$$

where (a) is due to (3.17) and the definition of a generating functional for a point process, (b) is due to (3.15) and the stationarity of the inter-cluster interference with respect to r_o, and (c) due to the isometric properties of the inter-cluster interference. □

3.8.4 Proof of Corollary 3.4.5

First, I must evaluate the transmission rate of intra-cluster communication. I compute $\mathrm{P_a}(\Gamma)$ in the standard way by re-arranging the $\mathrm{SINR_a}$ to

exploit the exponential fading such that

$$\mathbb{P}\left[\mathrm{SINR_a} > \Gamma\right] = \mathbb{P}\left[h_o > \left(r_o^{\alpha_\mathrm{m}}\theta + r_o^{\alpha_\mathrm{m}} I\right)\Gamma\right] \tag{3.85}$$

$$= \mathbb{E}\left[\exp\left(-r_o^{\alpha_\mathrm{m}}\theta\Gamma - r_o^{\alpha_\mathrm{m}} I\Gamma\right)\right] \tag{3.86}$$

$$= e^{-r_o^{\alpha_\mathrm{m}}\theta\Gamma}\mathbb{E}\left[\exp\left(-r_o^{\alpha_\mathrm{m}}\Gamma(I_\mathrm{a} + I_\mathrm{e})\right)\right] \tag{3.87}$$

$$= e^{-r_o^{\alpha_\mathrm{m}}\theta\Gamma}\mathcal{L}_\mathrm{a}(r_o^{\alpha_\mathrm{m}}\Gamma)\mathcal{L}_\mathrm{e}(r_o^{\alpha_\mathrm{m}}\Gamma), \tag{3.88}$$

where θ is defined as in Theorem 3.4.3 and the Laplace functionals of the interference as given in (3.28) and (3.29). Because λ_p only appears in $\mathcal{L}_\mathrm{e}$ outside the integration, I can invert (3.88) to obtain the transmission rate as

$$q(\epsilon, \Gamma) = \frac{-\log\left(\frac{1-\epsilon}{\exp(-r_o^{\alpha_\mathrm{m}}\theta\Gamma)\mathcal{L}_\mathrm{a}(r_o^{\alpha_\mathrm{m}}\Gamma)}\right)}{2\pi W(r_o^{\alpha_\mathrm{m}}\Gamma)}. \tag{3.89}$$

To evaluate $\mathrm{P_e}(\Gamma)$, I note that it is equivalent to to $\mathrm{P_a}(\Gamma)$, but r_o is replaced with r_e and must be integrated over $f_{r_\mathrm{e}}(r)$. □

3.8.5 Proof of Lemma 3.5.2

Let G_ϵ be the variable error-induced gain (e.g. (3.45)) as opposed to the perfect antenna gain $G_p = N^2$ and SINR^G be the SINR without the signal antenna gain. Further, let the ergodic rate of the network be

$$R = \mathbb{E}[\log_2(1 + G_p\mathrm{SINR}^G)], \tag{3.90}$$

and therefore the reduction in rate of the network is

$$\Delta R = \mathbb{E}[\log_2(1 + G_p \mathrm{SINR}^G)] - \mathbb{E}[\log_2(1 + G_\epsilon \mathrm{SINR}^G)] \tag{3.91}$$

$$= \mathbb{E}[\log_2(1 + G_p \mathrm{SINR}^G) - \log_2(1 + G_\epsilon \mathrm{SINR}^G)] \tag{3.92}$$

$$= \mathbb{E}\left[\log_2(G_p) + \mathcal{O}\left(\frac{1}{\mathrm{SINR}^G}\right) - \log_2(G_\epsilon) - \mathcal{O}\left(\frac{1}{\mathrm{SINR}^G}\right)\right] \tag{3.93}$$

$$= \mathbb{E}\left[\log_2\left(\frac{G_p}{G_\epsilon}\right) + \mathcal{O}\left(\frac{1}{\mathrm{SINR}^G}\right)\right]. \tag{3.94}$$

Isolating the signal antenna gain is due to Lemma 3.5.1. I use (3.45) to evaluate the expectation and note that $\log_2(N^2/N^2) = 0$. □

Chapter 4

Beam Training in Random mmWave Ad Hoc Networks

In the previous two chapters, I assumed that the communication link had been established. The transmitter and receiver were assumed to achieving the full gain from the antenna arrays. In this chapter, I focus on the overhead and effort required to align the antenna arrays. I evaluate the latency and user-perceived rate after accounting for the overhead of beam sweeping and mobility in the channel. Without a time constraint, exhaustive search provides the best beamforming pair at the receiver and transmitter. Due to latency concerns for the user, overhead in protocol design, and channel conditions changing, this approach cannot be used unless searching is done quickly. It is unclear if or when exhaustive beam sweeping is optimal or even tolerable with respect to latency and overhead for mmWave ad hoc networks.

4.1 Introduction

Beam sweeping and training for mmWave ad hoc networks was studied in [72–76]. A distributed algorithm is used to match users to access points for optimal beam training and beamwidth in [72]; an optimal beamwidth in an

interference free environment is shown to exist that balances throughput with training overhead. In [73], low-frequency 2.4GHz wireless LAN (WLAN) carries the control and coordination for synchronization of 60GHz WLAN. The results in [73] show that handshaking between neighbors by up to 55%, but the low-frequency band is not used for accelerating beam training. WLAN positioning techniques in the 5GHz band were used in [74] to aid the beamforming process for 60GHz WLANs; a similar out-of-band positioning technique is studied in [75] where the low-frequency information is used to get coarse alignment with the potential of fine beam alignment using in-band measurements. Both [74, 75] did not consider interference in the signal model as well as relying on the out-of-band measurements. Multi-user methods with hybrid architecture were studied in [76] to reduce the overhead of beam training as the number of users grows. The system model of [76] did not include interference, relies on a more complex hybrid architecture, and requires user diversity for full benefit.

The changes of angle-of-arrival (AoA) and angle-of-departure (AoD) due to channel variations are a large obstacle for mmWave communication for mobile environments. Beam tracking typically relates to tracking the small movements on a per OFDM symbol basis. I am concerned with beam failure events (i.e. require a complete beam re-alignment). Beam tracking was considered in [77, 78]. In [77], a hybrid architecture is used to collect information from multiple directions that is given to a probabilistic optimization model which accelerates the beam training and corrects alignment errors. Without

interference, the beam acquisition time is reduced by 50%, but it also required the hybrid architecture using 16 transmit and 6 receiver chains in the evaluation. The results of [78] require a continuous variation in the angles after beam sweeping to track properly; if the AoA or AoD suddenly changes due to mobility, the method does not support that. The impact of mmWave channel variation was studied in [79] for vehicular environments. The authors derive expressions for the beam coherence time, which showed that the antenna array beamwidth greatly affected the doppler spread of the fading signals. If the beams were too narrow, the rays cannot be tracked and the coherence time was small, but some directivity helps limit the doppler which aided the beam tracking is within the transmission block.

Beam alignment for mmWave networks within the cellular context was studied in [25, 26]. In a cellular system, the user may connect to the strongest base station, but in ad hoc networks, however, interference with neighboring users is possible. The user may not be able to connect to the closest user. In [25], (near)-orthogonal pilots provide synchronization and broadcast access to a mmWave cellular network. The orthogonality of the pilots allowed the base station and users to tolerate intra-cell interference and avoid collisions; in an uncoordinated ad hoc network, all users may not be beam sweeping at the same time making the use of pilots ineffective. Four beam sweeping methods for synchronization were studied in [26] with stochastic geometry, but the user assumed to connect to the strongest transmitter which is not necessarily the case with ad hoc networks. In [80], a context-aware method using side infor-

mation database is used to aid in mmWave cell discovery which illustrates the additional information provides substantial gains to mmWave cellular training time, but the dynamic nature of ad hoc networks makes database upkeep an additional overhead. The authors of [81] argue that out-of-band assistance (e.g. < 6GHz) was indispensable for quick mmWave cellular beam alignment; a method using the current LTE specifications was shown provide enough direction information in the low-frequency band to lower the beam sweeping time in the mmWave band, but the analysis assumed the other cellular base stations do not affect the training process.

4.2 Contributions

In this chapter, I characterize the overhead cost of beam alignment in terms of latency and rate reduction. I use stochastic geometry to model the user pair locations, the antenna array as a sectored antenna array, and line-of-sight (LOS) ball blockage model. I derive analytic expressions and bounds to be derived for the data transmission delay and the user perceived rate. The main contributions of the chapter are summarized as follows:

- Computation of the relative strength of the interfering users in a mmWave ad hoc network. The results show that despite the decreasing probability of a mainlobe collision between a user and interferer as the antenna array grows, the interferers with colliding mainlobes remain the dominant and thus the limiting source of an interference-limited scenario. In LOS and non-line-of-sight (NLOS) scenarios, mainlobe collisions are stronger by

a factor that is proportional to the array size given a sectored antenna model. I present results that show the increase in synchronization time due to a blockage event at the transmitter as well as a complete blockage event at the receiver. I show that blockage events at the transmitter are essentially nonrecoverable due to the degradation of signal power for fast training techniques while blockage events at the receiver may allow successful communication.

- Derivation of the expected data transmission delay of three different beamforming strategies as a function of transmission probability and antenna array size. I show that using omni-directional reception is optimal for mmWave ad hoc networks if the transmission probability is sufficiently low or if the antenna array size and training length is sufficiently large. In particular, I give expressions for the optimal transmission probability for minimizing the delay as well as well as the region where omni-directional reception is optimal.

- Characterization of the user-perceived ergodic rate when using each of the synchronization methods. Our results indicate that the optimal transmission probability for ergodic rate is typically larger than the optimal point for delay within a fixed transmission block; a similar conclusion holds for the array size. In the high mobility case where overhead is most costly, if the underlying user density is too high, the users must back off the channel too frequently for successful training to complete and data transmission to begin.

The rest of the chapter is organized as follows. Section 4.3 provides the system model and assumptions used in the chapter. Section 4.4.2 describes the data transmission delay and presents the analytic results. Section 4.4.3 develops the ergodic rate and the effect of overhead. I present the numerical results in Section 4.5 and conclude the chapter in Section 4.6. There are several appendices at the end of the chapter which provide detailed proofs.

4.3 System Model

In this section, I describe the uniform network model used to model the positions of the transmitters. I define the received signal model and enumerate the long and short term fading assumptions. I describe the proposed super-frame structure used to provide synchronization and training. Finally, I provide some mathematical preliminaries from prior work, to make the chapter self-contained. A summary of the key variables is given in Table 4.1.

4.3.1 Network Model

I build the transmitter and receiver location model from the standard homogeneous Poisson point process (PPP) [3, 21, 55]. I denote the collection of transmitter locations on $\mathbb{R}^2$ formed by the PPP Φ as the *uniform* network. I assume a slotted ALOHA style medium access control (MAC) with transmission probability ζ. I denote the intensity of Φ as $\lambda = \zeta\lambda_{\mathrm{u}}$ where λ_{u} is the intensity of all potential transmitters. The transmission probability ζ is an important parameter to tune the interference strength, as discussed further in

$\tau_{\text{syn+tr}}$	expected data transmission delay
β_y^x	delay ratio between x and y
R	ergodic rate
Φ	homogeneous Poisson point process (PPP)
λ_{u}	intensity of the PPP
ζ	ALOHA transmission probability
r_o	desired communication communication distance
R_{los}	LOS ball radius
SINR	SINR with PPP
Γ	SINR threshold for successful comm
$p(x)$	blockage probability function
α_{m}	path-loss exponent
A_{m}	path-loss intercept
N_o^{m}	noise power
N	number of antennas
$\mathcal{L}(z)$	Laplace functional of point process
$P_{\text{syn+tr}}$	probability of synch+training phase success
κ_{syn},κ_{tr}	antenna gain during synchronization or training phase
ρ	antenna gain probability
γ	mainlobe gain correction factor
η	ratio of mainlobe to sidelobe interference
T	slot time
T_{tot}	transmission interval time
S_{syn}, S_{tr}, S_{data}	number of synchronization, training or data slots

Table 4.1: System variables for Chapter 4

Section 4.3.4.2. Each transmitter has a receiver located at a fixed distance r_o away with the orientation with respect to the transmitter distributed uniformly in $[0, 2\pi]$ [21]; these receiver points are not part of Φ.

4.3.2 Received Signal Model

The received signal y_o of transmitted symbol x_o at the desired user pair is affected by the channel $\mathbf{H}$, the precoding vectors $\mathbf{f}$, the combining vectors $\mathbf{w}$, each interfering symbol x_i, and noise n

$$y_o = \mathbf{w}_o^* \mathbf{H}_o \mathbf{f}_o x_o + \sum_{i \in \Phi} \mathbf{w}_i^* \mathbf{H}_i \mathbf{f}_i x_i + n. \tag{4.1}$$

I assume $x_o, x_i \sim \mathcal{N}(0, P_o), \mathcal{N}(0, P_i)$ and $n \sim \mathcal{N}(0, N_o^{\mathrm{m}})$. I use the subscript o to indicate the signal of interest at the origin and i to indicate the interfering signal from user i. I model the channel as in prior work in mmWave by using the single-path model [9]. The path represents the LOS path or reflective surfaces in the physical world such as buildings or automobiles for a NLOS path. The effective channel $\mathbf{H}$ between a receiver and transmitter communicating at distance r is a composite value based on the large-scale path-loss $\ell(r)$, small-scale fading h, the antenna array response $\mathbf{a}(\theta)$ at the angle-of-arrival (AoA) θ, and the antenna response $\mathbf{a}(\phi)$ at the angle-of-departure (AoD) ϕ. The vector signal model for a single reflector is

$$\mathbf{H} = \sqrt{\ell(r) h} \mathbf{a}(\theta) \mathbf{a}^*(\phi). \tag{4.2}$$

I detail each term in the following paragraphs.

The optimal precoding and combining strategy for a single path without interference is to beamform towards the AoA and AoD. I assume the transmitter applies a precoding vector $\mathbf{f}$ so that $|\mathbf{a}^*(\phi)\mathbf{f}|^2 = G^{\text{tx}}(\phi)$; the receiver applies a combining vector $\mathbf{w}$ so that $|\mathbf{w}^*\mathbf{a}(\theta)|^2 = G^{\text{rx}}(\theta)$. Mobility in the network, however, causes the AoA or AOD of the path to change [82]. The beamforming solution is only valid for a finite amount of time. It is crucial, therefore, to avoid over training in high mobility environments.

I simplify the antenna response by using the sectored antenna model [25]. The sectored model reduces the antenna gain to either a mainlobe or sidelobe gain. The resultant gain for an array with N antennas at either the receiver or transmitter is

$$G^{\text{tx/rx}}(\theta,\phi) = \begin{cases} G_{\text{ml}}^{\text{tx/rx}} = \frac{2\pi}{\theta_{\text{ant}}}\frac{\gamma}{1+\gamma} & \theta,\phi \in [-\frac{\theta_{\text{ant}}}{2}, \frac{\theta_{\text{ant}}}{2}] \\ G_{\text{sl}}^{\text{tx/rx}} = \frac{2\pi}{2\pi-\theta_{\text{ant}}}\frac{1}{1+\gamma} & \text{otherwise} \end{cases}, \tag{4.3}$$

where θ_{ant} is the mainlobe beamwidth which is $\theta_{\text{ant}} = \frac{2\pi}{N}$. The mainlobe/sidelobe correction factor γ is representative of the front-to-back ratio of the antenna array which is the ratio between the maximum gain and the gain 180° from the maximum. I denote the gain of the mainlobe and sidelobe by $G_{\text{ml}}^{\text{tx/rx}}/G_{\text{sl}}^{\text{tx/rx}}$. The correction factor γ is computed so that the total energy transmitted by the array is always unity $G_{\text{ml}}^{\text{tx/rx}}\frac{\theta_{\text{ant}}}{2\pi} + G_{\text{sl}}^{\text{tx/rx}}\frac{2\pi-\theta_{\text{ant}}}{2\pi} = 1$, with $\gamma = \frac{2\pi}{C_0(2\pi-\theta_{\text{ant}})}$ for some constant C_0 [25]. Typical front-to-back ratios for arrays are on the order of the array size e.g. $\gamma \sim N$ [83]. I use the equivalence of $\gamma = N$ in our results to simplify the expressions.

At the same time, independently, the other users in the network are

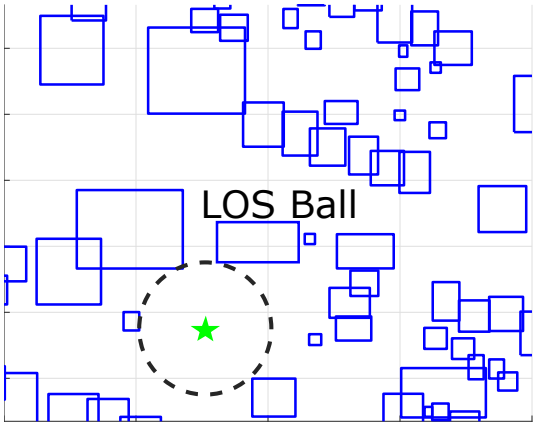

Figure 4.1: An example realization of the the PPP network with building blockages. The LOS ball model is a first-order approixmation that only considers the average LOS distance. This simplifies the blockage probability function $p(r)$ compared to other models, such as the exponential model [1]. All users inside the ball are considered LOS while all users outside the ball is considered NLOS.

transmitting in random directions. The resultant *system* gain $G^{\text{rx}}(\theta)G^{\text{tx}}(\phi)$ of the interfering signals is modeled as a discrete random variable

$$\kappa = \begin{cases} G^{\text{tx}}_{\text{ml}} G^{\text{rx}}_{\text{ml}} & \text{w.p. } \rho_{\text{ml,ml}} = \rho\left(G^{\text{tx}}_{\text{ml}}\right)\rho\left(G^{\text{rx}}_{\text{ml}}\right) \\ G^{\text{tx}}_{\text{ml}} G^{\text{rx}}_{\text{sl}} & \text{w.p. } \rho_{\text{ml,sl}} = \rho\left(G^{\text{tx}}_{\text{ml}}\right)\rho\left(G^{\text{rx}}_{\text{sl}}\right) \\ G^{\text{tx}}_{\text{sl}} G^{\text{rx}}_{\text{ml}} & \text{w.p. } \rho_{\text{sl,ml}} = \rho\left(G^{\text{tx}}_{\text{sl}}\right)\rho\left(G^{\text{rx}}_{\text{ml}}\right) \\ G^{\text{tx}}_{\text{sl}} G^{\text{rx}}_{\text{sl}} & \text{w.p. } \rho_{\text{sl,sl}} = \rho\left(G^{\text{tx}}_{\text{sl}}\right)\rho\left(G^{\text{rx}}_{\text{sl}}\right) \end{cases} \tag{4.4}$$

where $\rho(\cdot)$ is the probability of the transmit or receive beam pattern occurring. For example, $\rho\left(G^{\text{tx}}_{\text{sl}}\right)$ is the probability that the interfering transmitter sidelobe is pointed towards the receiver; likewise, $\rho\left(G^{\text{rx}}_{\text{sl}}\right)$ is the probability the receiver sidelobe is pointed towards an interfering transmitter. The sidelobe probabilities are calculated from the mainlobe probabilities $\rho\left(G^{\text{tx/rx}}_{\text{sl}}\right) = 1 - \rho\left(G^{\text{tx/rx}}_{\text{ml}}\right)$.

The short term effects are representative of typical fast fading effects

[34]. I assume a narrowband channel model where the fast fading channel coefficient h is a random variable. Wideband channels are converted to such narrowband models via multicarrier techniques such as OFDM. The long term channel effects are due to phenomena like building reflections or blockage that change the path-loss. I use the standard unbounded path-loss model

$$\ell(r) = \frac{A_{\mathrm{m}}}{r^{\alpha_{\mathrm{m}}}} \tag{4.5}$$

where α_{m} is the path-loss exponent (PLE) and A_{m} is the path-loss intercept. The path-loss intercept represents the power loss in the first meter of transmission. This model is valid for far-field communication and if the interference is greater than $1m$ away; in the case an interfering user is within $1m$, I do not account for the near-field for tractability as is common in other stochastic geometry work [1, 25, 26]. Measurements show a lower PLE for line-of-sight (LOS) versus non-line-of-sight (NLOS) signals [34]. Both the desired signal and the interference signals are either LOS or NLOS. This discrepancy is largely caused by building blockage. The difference between the signals is quantified by the distance dependent path-loss function $p(r)$ which gives the probability that a user at distance r is LOS. I use the LOS ball blockage model where all users within a distance R_{los} are considered LOS while all users outside that distance are considered NLOS; as a result, $p(r) = \mathbb{1}_{\{r \leq R_{\mathrm{los}}\}}$. The LOS distance R_{los} is chosen based on the average LOS view for a specific geographic location or area. From the exponential random shape model [38, 48], R_{los} is calculated so the average number of LOS transmitters remains the same between the

models. In [38], the calculated values for Chicago and Manhattan are $87.13m$ and $90.42m$, for example.

Simplifying the received signal model yields

$$y_o = \sqrt{A_{\mathrm{m}} r_o^{-\alpha_{\mathrm{m}}} h_o \kappa_o} x_o + \sum_{i \in \Phi} \sqrt{A_{\mathrm{m}} d_i^{-\alpha_{\mathrm{m}}} h_i \kappa_i} x_i + n \tag{4.6}$$

The received signal to interference ratio (SINR) is the source of the metrics used throughout the chapter. The transmit power $P_o(P_i)$ is equal between all users. The noise power of the receiver is N_o^{m}. The random distance between the receiver of interest and each interfering user is d_i. The SINR of the received signal is

$$\mathrm{SINR} = \frac{P_o A_{\mathrm{m}} \kappa_o h_o r_o^{-\alpha_{\mathrm{m}}}}{N_o^{\mathrm{m}} + \sum_{\Phi} P_i A_{\mathrm{m}} \kappa_i h_i d^{-\alpha_{\mathrm{m}}}}. \tag{4.7}$$

The SINR changes on a slot by slot basis each transmission because of the new snapshot of transmitters and different short term fading.

4.3.3 Transmission Interval Access Method

I assume the transmissions follow the time-slotted method shown in Fig. 4.2. For simplicity, the network uses a fixed transmit time T sec for each transmission opportunity. Each user transmits during a transmission slot with probability ζ. Each transmission slot is a small chunk of data such as an OFDM symbol. I assume that overhead within these symbols, e.g. cyclic prefix, is included in T. I note that recent proposals to 5G standards have included using the cyclic prefix to account for beam switching time as well; therefore,

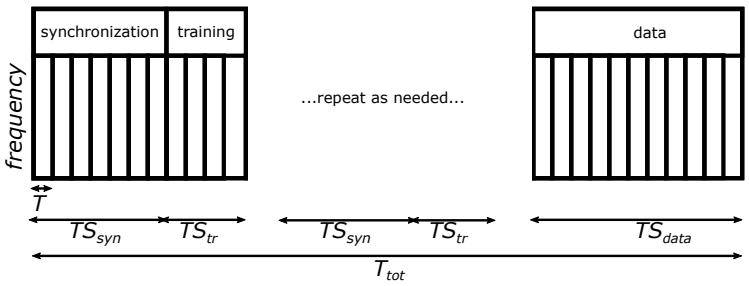

Figure 4.2: The time-slotted design of the proposed system. A slot is T sec long. There are S_{syn} slots for synchronization, S_{tr} slots for training, and S_{data} slots for data. The training block may be repeated if needed. The total time per transmission interval is T_{tot} sec.

sweeping over the beams on a per OFDM symbol is feasible [84]. I denote the number of transmission slots for synchronization, training, and data as S_{syn}, S_{tr}, and S_{data}. The total time a user spends synchronizing and training is then $\frac{T\cdot(S_{\text{syn}}+S_{\text{tr}})}{\zeta}$ sec. The whole transmission block is the *transmission interval* which includes the *synchronization*, *training*, and *data* slots and lasts for T_{tot} sec. Because of the network conditions, I allow for the possibility to have multiple synchronization and training blocks per transmission interval. The number of these blocks plays an important role in the latency. The system is considered to be invariant to small-scale fading over the T sec transmission slot. Additionally, the network is assumed to invariant to large-scale fading effects (e.g AoA / AoD / blockage) for T_{tot} sec. If ζ is sufficiently small, it is possible for $\frac{T\cdot(S_{\text{syn}}+S_{\text{tr}})}{\zeta} > T_{\text{tot}}$ because of the random access in the channel. In this situation, no data communication occurs.

The mobility of the users in the network is captured by the value of T_{tot} which is the time that the long-term channel effects are valid. The mobility of

the network includes pedestrians walking or vehicular movement, but mobility also includes effects such as local handset movement (i.e, moving a handset from one ear to another or removing a phone from a pocket). These local effects will change the AoA and AoD. There are proposals to use inertial measurement units (IMUs) in smartphones to track these changes, but the efficacy of these approaches is unknown in real systems [77]. I assume that the small local changes are tracked by the receiver, but a new beamforming solution must be computed every T_{tot} sec.

I use three synchronization and training methods: *baseline*, *fast-training*, and *fast-synch-ronization and training*. These methods were studied in [26] for a cellular environment. The methods are variations on the beamsweeping algorithms from standards such as 802.11ad [67]. During each transmission slot of synchronization and training, the user pair sweeps possible beam combinations. I consider the *correct* beam combination when the mainlobes of each user are aligned with total gain $G^{\text{tx}}G^{\text{rx}} = \left(N\frac{\gamma}{1+\gamma}\right)^2$. For all methods, during the synchronization phase, one user (e.g. the primary) transmits the beacon-like frames while the other user (e.g. the secondary) listens; during the training phase, the secondary user sends feedback over one or many beams while the primary user listens. Because there is a single path in the channel, there is a unique best sector where $G^{\text{tx}} = N\frac{\gamma}{1+\gamma}$ and $G^{\text{rx}} = N\frac{\gamma}{1+\gamma}$. In [26], the best trade-off between initial delay and end user throughput for a cellular system is to have a coarse synchronization phase while refining the beam pattern in the training phase. Table 4.2 provides a summary of the beamforming

methods used in the chapter.

In the baseline method, during the synchronization phase, each user in the dipole pair sweeps over its beam patterns which takes $S_{\text{syn}} = N^2$ slots with antenna gain $\kappa_{\text{syn}} = \left(N\frac{\gamma}{1+\gamma}\right)^2$; during the training phase, the primary user sweeps over its beams again while the secondary user transmits using the best beam from the synchronization phase; this takes $S_{\text{tr}} = N$ slots with antenna gain $\kappa_{\text{tr}} = \left(N\frac{\gamma}{1+\gamma}\right)^2$.

In the fast-training method, during the synchronization phase, each user in the dipole pair sweeps over its beam patterns which takes $S_{\text{syn}} = N^2$ slots with antenna gain $\kappa_{\text{syn}} = \left(N\frac{\gamma}{1+\gamma}\right)^2$. During the training phase, the primary user listens omni-directionally while the other user fixes its beam on the best result from the synchronization phase; this takes $S_{\text{tr}} = 1$ slot with antenna gain $\kappa_{\text{tr}} = N\frac{\gamma}{1+\gamma}$.

In the fast-synchronization and training method, during the synchronization phase, the primary user sweeps over its beam patterns while the secondary user listens omni-directionally which takes $S_{\text{syn}} = N$ slots with antenna gain $\kappa_{\text{syn}} = N\frac{\gamma}{1+\gamma}$. During the training phase, the roles are swapped; this takes another $S_{\text{tr}} = N$ slots with antenna gain $\kappa_{\text{tr}} = N\frac{\gamma}{1+\gamma}$.

4.3.4 Technical Preliminaries

In this section, I summarize the main result on success probability of mmWave ad hoc networks from prior work [56]. I define the mainlobe/sidelobe interference ratio which gives the relative strength of the interference in the

Method	**Synchronization Phase Values**	**Training Phase Values**
Baseline	$G_{\text{ml}}^{\text{tx}} = N\frac{\gamma}{1+\gamma}$, $G_{\text{ml}}^{\text{rx}} = N\frac{\gamma}{1+\gamma}$, $\rho\left(G_{\text{ml}}^{\text{tx}}\right) = \frac{1}{N}$, $\rho\left(G_{\text{ml}}^{\text{rx}}\right) = \frac{1}{N}$, $S_{\text{syn}} = N^2$	$G_{\text{ml}}^{\text{tx}} = N\frac{\gamma}{1+\gamma}$, $G_{\text{ml}}^{\text{rx}} = N\frac{\gamma}{1+\gamma}$, $\rho\left(G_{\text{ml}}^{\text{tx}}\right) = \frac{1}{N}$, $\rho\left(G_{\text{ml}}^{\text{rx}}\right) = \frac{1}{N}$, $S_{\text{tr}} = N$
Fast Training	$G_{\text{ml}}^{\text{tx}} = N\frac{\gamma}{1+\gamma}$, $G_{\text{ml}}^{\text{rx}} = N\frac{\gamma}{1+\gamma}$, $\rho\left(G_{\text{ml}}^{\text{tx}}\right) = \frac{1}{N}$, $\rho\left(G_{\text{ml}}^{\text{rx}}\right) = \frac{1}{N}$, $S_{\text{syn}} = N^2$	$G_{\text{ml}}^{\text{tx}} = N\frac{\gamma}{1+\gamma}$, $G_{\text{ml}}^{\text{rx}} = 1$, $\rho\left(G_{\text{ml}}^{\text{tx}}\right) = \frac{1}{N}$, $\rho\left(G_{\text{ml}}^{\text{rx}}\right) = 1$, $S_{\text{tr}} = 1$
Fast synchronization & Training	$G_{\text{ml}}^{\text{tx}} = N\frac{\gamma}{1+\gamma}$, $G_{\text{ml}}^{\text{rx}} = 1$, $\rho\left(G_{\text{ml}}^{\text{tx}}\right) = \frac{1}{N}$, $\rho\left(G_{\text{ml}}^{\text{rx}}\right) = 1$, $S_{\text{syn}} = N$	$G_{\text{ml}}^{\text{tx}} = N\frac{\gamma}{1+\gamma}$, $G_{\text{ml}}^{\text{rx}} = 1$, $\rho\left(G_{\text{ml}}^{\text{tx}}\right) = \frac{1}{N}$, $\rho\left(G_{\text{ml}}^{\text{rx}}\right) = 1$, $S_{\text{tr}} = N$

Table 4.2: Values of slot usages and gain during a transmission interval.

main and side lobes. I also define user blockage scenarios using the LOS ball model to add tractability to transmitter and receiver blockage events.

4.3.4.1 Probability of Success

The probability of success of a packet transmission is

$$P(\Gamma) = \mathbb{P}[\text{SINR} > \Gamma], \tag{4.8}$$

where Γ is the decoding threshold based on the modulation and coding rate of the packet. Our previous work [56, 85–87] considered the probability of success in various network configurations during data transmission. The generic results for the success probability are

$$P(\Gamma) = \underbrace{e^{-\frac{r_o^{\alpha_{\text{m}}}\Gamma}{\kappa_o}\frac{N_o^{\text{m}}}{P_o A_{\text{m}}}}}_{\text{signal}} \underbrace{\mathcal{L}_\Phi(z)}_{\text{interference}}, \tag{4.9}$$

where $\mathcal{L}_\Phi(z)$ is the Laplace functional of the interference. The specific evaluation of $\mathcal{L}_\Phi(z)$ depends on the network assumptions.

In the case of a uniform PPP network described in Section II.A, $\mathcal{L}_\Phi(z) = \mathcal{L}_{\rm p}(z)$ with

$$\mathcal{L}_{\rm p}(z) = \exp\left(-2\pi\zeta\lambda_{\rm u}\sum_i \rho_i \int_0^\infty \left[1-\left(1+\frac{z\kappa_i}{x^{\alpha_{\rm m}}}\right)^{-1}\right] p(x)xdx\right), \qquad (4.10)$$

and $i \in \{({\rm ml},{\rm ml}),({\rm ml},{\rm sl}),({\rm sl},{\rm ml}),({\rm sl},{\rm sl})\}$ is the possible gain of the interfering links according to (4.4). For compactness of the notation, I denote the integral of the interference within the Laplace function as

$$\Theta = 2\pi\lambda_{\rm u}\sum_i \rho_i \int_0^\infty \left[1-\left(1+\frac{z\kappa_i}{x^{\alpha_{\rm m}}}\right)^{-1}\right] p(x)xdx. \qquad (4.11)$$

I also write the desired signal term from the exponential in (4.9) as

$$\Omega = \frac{r_o^{\alpha_{\rm m}}\Gamma}{\kappa_o}\frac{N_o^{\rm m}}{P_o A_{\rm m}}. \qquad (4.12)$$

The probability of success in the uniform network is then compactly written as

$$P\left(\Gamma\right) = e^{-\Omega-\zeta\Theta}. \qquad (4.13)$$

Throughout the chapter, I compare the different access methods or the different stages of access. To do so, I use the notation Ω_y^x and Θ_y^x to represent the signal or interference of y stage of x method. For example, $\Omega_{\rm syn}^{\rm base}$ is the signal term of the base method during the synchronization phase (i.e. $\kappa_o = \kappa_{\rm syn}$).

In our previous work, the integral within the Laplace functional is left to numeric integration when evaluated. For the LOS ball blockage model, the

integral within the Laplace functional simplifies to a semi-closed form for the LOS interference with

$$\int_0^\infty \left[1-\left(1+\frac{z\kappa}{x^{\alpha_\mathrm{m}}}\right)^{-1}\right] p(x)xdx = \int_0^\infty \left[1-\left(1+\frac{z\kappa}{x^{\alpha_\mathrm{m}}}\right)^{-1}\right] \mathbb{1}_{\{x\leq R_\mathrm{los}\}}xdx \tag{4.14}$$

$$= \int_0^{R_\mathrm{los}} \left[1-\left(1+\frac{z\kappa}{x^{\alpha_\mathrm{m}}}\right)^{-1}\right] xdx \tag{4.15}$$

$$= {}_2F_1\left(1, \frac{2}{\alpha_\mathrm{m}}, \frac{2+\alpha_\mathrm{m}}{\alpha_\mathrm{m}}, -\frac{-R_\mathrm{los}^{\alpha_\mathrm{m}}}{z\kappa}\right), \tag{4.16}$$

where ${}_2F_1(\cdot)$ is the Gauss hypergeometric function. While (4.16) does not evaluate to simpler functions for arbitrary PLEs, if $\alpha_\mathrm{m}=2$ which is a common value for LOS communication, I simplify (4.16) when $\alpha_\mathrm{m}\to 2$ which leads to the following Theorem.

Theorem 4.3.1. *The interference integral under the LOS ball model for LOS interference is*

$$\Theta = 2\pi\lambda_\mathrm{u}\sum_i \rho_i \frac{z\kappa_i}{2}\log\left(1+\frac{R_\mathrm{los}^2}{z\kappa_i}\right) + \mathcal{O}\left(\alpha_\mathrm{m}-2\right) \tag{4.17}$$

while the interference integral under the LOS ball model for NLOS interference is

$$\Theta = 2\pi\lambda_\mathrm{u}\sum_i \rho_i \frac{\sqrt{z\kappa_i}}{2}\mathrm{atan}\left(\frac{\sqrt{z\kappa_i}}{R_\mathrm{los}^2}\right) + \mathcal{O}\left(\alpha_\mathrm{m}-4\right). \tag{4.18}$$

Proof. I begin with

$${}_2F_1\left(1, \frac{2}{\alpha_\mathrm{m}}, \frac{2+\alpha_\mathrm{m}}{\alpha_\mathrm{m}}, -\frac{-R_\mathrm{los}^{\alpha_\mathrm{m}}}{z\kappa}\right) = \frac{z\kappa}{2}\log\left(1+\frac{R_\mathrm{los}^2}{z\kappa}\right) + \mathcal{O}\left(\alpha_\mathrm{m}-2\right) \tag{4.19}$$

$$\leq \frac{z\kappa}{2}\log\left(1+\frac{R_\mathrm{los}^2}{z\kappa}\right). \tag{4.20}$$

In other stochastic geometry work, it is typical to restrict the PLE to $\alpha_{\mathrm{m}} > 2$. This is not needed in our system model because of the LOS ball blockage model. The restriction of $\alpha_{\mathrm{m}} > 2$ prevents the situation of infinite interference as the integration bounds tend towards infinity. With the LOS ball model, the integral in (4.20) is finite because it only goes to R_{los}.

The NLOS interference (i.e. users with $||x|| > R_{\mathrm{los}}$) is similarly simplified when $\alpha_{\mathrm{m}} \to 4$ which is a common parameter for NLOS mmWave communication. The NLOS interference in the LOS ball model is

$$\int_0^\infty \left[1 - \left(1 + \frac{z\kappa}{x^{\alpha_{\mathrm{m}}}}\right)^{-1}\right] p(x) x dx = \int_0^\infty \left[1 - \left(1 + \frac{z\kappa}{x^{\alpha_{\mathrm{m}}}}\right)^{-1}\right] \mathbb{1}_{\{x > R_{\mathrm{los}}\}} x dx \tag{4.21}$$

$$= \int_R^\infty \left[1 - \left(1 + \frac{z\kappa}{x^{\alpha_{\mathrm{m}}}}\right)^{-1}\right] x dx \tag{4.22}$$

$$= z\kappa R^{2-\alpha_{\mathrm{m}}} \frac{{}_2F_1\left(1, \frac{\alpha_{\mathrm{m}}-2}{\alpha_{\mathrm{m}}}, 2 - \frac{2}{\alpha_{\mathrm{m}}}, -z\kappa R_{\mathrm{los}}^{-\alpha_{\mathrm{m}}}\right)}{\alpha_{\mathrm{m}} - 2} \tag{4.23}$$

$$= \frac{\sqrt{z\kappa}}{2} \mathrm{atan}\left(\frac{\sqrt{z\kappa}}{R_{\mathrm{los}}^2}\right) + \mathcal{O}\left(\alpha_{\mathrm{m}} - 4\right). \tag{4.24}$$

Equation (4.24) is either an overestimate or underestimate, depending on the specific NLOS PLE. If $\alpha_{\mathrm{m}} \geq 4$ which is typical, (4.24) is an upper bound on the interference strength. □

4.3.4.2 Mainlobe-sidelobe Ratio

The interference in the network model implicitly assumes that there are four classes of interfering users: (1) those with mainlobes directed towards the receiver's mainlobe, (2) those with mainlobes directed towards the receiver's

sidelobe, (3) those with sidelobes directed towards the receiver's mainlobe, and (4) those with sidelobes directed towards the receiver's sidelobe. For our analysis and simplicity, because I assume each user has the same number of antennas, there are three classes of interfering users (2) and (3) mainlobe sidelobe combination at the receiver and transmitter results in the same gain. If I focus on the Laplace functional of (4.10), the summation over i represents the contribution from each interfering user class. The relative degradation of each user class to the overall success of communication is quantified. I define a metric, independent of user density, called the mainlobe-sidelobe ratio

$$\eta = \frac{p_{\mathrm{ml,ml}} \int_0^\infty \left[1 - \left(1 + \frac{z\kappa_{\mathrm{ml,ml}}}{x^{\alpha_{\mathrm{m}}}}\right)^{-1}\right] p(x) x dx}{\sum_{i \neq_{\mathrm{ml,ml}}} p_i \int_0^\infty \left[1 - \left(1 + \frac{z\kappa_i}{x^{\alpha_{\mathrm{m}}}}\right)^{-1}\right] p(x) x dx}. \tag{4.25}$$

Using the (4.20), the relative interference between class 1 and class 4 interfering users is

$$\eta = \frac{p_{\mathrm{ml,ml}} \kappa_{\mathrm{ml,ml}} \log\left(1 + \frac{R_{\mathrm{los}}^2}{r_o^{\alpha_{\mathrm{m}}} \kappa_{\mathrm{ml,ml}}}\right)}{p_{\mathrm{sl,sl}} \kappa_{\mathrm{sl,sl}} \log\left(1 + \frac{R_{\mathrm{los}}^2}{r_o^{\alpha_{\mathrm{m}}} \kappa_{\mathrm{sl,sl}}}\right)} \tag{4.26}$$

$$= \frac{\left(\frac{1}{N}\right)^2 \left(N \frac{\gamma}{1+\gamma}\right)^2 \log\left(1 + \frac{R_{\mathrm{los}}^2}{r_o^{\alpha_{\mathrm{m}}} \left(N \frac{\gamma}{1+\gamma}\right)^2}\right)}{\left(1 - \frac{1}{N}\right)^2 \left(\frac{N}{N-1} \frac{1}{1+\gamma}\right)^2 \log\left(1 + \frac{R_{\mathrm{los}}^2}{r_o^{\alpha_{\mathrm{m}}} \left(\frac{N}{N-1} \frac{1}{1+\gamma}\right)^2}\right)} \tag{4.27}$$

$$= \frac{N^2 \log\left(1 + \frac{R_{\mathrm{los}}^2}{r_o^{\alpha_{\mathrm{m}}}}\right)}{\log\left(1 + \frac{R_{\mathrm{los}}^2 N^2 (N-1)^2}{r_o^{\alpha_{\mathrm{m}}}}\right)}, \tag{4.28}$$

where I leverage the equivalence of the front-to-back ratio $\gamma = N$. Whereas

the relative interference between class 1 and class 2/3 interfering users is

$$\eta = \frac{p_{\mathrm{ml,ml}}\kappa_{\mathrm{ml,ml}} \log\left(1 + \frac{R_{\mathrm{los}}^2}{r_o^{\alpha_{\mathrm{m}}}\kappa_{\mathrm{ml,ml}}}\right)}{2p_{\mathrm{ml,sl}}\kappa_{\mathrm{ml,sl}} \log\left(1 + \frac{R_{\mathrm{los}}^2}{r_o^{\alpha_{\mathrm{m}}}\kappa_{\mathrm{ml,sl}}}\right)} \tag{4.29}$$

$$= \frac{\left(\frac{1}{N}\right)^2 \left(N\frac{\gamma}{1+\gamma}\right)^2 \log\left(1 + \frac{R_{\mathrm{los}}^2}{r_o^{\alpha_{\mathrm{m}}}\left(N\frac{\gamma}{1+\gamma}\right)^2}\right)}{2\left(1-\frac{1}{N}\right)\left(\frac{1}{N}\right)\left(\frac{N}{N-1}\frac{1}{1+\gamma}\right)\left(N\frac{\gamma}{1+\gamma}\right)\log\left(1 + \frac{R_{\mathrm{los}}^2}{r_o^{\alpha_{\mathrm{m}}}\left(\frac{N}{N-1}\frac{1}{1+\gamma}\right)\left(N\frac{\gamma}{1+\gamma}\right)}\right)} \tag{4.30}$$

$$= \frac{N\log\left(1 + \frac{R_{\mathrm{los}}^2}{r_o^{\alpha_{\mathrm{m}}}}\right)}{2\log\left(1 + \frac{R_{\mathrm{los}}^2 N(N-1)}{r_o^{\alpha_{\mathrm{m}}}}\right)}. \tag{4.31}$$

With $\gamma = N$, (4.28) and (4.31) show that even with the decreasing the probability of the mainlobes aligning, the interference caused by class 1 users remains the dominant factor for all antenna configurations. The logarithm in the denominator does grow faster than the logarithm in the numerator in both (4.28) and (4.31) but the pre-log term dominates. Using similar logic, the same relationship between the interference is shown in the NLOS case.

Comment: Class 1 interfering users are the primary limiting interference source. Because of this, any access method should attempt to remedy this source of degradation. It can be checked with Campbell's Theorem that the expected power of the LOS interference is invariant to the antenna array size; this is due to the unity total radiated power constraint on the antenna array. The utility of the antenna array is a bit of sleight-of-hand; the gain from the antenna array is the boost to the signal strength. Ironically, as the array size grows, the proportion of interference coming from class 1 interference grows. The issue of class 1 interference is an extreme case of the hidden

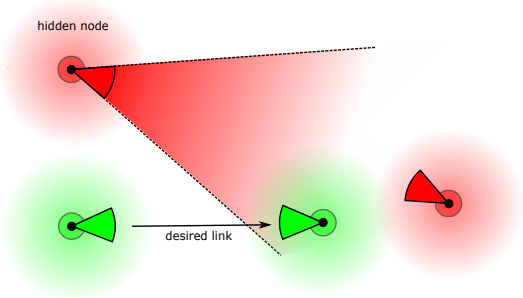

Figure 4.3: An example illustration of the hidden node issue with a class 1 interfering user.

node problem with carrier sense protocols such as 802.11. Fig. 4.3 shows an example of issue. The transmitter of interest is outside the mainlobe of the class 1 interfering user. Because of this, no carrier sense will be reliable as the interference is hidden to the transmitter as the SINR at the receiver will be degraded by the interference. I use ζ to reduce the interference which is not as robust as analyzing a collision avoidance method like RTS-CTS frames but remains tractable.

4.3.4.3 Network Scenarios

I consider three network situations shown in Fig. 4.4. The first scenario in Fig. 4.4a consists of a LOS signal path, but also strong LOS interference nearby. In this case, $r_o < R_{\text{los}}$. This is the primary scenario I consider in this chapter. The second scenario in Fig. 4.4b consists of strong LOS interference, but the signal path is greater than the LOS distance so the desired signal is NLOS. In this situation, I show that establishing communication is difficult, even with large antenna arrays. In this case, $r_o > R_{\text{los}}$. The third scenario in

Fig. 4.4c consists of nearly all NLOS signals. In this scenario, the blockage is large so LOS signals (both desired and interference) are unlikely. In this case, $r_o >> R_{\text{los}}$ and $R_{\text{los}} \to 0$.

4.4 Quantifying Overhead

In this section, I define the data transmission delay metric and compute closed-form solutions for PPP networks with PLEs of $\alpha_{\text{m}} = 2$ and $\alpha_{\text{m}} = 4$. I calculate the ratio between the baseline method and the fast-synchronization method when encountering a blockage event. I derive a formula for the minimum delay with respect to the number of antennas and user density. I conclude the section by computing the user-perceived ergodic rate which is affected by the data transmission delay and user density. Because I am interested in evaluating the sequential success or failure of packet transmissions, the correlation between each access must be considered.

4.4.1 Independence Between Attempts

Typically in stochastic geometry analysis, the location of the users in the PPP is averaged out. As shown in [88, 89], the correlation between transmissions may cause a large difference in the results. In [89], the data transmission delay for cellular users may be infinite under certain conditions for static users. Because some users will be stuck on cell edges, the training time for those users is infinite. This issue is remedied partially by the channel access parameter ζ because the cell edge effect disappears when a base-station is

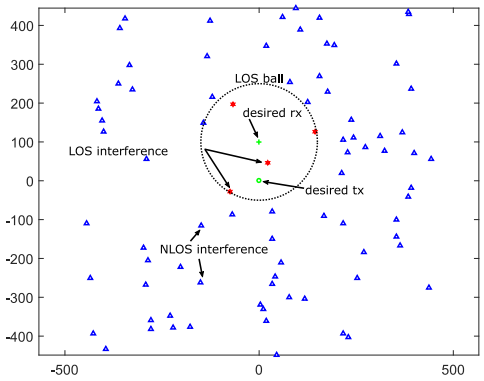

(a) The network is primarily limited by the LOS interference, but a strong LOS signal remains.

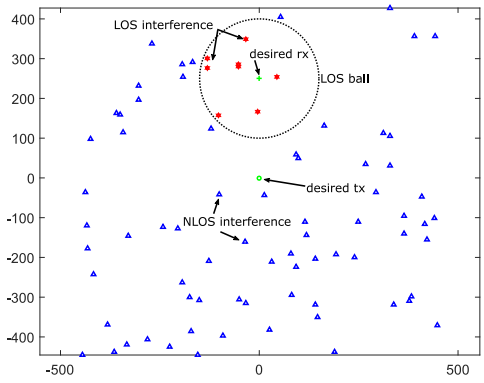

(b) The network is primarily limited by the LOS interference, but without a LOS signal path, the SINR will suffer.

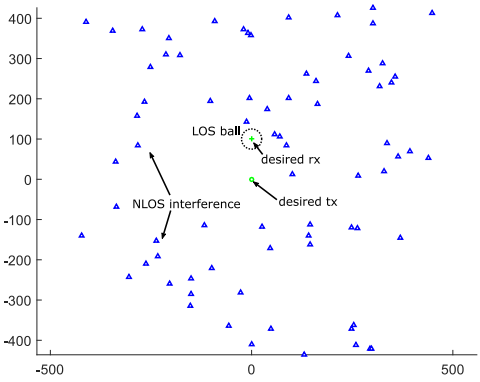

(c) In extremely dense blockage scenarios, all signals are likely to be NLOS.

Figure 4.4: The network scenarios detailed in Section 4.3.4.3. Fig. 4.4a is normal operation. Fig. 4.4b is a transmitter blockage scenario. Fig. 4.4c is a receiver blockage scenario.

silent. Consider, however, the sequence of active transmitters in time-slot s as $\Phi_s \subseteq \Phi$ where Φ is the realization of the PPP at time-slot s. In the case where $\zeta = 1$ and the users are not moving, each time-slot experiences interference from the same interfering locations. The success probability in this case was studied in [88, Theorem 1] which concluded that for $\alpha_{\mathrm{m}} \to 2$ the correlation between channel access is small, even for $\zeta \to 1$. Evaluating [88, Theorem 1, (24)] over the LOS ball from 0 to R_{los} for two successes (i.e. the joint probability), the integral of the interference can be studied similar to Theorem 4.3.1 which yields

$$\Theta_s = \zeta z\kappa \left(\log\left(1 + \frac{R_{\mathrm{los}}^2}{z\kappa}\right) - \frac{\zeta R_{\mathrm{los}}^2}{2(z\kappa + R_{\mathrm{los}}^2)} \right). \tag{4.32}$$

The $\frac{1}{2}$ from Theorem 4.3.1 is lost due to the *squaring* effect of the two attempts. The trailing term, however, indicates that effect of the interference is *less* when considering both probabilities. This is supported by the Monte-carlo simulations in Fig. 4.5. The simulations were run over $10,000$ iterations that simulated a network layout and then either moving the users, as in Fig. 4.5a, or using a different subset as transmitters 4.5b. In general, the movement of the users has a small effect on the SINR distribution while the ζ has a very large effect. For $\zeta < 0.5$, the SINR between transmissions is uncorrelated.

4.4.2 Data Transmission Delay

The data transmission delay is the time it takes for the synchronization and training phases to complete. During the synchronization and training phases, the transmitter and receiver realign their beams. The synchronization

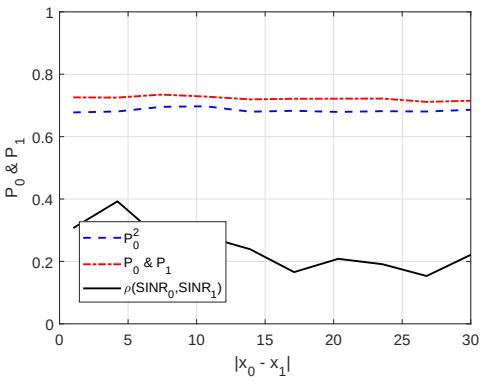

(a) The correlation in SINR over small distances.

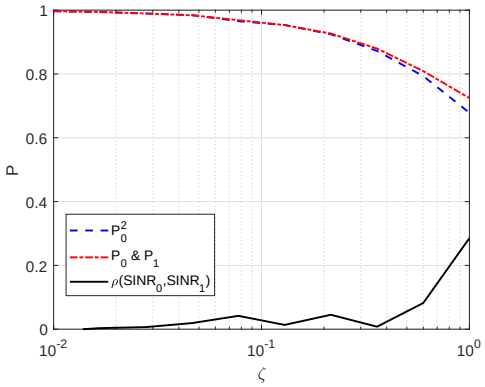

(b) The correlation in SINR over different transmit probabilities.

Figure 4.5: Monte-carlo simulations were used to generate the SINR over multiple slots using the same network distribution. In (a), the users move a random distance between slots. In (b), different subsets of the network access the channel in the subsequent slots. The small movement has a minor effect on the correlated behavior, but the access probability ζ has a very strong effect. For $\zeta < 0.5$, the SINR values between subsequent channel accesses is largely uncorrelated.

and training phases of the transmission interval are considered successful if the transmission during the desired beam in the synchronization and training phases exceeds an SINR threshold. I denote SINR_{syn} as the SINR during the synchronization phase and SINR_{tr} as the SINR during the training phase. The variables for SINR_{syn} and SINR_{tr} are the same as (4.7), but with the gain values appropriately chosen according to Table 4.2. Because the receiver experiences a different fading and interference realization in each transmission slot and the results present in Section 4.4.1, the SINR of the training phase is assumed to be independent of the synchronization phase for the remainder of the chapter. The probability of success for both phases $P_{\text{syn+tr}}$ is the product of the individual success probabilities. Specifically,

$$P_{\text{syn+tr}} = \mathbb{P}\left[\text{SINR}_{\text{syn}} > \Gamma\right] \mathbb{P}\left[\text{SINR}_{\text{tr}} > \Gamma\right], \tag{4.33}$$

where the threshold for success Γ is chosen to match the sensitivity of a low rate control signal (e.g -4 dBm to 0 dBm).

I treat each synchronization and training block (e.g. $S_{\text{syn}} + S_{\text{tr}}$ slots) as a Bernoulli random variable with probability $P_{\text{syn+tr}}$. The number of synchronization and training blocks $\nu_{\text{disc+tr}}$ until successful beam alignment is a geometric random variable. The expected time to begin transmission is then [26]

$$\tau_{\text{syn+tr}} = \mathbb{E}\left[\nu_{\text{disc+tr}} \frac{TS_{\text{syn}} + TS_{\text{tr}}}{\zeta}\right]. \tag{4.34}$$

I do not include the total transmission interval T_{tot} in the delay time. Because users in the uniform network are dipole pairs, if the training phase is

not successful, the users will simply restart the training phase. In a low mobility situation, $T_{\text{tot}} >> T$, the effect of overhead per transmission interval is negligible. As such, $\frac{TS_{\text{syn}}+TS_{\text{tr}}}{T_{\text{tot}}} \to 0$. The metric of interest is therefore the data transmission delay.

The first result gives the expected data transmission delay.

Corollary 4.4.1. *The expected data transmission delay $\tau_{\text{syn+tr}}$ of a mmWave ad hoc network with uniform spatial deployment is*

$$\tau_{\text{syn+tr}} = e^{\Omega_{\text{syn}}+\Omega_{\text{tr}}} e^{\zeta(\Theta_{\text{syn}}+\Theta_{\text{tr}})} \left(\frac{TS_{\text{syn}} + TS_{\text{tr}}}{\zeta} \right). \tag{4.35}$$

Proof. Because $\nu_{\text{disc+tr}}$ is a geometric random variable, the expected number of trials until the first success is the reciprocal of the success probability $P_{\text{syn+tr}}$ and (4.34) simplifies to

$$\tau_{\text{syn+tr}} = \frac{1}{P_{\text{syn+tr}}} \frac{TS_{\text{syn}} + TS_{\text{tr}}}{\zeta}. \tag{4.36}$$

In the case of a uniform PPP network,

$$P_{\text{syn+tr}} = e^{-r_o^{\alpha_{\text{m}}} \frac{N_o^{\text{m}}\Gamma}{P_o A_{\text{m}}} \left(\frac{1}{\kappa_{\text{syn}}}+\frac{1}{\kappa_{\text{tr}}}\right)} \mathcal{L}_{\text{p}} \left(r_o^{\alpha_{\text{m}}} \frac{\Gamma}{\kappa_{\text{syn}}} \right) \mathcal{L}_{\text{p}} \left(r_o^{\alpha_{\text{m}}} \frac{\Gamma}{\kappa_{\text{tr}}} \right) \tag{4.37}$$

where $\mathcal{L}_{\text{p}}(z)$ is (4.10). The inversion of the exponential removes the negation which yields the results using the notation developed in Section II. □

Comment: Corollary 4.4.1 shows that the transmission probability ζ is an important parameter as it affects the strength of the interference as well as the the time the training takes to complete. The *effective* transmitter density

λ, as shown in Section 4.3.1, is the product of the *potential* transmitter density λ_{u} and the transmission probability ζ. In our previous work [85–87], I only considered the *effective* transmitter density as ζ only affected the transmitting density. Because reducing ζ increases the expected training time $TS_{\mathrm{syn}} + TS_{\mathrm{tr}}$ in (4.34), I must consider ζ and λ_{u} separately. The relationship between these values is important to consider as ζ allows sufficient reduction of the interference in dense deployments, but as a result, the synchronization and training time takes much longer. I show the interplay of these values in Section 4.5.

I define the blockage events as transitions between the scenarios from Fig. 4.4. Scenario 1 in Fig. 4.4a is normal, desired operation. Scenario 2 is Fig. 4.4b, and Fig. 4.4c is scenario 3. I define a *transmitter* blockage as the transition from 1 to 2. With transmitter blockage, the receiver still has LOS interference, but the desired path from the transmitter to receiver becomes blocked. For example, if the transmitter turns a corner on a street, the desired LOS path is blocked. Conversely, I define a *receiver* blockage event as the transition from 1 to 3 because the receiver experiences heavy blockage, most signals become NLOS. For example, a user entering a vehicle may block all LOS paths from nearby transmitters.

It is useful to directly compare the various methods presented in Section 4.3.3. The following Corollary quantifies the increase in delay when moving from network scenario (1) to network scenario (2). Consider the situation when $r_o = R_{\mathrm{los}} - \epsilon$. The users are operating in LOS signal region with delay

$\tau^{(1)}_{\text{syn+tr}}$. If the signal becomes NLOS due to a transmitter blockage event, i.e. $r_o = R_{\text{los}} + \epsilon$, this models a blockage event. Now the delay is $\tau^{(2)}_{\text{syn+tr}}$.

Corollary 4.4.2. *Given the common term*

$$C = \frac{N+1}{N} + 4\pi\zeta\lambda_{\text{u}}\left(\Gamma\log\left(1+\frac{R^2_{\text{los}}}{\Gamma r_o^4}\right) - \Gamma\log\left(1+\frac{R^2_{\text{los}}}{\Gamma r_o^2}\right)\right), \tag{4.38}$$

a path-loss exponent of 2*, and a NLOS path-loss exponent of* 4*, the increase in expected transmission delay due to a transmitter blockage event for the baseline method is approximated by*

$$\beta^{(1)\text{base}}_{(2)\text{base}} = \exp\left(\frac{C}{N^2}\left(r_o^4 - r_o^2\right)\right), \tag{4.39}$$

and the increase in expected transmission delay due to a transmitter blockage event for the fast-synchronization method is approximated by

$$\beta^{(1)\text{fast}-\text{syn}}_{(2)\text{fast}-\text{syn}} = \exp\left(\frac{C}{N}\left(r_o^4 - r_o^2\right)\right). \tag{4.40}$$

Proof. The proof is presented in Appendix 4.7.1. □

Comment: The transmitter blockage scenario is the worst possible scenario because the transmitter is blocked. The desired signal becomes NLOS while the interference remains LOS. As I show in Section 4.5, the increase in $\tau_{\text{syn+tr}}$ is large for the fast-synchronization method as the increase in delay decays only with $\frac{1}{N}$. The decay according to $\frac{1}{N^2}$ in the exhaustive method allows the baseline method to be *blockage tolerant* as I show in Section 4.5.

The following Corollary quantifies the increase in delay when moving from network scenario (1) to network scenario (3). If the signal becomes NLOS

due to a receiver blockage event, i.e. $R_{\text{los}} \to 0$, this models the transition from (1) to (3). Now the delay is $\tau^{(3)}_{\text{syn+tr}}$.

Corollary 4.4.3. *Given the common term*

$$D = \left(r_o^2 - 1\right) \frac{N+1}{N} + 4\pi\zeta\lambda_{\text{u}} \left(\sqrt{\Gamma} \text{atan}\left(\frac{R_{\text{los}}^2}{\Gamma r_o^4}\right) - \Gamma \log\left(1 + \frac{R_{\text{los}}^2}{\Gamma r_o^2}\right)\right), \tag{4.41}$$

a LOS path-loss exponent of 2*, and a NLOS path-loss exponent of* 4*, the increase in expected transmission delay due to a receiver blockage event for the baseline method is approximated by*

$$\beta^{(1)\text{base}}_{(3)\text{base}} = \exp\left(\frac{r_o^2}{N^2} D\right), \tag{4.42}$$

and the increase in expected transmission delay due to a receiver blockage event for the fast-synchronization method is approximated by

$$\beta^{(1)\text{fast}-\text{syn}}_{(3)\text{fast}-\text{syn}} = \exp\left(\frac{r_o^2}{N} D\right). \tag{4.43}$$

Proof. The proof is presented in Appendix 4.7.2. □

Comment: The increase in the transmission delay is better tolerated in the case of a receiver blockage event because of the r_o^2 term rather than $r_o^4 - r_o^2$. While signal is NLOS, the interference is NLOS as well. The same trend with regard to antenna scaling is evident. The fast-synchronization and training method is less tolerant of (1) to (3) blockage events, but it is possible to still have successful communication.

In each training method, there is a balance between the mutual interference reduction by users transmitting with probability ζ and the increase in the overall training time. Using Corollary 4.4.1, I present results for the minimum delay with respect transmission opportunity ζ and number of antennas N. The optimal ζ is presented in the following Corollary.

Corollary 4.4.4. *The minimum delay in a uniform mmWave ad hoc network occurs with a transmission opportunity of*

$$\hat{\zeta} = \frac{1}{\Theta_{\text{syn}} + \Theta_{\text{tr}}}, \tag{4.44}$$

where Θ_{syn} *is the interference during synchronization and* Θ_{tr} *is interference during training.*

Proof. The proof is presented in Appendix 4.7.3. □

Comment: Corollary 4.4.4 shows that, surprisingly, the optimal transmission probability is only a function of the interference strength. The synchronization and training time term $TS_{\text{syn}} + TS_{\text{tr}}$ disappears even though the latency is heavily affected by that term.

4.4.3 Ergodic Rate with Overhead

After the training phase is completed, the remaining time in the transmission interval is used for data. I use ergodic rate as the metric to measure the rate. I define the ergodic rate as

$$R_{\text{u}} = \mathbb{E}_{\mathcal{P},h,\kappa}\left[\sum_{i\in\mathcal{P}} \log_2\left(1 + \text{SINR}_i\right)\right], \tag{4.45}$$

where the expectation is taken over the random PPP points $\mathcal{P}$, random fading h per slot T, and the random interference antenna gain κ. In the high mobility region, the per transmission interval overhead is expensive as T_{tot} is small. In this region, I let $\frac{TS_{\text{syn}}+TS_{\text{tr}}}{M} \rightarrow \epsilon$.

In the uniform network case, the user perceived ergodic rate is heavily affected by the transmission probability ζ. The user perceived rate of the network is

$$R = \left(1 - \frac{\min\left(\tau_{\text{syn+tr}}, T_{\text{tot}}\right)}{T_{\text{tot}}}\right)(\zeta)\,\mathbb{E}_{\mathcal{P},h,\kappa}\left[\sum_{i\in\mathcal{P}} \log_2\left(1+\text{SINR}_i\right)\right], \qquad (4.46)$$

where the first term on the right hand side represents the expected overhead in transmission interval. I note that for certain network situations (e.g. small T_{tot}), it is possible for the synchronization to take the entire T_{tot} sec to complete; in this scenario, the effective rate is zero as the beamforming must be re-done after the T_{tot} sec. The second term adjusts the ergodic rate for transmission probability because the remaining time left per transmission interval is reduced by ζ; while there are S_{data} slots, only ζS_{data} slots on average will be used. I include this term because I am interested in the *user perceived* rate of bits/sec/Hz not bits/slot/Hz. Because I use the transmission probability as an interference reduction method, I must reduce the data rate as well to keep the comparisons fair. The final term is the ergodic rate of the network. Analytic solutions to the ergodic rate are available for both uniform and clustered networks in our previous work [85, 87]. For a uniform network, the ergodic

rate is

$$R_{\mathrm{u}} = \frac{1}{\log(2)} \int_0^{\infty} \frac{e^{-z\Omega}}{z} \left[1 - (1+z)^{-1}\right] \mathcal{L}_{\mathrm{p}} \left(z \frac{r_o^{\alpha_{\mathrm{m}}} \Gamma}{\kappa_o} \right) dz \tag{4.47}$$

with Ω and $\mathcal{L}_{\mathrm{p}}$ defined above. I use numerical integration methods to evaluate (4.47).

4.5 Results

In this section I provide numerical results to illustrate the effectiveness of different beamforming solutions and methods. I present results by varying both the transmission probability ζ and the number of antennas N. I present the results for the three network scenarios described in Section 4.3.4.3. The system parameters correspond to a generic wideband mmWave system (e.g. OFDM 160MHz) and are summarized in Table 4.3. At 160MHz with an 2048 FFT size, the FFT period is $12.8\mu s$. The total slot time is $T = 15\mu s$ which includes all overhead including cyclic prefix and interframe spacing. The transmission interval is $T_{\mathrm{tot}} = 100ms$. The number of slots per interval is $\frac{T_{\mathrm{tot}}}{T} = 6,666$. The maximum number of antennas is $N_{\max} = 64$ which could require up to $N_{\max}^2 + N_{\max} = 4,160$ training slots per transmission interval depending on the beamforming method. The SINR threshold for the synchronization and training phases is set to $\Gamma = 0$ dBm. The LOS distance was set to $R_{\mathrm{los}} = 250$ with the communication distance $r_o = 100$. The PLE was set to $\alpha_{\mathrm{m}} = 2$ for LOS and $\alpha_{\mathrm{m}} = 4$ for NLOS.

Typically mmWave devices operate with a predetermined codebook

Variable	Value
system bandwidth	160MHz
T	$15\mu s$
T_{tot}	$100ms$
$S_{\text{syn}} + S_{\text{tr}} + S_{\text{data}}$	$6,666$ slots
$N_{\max}$	64
Γ	0 dBm
R_{los}	$250m$
r_o	$100m$
LOS PLE	2
NLOS PLE	4
N_o^{m}	-92 dBm
A_{m}	60 dB
P	1 W (30 dBm)

Table 4.3: Simulation variable values

of beamforming vectors. The number of codewords within the codebook is not limited to the number of antennas within the mmWave array; it may be larger or smaller than the number of antennas. For this reason, the number of antennas listed in the results is the codebook side. There are methods, for example, to create the beam pattern of an antenna with 4 elements from an array with 16 elements [90]. I vary the number of antennas, but in effect, I am varying the codebook size.

In Fig 4.6 and 4.7, the transmission opportunity was set to $\zeta = 0.5$ and the intensity of the PPP $\lambda_{\text{u}} = 5 \times 10^{-4}$. The results in Fig. 4.6 and 4.7 show that for ad hoc networks, the exhaustive search is optimal depending on the array size, where the overhead for exhaustive search becomes too cumbersome. This is different than the cellular case of [26] where the fast case reduces

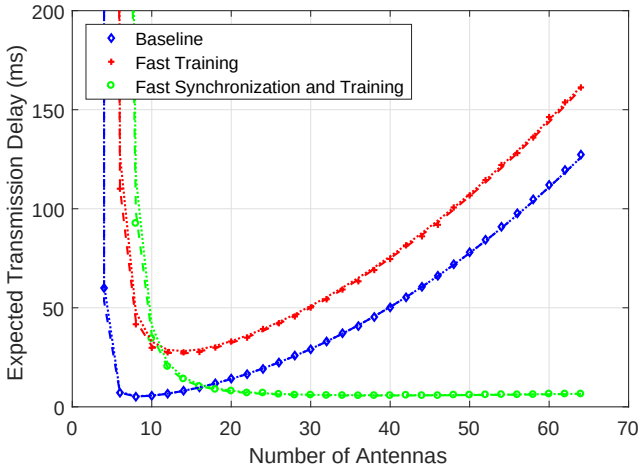

Figure 4.6: The markers correspond to simulation results while the dashed lines correspond to Corollary 4.4.1. With a low number of antennas, the baseline method performs best because of the directionality. The overhead with training the entire array quickly becomes large.

overhead to increase user perceived throughput regardless of array size. The difference is because the proximate interference of ad hoc networks ruins the fast methods. When the receiver is using an omni-directional antenna, it is not rejecting any of the nearby interference. When the number of antennas is large, the fast-synchronization and training becomes better because the single directional antenna provides enough gain to overcome the interference; additionally, overhead grows as N whereas the exhaustive search grows as N^2. For the network parameters chosen, the fast-training method provides no benefit. The decrease in the training block time is overpowered by the decrease in the success probability of the training phase. A similar trend is shown in Fig. 4.7. At smaller array sizes, the baseline method is optimal as a way to eliminate interference while the effect of the N^2 overhead is tolerable. It is

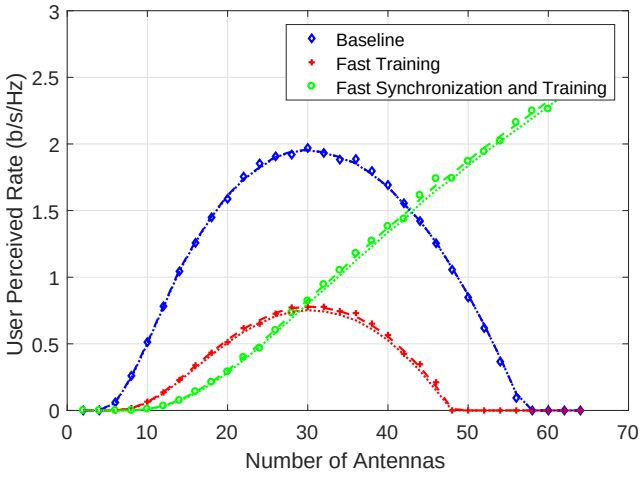

Figure 4.7: The markers correspond to simulation results while the dashed lines correspond to (4.47). A similar trend is shown here where the baseline method performs best in low array sizes. The user perceived rate goes to zero for high array sizes because the training on average will not complete before a new solution is needed.

interesting to note that minimum of Fig. 4.6 and the maximum of Fig. 4.7 occur at different array sizes. The lowest transmission delay occurs at $N = 5$ while the maximum rate occurs at $N = 30$. At the minimum delay of $N = 4$, the user perceived rate is is about 25% lower than the maximum possible rate for the network configuration; conversely, the minimum delay is 80% less than the delay at the maximum rate.

In Fig 4.8 and 4.9, the antenna array size was set to $N = 16$ and the intensity of the PPP $\lambda_{\mathrm{u}} = 1 \times 10^{-3}$. Fig. 4.8 and 4.9 illustrate the balance between the transmission probability and the success of the training phase for the fast-synchronization and training phase. If ζ is too small, the training block term $TS_{\mathrm{syn}} + TS_{\mathrm{tr}}$ increases the latency undesirably. If ζ is too large, the

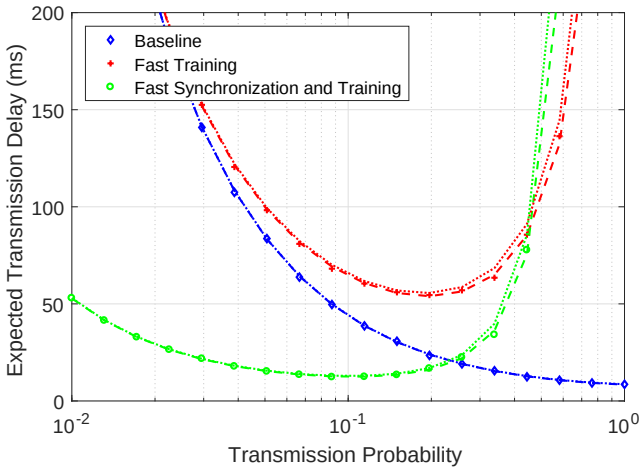

Figure 4.8: The markers correspond to simulation results while the dashed lines correspond to Corollary 4.4.1. If the fast-synchronization method is too aggressive with the channel, the aggregate interference limits the link performance. If the channel is underused, however, the packets are received but the training time increases due to utilization.

omni-directional reception of the method cannot eliminate the interference and success probability of the phase $P_{\text{syn+tr}}$ decreases extremely fast. Conversely, the baseline method is aggressive with the transmission probability because the interference is canceled by the array gain while the training block time increases as N^2. Again, Fig. 4.8 shows the ineffectiveness of the fast-training method. It suffers the same N^2 training block time growth, but also suffers from decreased $P_{\text{syn+tr}}$ during the training phase which causes the latency to be unbearable at high ζ.

In Fig. 4.10, I plot the optimal transmission probability ζ to minimize the delay. Because of the increase by N^2 in the training time, the base method is very aggressive with the channel in nearly all cases. The optimal ζ quickly

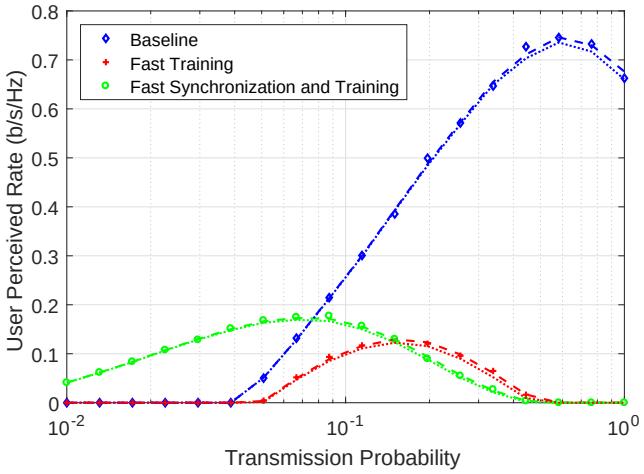

Figure 4.9: The markers correspond to simulation results while the dashed lines correspond to (4.47). The baseline method is very aggressive with the channel.

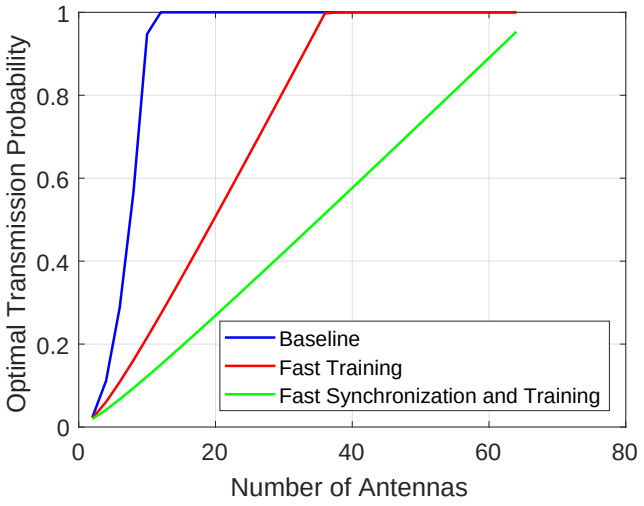

Figure 4.10: The solid lines correspond to correspond to Corollary 4.4.4. Even with many antennas, the fast synchronization method must back off on the channel to reduce interference.

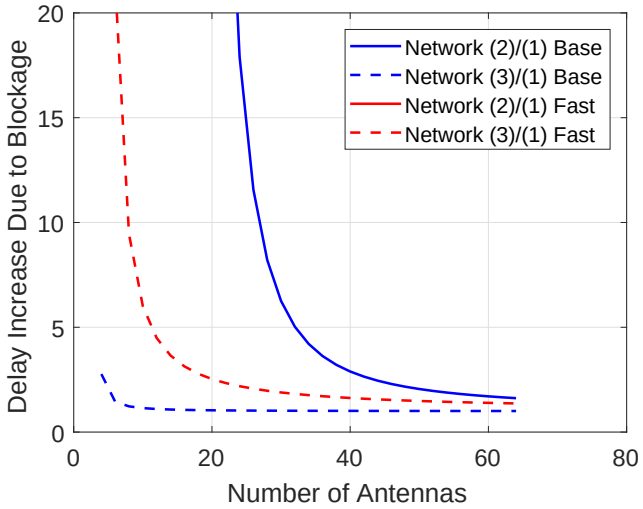

Figure 4.11: The solid lines correspond to correspond to Corollary 4.4.2 while the dashed lines correspond to Corollary 4.4.3. In general, blockage events at the receiver are tolerated better than blockage events at the transmitter.

goes to 1. Fig. 4.10 again shows the sensitivity of the fast-synchronization and training method to the interference. Even when $N = 64$, it is optimal to back off transmission slightly in order to minimize the delay in the network.

Fig. 4.11 shows the multiplying factor when encountering a blockage event at the transmitter (solid curves) or receiver (dashed curves). The blockage event at the transmitter is not shown for the fast synchronization method because the expected delay is greater than 20 for all the antenna values. If the blockage event occurs at the receiver, the fast synchronization method encounters roughly 2.5× increase in the delay if 20 antennas are used.

4.6 Conclusions

In this chapter, I developed a framework to analyze the impact of overhead in synchronization and training methods of mmWave ad hoc networks. I explored the balance in optimizing two important next-generation metrics: latency and rate. The derived equations show that the transmission probability and antenna array size that maximizes rate is different than the the value that minimizes latency. Exhaustive search sweeping is much more tolerant of interference but must be very aggressive with the channel to minimize the delay. I showed that if omni-directional reception is used, the transmission probability must be carefully tuned; too conservative of a transmission probability under utilizes the channel, but too high of a transmission probability creates too much interference at the receiver. Additionally, I define three different network operating scenarios and show that blockage events at the receiver are tolerated much more in terms of increased delay or lost rate as compared to blockage events at the transmitter.

4.7 Appendix

4.7.1 Proof of Corollary 4.4.2

The ratio for the baseline method is

$$\beta = \frac{\tau^{(2)}_{\text{syn+tr}}}{\tau^{(1)}_{\text{syn+tr}}} \tag{4.48}$$

$$= \frac{\exp\left(r_o^4\Omega'\left(\frac{1}{\kappa_{\text{syn}}}+\frac{1}{\kappa_{\text{tr}}}\right)+\Theta^{(2)}_{\text{syn}}+\Theta^{(2)}_{\text{tr}}\right)\frac{TS^{\text{base}}_{\text{syn}}+TS^{\text{base}}_{\text{tr}}}{\zeta}}{\exp\left(r_o^2\Omega'\left(\frac{1}{\kappa_{\text{syn}}}+\frac{1}{\kappa_{\text{tr}}}\right)+\Theta^{(1)}_{\text{syn}}+\Theta^{(1)}_{\text{tr}}\right)\frac{TS^{\text{base}}_{\text{syn}}+TS^{\text{base}}_{\text{tr}}}{\zeta}}, \tag{4.49}$$

where Ω' is Ω without the κ and r_o terms. I suppress the Ω' term in the following equations to minimize the clutter. In the next step, I only consider the class 1 interference when calculating the gain

$$\beta = \exp\Bigg(\left(r_o^4 - r_o^2\right) \frac{N+1}{N^3} + 4\pi\zeta\lambda_{\mathrm{u}} \left(\frac{\Gamma r_o^4 \log\left(1+\frac{R_{\mathrm{los}}^2}{\Gamma r_o^4}\right)}{N^2} - \frac{\Gamma r_o^2 \log\left(1+\frac{R_{\mathrm{los}}^2}{\Gamma r_o^2}\right)}{N^2} \right) \Bigg) \tag{4.50}$$

$$= \exp\Bigg(\left(r_o^4 - r_o^2\right) \frac{1}{N^2} \Bigg(\frac{N+1}{N} + 4\pi\zeta\lambda_{\mathrm{u}} \left(\Gamma \log\left(1+\frac{R_{\mathrm{los}}^2}{\Gamma r_o^4}\right) - \Gamma \log\left(1+\frac{R_{\mathrm{los}}^2}{\Gamma r_o^2}\right) \right) \Bigg) \Bigg), \tag{4.51}$$

which yields the result. For the ratio between of the fast-synchronization method, I skip to the last few steps

$$\beta = \exp\Bigg(\left(r_o^4 - r_o^2\right) \frac{N+1}{N^2} + 4\pi\zeta\lambda_{\mathrm{u}} \left(\frac{\Gamma r_o^4 \log\left(1+\frac{R_{\mathrm{los}}^2}{\Gamma r_o^4}\right)}{N} - \frac{\Gamma r_o^2 \log\left(1+\frac{R_{\mathrm{los}}^2}{\Gamma r_o^2}\right)}{N} \right) \Bigg) \tag{4.52}$$

$$= \exp\Bigg(\left(r_o^4 - r_o^2\right) \frac{1}{N} \Bigg(\frac{N+1}{N} + 4\pi\zeta\lambda_{\mathrm{u}} \left(\Gamma \log\left(1+\frac{R_{\mathrm{los}}^2}{\Gamma r_o^4}\right) - \Gamma \log\left(1+\frac{R_{\mathrm{los}}^2}{\Gamma r_o^2}\right) \right) \Bigg) \Bigg), \tag{4.53}$$

which completes the proof. □

4.7.2 Proof of Corollary 4.4.3

The ratio proof is similar as the previous Corollary and I begin with the base again

$$\beta = \frac{\tau^{(2)}_{\text{syn+tr}}}{\tau^{(1)}_{\text{syn+tr}}} \tag{4.54}$$

$$= \frac{\exp\left(r_o^4\Omega'\left(\frac{1}{\kappa_{\text{syn}}}+\frac{1}{\kappa_{\text{tr}}}\right)+\Theta^{(2)}_{\text{syn}}+\Theta^{(2)}_{\text{tr}}\right)^{\frac{TS^{\text{base}}_{\text{syn}}+TS^{\text{base}}_{\text{tr}}}{\zeta}}}{\exp\left(r_o^2\Omega'\left(\frac{1}{\kappa_{\text{syn}}}+\frac{1}{\kappa_{\text{tr}}}\right)+\Theta^{(1)}_{\text{syn}}+\Theta^{(1)}_{\text{tr}}\right)^{\frac{TS^{\text{base}}_{\text{syn}}+TS^{\text{base}}_{\text{tr}}}{\zeta}}}, \tag{4.55}$$

where Ω' is Ω without the κ and r_o terms. In the next step, I only consider the class 1 interference when calculating the gain

$$\beta = \exp\Bigg(\left(r_o^4 - r_o^2\right)\frac{N+1}{N^3} + 4\pi\zeta\lambda_{\text{u}}\left(\frac{\sqrt{\Gamma}r_o^2\text{atan}\left(\frac{R^2_{\text{los}}}{\sqrt{\Gamma}r_o^2}\right)}{N^2} - \frac{\Gamma r_o^2\log\left(1+\frac{R^2_{\text{los}}}{\Gamma r_o^4}\right)}{N^2}\right)\Bigg) \tag{4.56}$$

$$= \exp\left(\frac{r_o^2}{N^2}\left(\left(r_o^2-1\right)\frac{N+1}{N} + 4\pi\zeta\lambda_{\text{u}}\left(\sqrt{\Gamma}\text{atan}\left(\frac{R^2_{\text{los}}}{\Gamma r_o^4}\right) - \Gamma\log\left(1+\frac{R^2_{\text{los}}}{\Gamma r_o^2}\right)\right)\right)\right), \tag{4.57}$$

which yields the result. The proof for the fast synchronization method follows in the same way as before. □

4.7.3 Proof of Corollary 4.4.4

First, I show that the expected delay time (4.35) is strictly convex function in ζ. I express (4.35) generically as

$$f(\zeta) = e^{\Omega+\zeta\Theta}\frac{c}{\zeta}, \tag{4.58}$$

with first and second derivatives as

$$f'(\zeta) = e^{\Omega+\zeta\Theta}\frac{c(\zeta\Theta - 1)}{\zeta^2} \tag{4.59}$$

$$f''(\zeta) = e^{\Omega+\zeta\Theta}\frac{c(\zeta\Theta^2 - 2\zeta\Theta + 2)}{\zeta^3}. \tag{4.60}$$

The first term $e^{\Omega+\zeta\Theta}$ is strictly positive. The polynomial $\zeta\Theta^2 - 2\zeta\Theta + 2$ has no real solutions for any $\zeta \in (0, 1)$; from the quadratic formula, $\sqrt{4\zeta^2 - 8\zeta}$ is always negative. The polynomial is therefore strictly positive as well. The time constant c is always strictly positive. Lastly, the denominator ζ^3 is always positive as the transmission probability must also be strictly positive for non-zero ζ.

Because the function is strictly convex, it suffices to find the zero point of the first derivative. The minimum delay is achieved by solving (4.59) for ζ which yields the desired result. □

Chapter 5

Conclusion

This section gives a summary of the contributions of the dissertation in Section 5.1. Potential avenues for future research are detailed in Section 5.2.

5.1 Summary

In this dissertation, I develop a framework for analyzing mmWave ad hoc networks using stochastic geometry. The three major contributions of this dissertation are as follows:

In Chapter 2, I formulate the performance of mmWave ad hoc networks by incorporating random factors of a mmWave ad hoc network such as building blockage, antenna alignment, interferer position, and user position. Using a similar framework, I compare and contrast the performance against a lower frequency UHF ad hoc network. I argue for LOS-aware protocols due to the large performance increase from LOS communication at mmWave. I include discussion of the INR when a network is operating at the transmission capacity.

In Chapter 3, I characterize the ergodic rate of mmWave ad hoc networks for two different spatial distributions of transmitters: uniform networks (e.g. a Poisson point process) and a LOS cluster process (e.g. Poisson clus-

ter process). An antenna scaling trend, as transmitter density increases, of uniform mmWave ad hoc networks is derived. The result indicates that the number of antennas can scale sub-linearly with transmitter density while clustered ad hoc networks must scale linearly with user density. I define and develop a relationship between the SINR for communication within a cluster (intra-cluster) and between clusters (inter-cluster) which gives the proximity of the nearest cluster while maintaining rate requirements within a cluster. I characterize of the effect of random beam misalignment between the desired user pairs.

In Chapter 4, I characterize the overhead cost of beam alignment in terms of latency and rate reduction. I show that blockage events at the transmitter are essentially nonrecoverable due to the degradation of signal power for fast training techniques while blockage events at the receiver may allow successful communication. I show that using omni-directional reception is optimal for mmWave ad hoc networks if the transmission probability is sufficiently low or if the antenna array size and training length is sufficiently large. In particular, I give expressions for the optimal transmission probability for minimizing the delay as well as well as the region where omni-directional reception is optimal. The results indicate that the optimal transmission probability for ergodic rate is typically larger than the optimal point for delay within a fixed transmission block; a similar conclusion holds for the array size. In the high mobility case where overhead is most costly, if the underlying user density is too high, the users must back off the channel too frequently for successful

training to complete and data transmission to begin.

5.2 Future Research Directions

In this section, I present some new directions and extensions of the work developed in my dissertation for further investigation and characterization of mmWave ad hoc networks.

1. **LOS Relaying:** As shown in Chapter 2, mmWave ad hoc networks are extremely limited if the desired signal is NLOS while there are LOS interference signals. The underlying point process assumes that there are users remaining silent during each transmission. These silent users can potentially serve as relays for long NLOS mmWave links in ad hoc networks. Relaying has been studied extensively in the past for ad hoc and cellular networks [91, 92]. Relaying is part of the IEEE 802.11ad standard as both amplify-and-forward and decode-and-forward [67]. Because of the vastly different path-loss exponents between LOS and NLOS communication, relaying may prove to be a huge boon for mmWave networks. Depending on the link distance, the received relay signal may potentially be several 10s of dB stronger than the direct link. In order to extend the framework from Chapter 2 to account for relaying, the SINR can be evaluated over two, potentially correlated, transmissions. The problem of mmWave relaying with stochastic geometry is investigated in [93], but the authors do not include interference in the signal metrics.

2. **Improved Beam Training Methods:** The framework developed in Chapter 4 provides a method to evaluate peer-to-peer beamforming, but several extensions can be made. First, the analysis of overhead in the peer-to-peer case does not consider any enhancements and detriments by training multiple users during the same transmission interval. In a clustered environment with many users (e.g. a WLAN access point), the access point may only have to beam sweep once which saves time, but each added user adds overhead as well. Second, any optimization to the transmitted waveform are not consider. In the peer-to-peer environment, the OFDM waveform can be compressed in frequency to reduce the noise figure at the receiver which would help the reception in noise-limited environments. Third, the alignment error model developed in Chapter 3 is not included. The quality of the alignment and channel estimate depends on the amount of training sent in the control packets. This additional overhead is not considered.

3. **Real Hardware Prototype:** The trends and system guidelines developed in this dissertation should be validated against a real hardware prototype. Unfortunately, the cost and difficulty to acquire mmWave hardware, especially the active phased antenna arrays, is high and such an endeavor was not possible during the completion of this dissertation. The previous generation of wireless standards (e.g. 3GPP LTE and IEEE 802.11n/ac) were prototyped using software defined radio (SDR) platforms. A particular popular platform is the National Instruments

/ Ettus USRP (Universal Software Radio Peripheral). As of this writing, the largest baseband bandwidth available in the USRP platform is 160MHz [94]. In lieu of wider bandwidth USRP option, current and future mmWave ad hoc protocols may be prototyped at baseband using a limited bandwidth, but upconverted to mmWave using an external mixer. National Instruments also offers a full mmWave transceiver system with a 2GHz bandband bandwidth, but the cost is nearly $\$200,000$ for a single bi-directional link with no phased array [95]. Once affordable mmWave phased arrays are available, more sophisticated beam tracking and beam training methods can be tested.

Bibliography

[1] T. Bai and R. W. Heath Jr., "Coverage and Rate Analysis for Millimeter-Wave Cellular Networks," *IEEE Trans. Wireless Commun.*, vol. 14, no. 2, pp. 1100–1114, Feb 2015.

[2] What Drives Data Usage? [Online]. Available: http://www.nielsen.com/us/en/insights/news/2016/what-drives-data-usage.html

[3] J. Andrews *et al.*, "Rethinking information theory for mobile ad hoc networks," *IEEE Commun. Mag.*, vol. 46, no. 12, pp. 94–101, 2008.

[4] "IEEE Standard for Information Technology - Telecommunications and Information Exchange Between Systems - Local and Metropolitan Area Networks - Specific Requirements - Part 11: Wireless LAN Medium Access Control (MAC) and Physical Layer (PHY) Specifications," *IEEE Std 802.11-2007 (Revision of IEEE Std 802.11-1999)*, pp. 1–1076, June 2007.

[5] "IEEE Standard for High Data Rate Wireless Multi-Media Networks," *IEEE Std 802.15.3-2016 (Revision of IEEE Std 802.15.3-2003*, pp. 1–510, July 2016.

[6] Bluetooth Core Specification. [Online]. Available: https://www.bluetooth.com/specifications/bluetooth-core-specification

[7] D. Gislason, *Zigbee Wireless Networking*, pap/onl ed. Newton, MA, USA: Newnes, 2008.

[8] J. Singh, S. Ponnuru, and U. Madhow, "Multi-Gigabit communication: the ADC bottleneck," in *Ultra-Wideband, 2009. ICUWB 2009. IEEE International Conference on*, 2009, pp. 22–27.

[9] A. Alkhateeb, O. El Ayach, G. Leus, and R. Heath, "Hybrid precoding for millimeter wave cellular systems with partial channel knowledge," in *Information Theory and Applications Workshop (ITA), 2013*, 2013, pp. 1–5.

[10] O. El Ayach, S. Rajagopal, S. Abu-Surra, Z. Pi, and R. W. Heath, Jr, "Spatially Sparse Precoding in Millimeter Wave MIMO Systems," *submitted to IEEE Trans. Wireless Commun.*, May 2013.

[11] T. Rappaport, E. Ben-Dor, J. Murdock, and Y. Qiao, "38 GHz and 60 GHz angle-dependent propagation for cellular amp; peer-to-peer wireless communications," in *Proc. of IEEE International Conference on Communications (ICC)*, Jun 2012, pp. 4568–4573.

[12] T. Rappaport, S. Sun, R. Mayzus, H. Zhao, Y. Azar, K. Wang, G. Wong, J. Schulz, M. Samimi, and F. Gutierrez, "Millimeter Wave Mobile Communications for 5G Cellular: It Will Work!" *IEEE Access*, vol. 1, pp. 335–349, 2013.

[13] P. Gupta and P. Kumar, "The capacity of wireless networks," *IEEE Trans. Inf. Theory*, vol. 46, no. 2, pp. 388–404, Mar. 2000.

[14] F. Baccelli and S. Zuyev, "Stochastic Geometry Models of Mobile Communication Networks," in *Frontiers in queueing: models and applications in science and engineering*. CRC Press, 1996, pp. 227–243.

[15] K. Huang, J. Andrews, D. Guo, R. Heath, and R. Berry, "Spatial Interference Cancellation for Multiantenna Mobile Ad Hoc Networks," *IEEE Trans. Inf. Theory*, vol. 58, no. 3, pp. 1660–1676, 2012.

[16] A. Hunter, J. Andrews, and S. Weber, "Transmission capacity of ad hoc networks with spatial diversity," *IEEE Trans. Wireless Commun.*, vol. 7, no. 12, pp. 5058–5071, 2008.

[17] N. Lee, F. Baccelli, and R. W. Heath Jr., "Spectral Efficiency Scaling Laws in Dense Random Wireless Networks With Multiple Receive Antennas," *IEEE Trans. Inf. Theory*, vol. 62, no. 3, pp. 1344–1359, March 2016.

[18] X. Lin, J. G. Andrews, and A. Ghosh, "Spectrum Sharing for Device-to-Device Communication in Cellular Networks," *IEEE Trans. Wireless Commun.*, vol. 13, no. 12, pp. 6727–6740, dec 2014.

[19] R. Vaze and R. Heath, "Transmission Capacity of Ad-hoc Networks With Multiple Antennas Using Transmit Stream Adaptation and Interference

Cancellation," *IEEE Trans. Inf. Theory*, vol. 58, no. 2, pp. 780–792, 2012.

[20] S. Weber, J. Andrews, and N. Jindal, "An Overview of the Transmission Capacity of Wireless Networks," *IEEE Trans. Commun.*, vol. 58, no. 12, pp. 3593–3604, 2010.

[21] F. Baccelli and B. Blaszczyszyn, *Stochastic Geometry and Wireless Networks, Volume I - Theory*. NoW Publishers, 2009, vol. 1. [Online]. Available: http://hal.inria.fr/inria-00403039

[22] F. Baccelli, B. Blaszczyszyn, and P. Muhlethaler, "An Aloha protocol for multihop mobile wireless networks," *IEEE Trans. Inf. Theory*, vol. 52, no. 2, pp. 421–436, Feb 2006.

[23] T. Rappaport, R. W. Heath Jr., R. C. Daniels, and J. Murdock, *Millimeter Wave Wireless Communications*. Prentice-Hall, September 2014.

[24] J. G. Andrews, S. Buzzi, W. Choi, S. V. Hanly, A. Lozano, A. C. K. Soong, and J. C. Zhang, "What Will 5G Be?" *IEEE Journal on Selected Areas in Communications*, vol. 32, no. 6, pp. 1065–1082, Jun. 2014.

[25] A. Alkhateeb, Y. H. Nam, M. S. Rahman, C. Zhang, and R. Heath, "Initial Beam Association in Millimeter Wave Cellular Systems: Analysis and Design Insights," *IEEE Transactions on Wireless Communications*, vol. PP, no. 99, pp. 1–1, 2017.

[26] Y. Li, J. G. Andrews, F. Baccelli, T. D. Novlan, and J. C. Zhang, "Design and Analysis of Initial Access in Millimeter Wave Cellular Networks," *CoRR*, vol. abs/1609.05582, 2016. [Online]. Available: http://arxiv.org/abs/1609.05582

[27] R. Vaze, K. Truong, S. Weber, and R. Heath, "Two-Way Transmission Capacity of Wireless Ad-hoc Networks," *IEEE Trans. Wireless Commun.*, vol. 10, no. 6, pp. 1966–1975, 2011.

[28] J. Andrews, R. Ganti, M. Haenggi, N. Jindal, and S. Weber, "A primer on spatial modeling and analysis in wireless networks," *IEEE Commun. Mag.*, vol. 48, no. 11, pp. 156–163, Nov. 2010.

[29] R. Ramanathan, J. Redi, C. Santivanez, D. Wiggins, and S. Polit, "Ad hoc networking with directional antennas: a complete system solution," *IEEE J. Sel. Areas Commun.*, vol. 23, no. 3, pp. 496–506, 2005.

[30] S. Bellofiore, J. Foutz, R. Govindarajula, I. Bahceci, C. Balanis, A. Spanias, J. Capone, and T. Duman, "Smart antenna system analysis, integration and performance for mobile ad-hoc networks (MANETs)," *IEEE Trans. Antennas Propag.*, vol. 50, no. 5, pp. 571–581, 2002.

[31] J. Winters, "Smart antenna techniques and their application to wireless ad hoc networks," *IEEE Trans. Wireless Commun.*, vol. 13, no. 4, pp. 77–83, 2006.

[32] R. Choudhury, X. Yang, R. Ramanathan, and N. Vaidya, "On designing MAC protocols for wireless networks using directional antennas," *IEEE Trans. Mobile Comput.*, vol. 5, no. 5, pp. 477–491, 2006.

[33] D5.1 Channel Modeling and Characterization. [Online]. Available: http://www.miweba.eu/wp-content/uploads/2014/07/MiWEBA_D5.1_v1.011.pdf

[34] T. S. Rappaport, G. R. MacCartney, M. K. Samimi, and S. Sun, "Wideband Millimeter-Wave Propagation Measurements and Channel Models for Future Wireless Communication System Design," *IEEE Trans. Commun.*, vol. 63, no. 9, pp. 3029–3056, Sept 2015.

[35] F. Baccelli and B. Blaszczyszyn, *Stochastic Geometry and Wireless Networks, Volume II - Applications.* NoW Publishers, 2009, vol. 2. [Online]. Available: http://hal.inria.fr/inria-00403040

[36] R. Gowaikar, B. Hochwald, and B. Hassibi, "Communication over a wireless network with random connections," *IEEE Trans. Inf. Theory*, vol. 52, no. 7, pp. 2857–2871, Jul. 2006.

[37] T. Bai and R. W. Heath Jr., "Coverage analysis for millimeter wave cellular networks with blockage effects," in *2013 IEEE Global Conference on Signal and Information Processing.* IEEE, Dec. 2013, pp. 727–730.

[38] M. Kulkarni, S. Singh, and J. Andrews, "Coverage and rate trends in

dense urban mmWave cellular networks," in *Global Communications Conference (GLOBECOM), 2014 IEEE*, Dec 2014, pp. 3809–3814.

[39] S. Singh, M. N. Kulkarni, A. Ghosh, and J. G. Andrews, "Tractable Model for Rate in Self-Backhauled Millimeter Wave Cellular Networks," *IEEE Journal on Selected Areas in Communications*, vol. 33, no. 10, pp. 2196–2211, Oct 2015.

[40] K. Venugopal, M. C. Valenti, and R. W. Heath Jr., "Device-to-Device Millimeter Wave Communications: Interference, Coverage, Rate, and Finite Topologies," *CoRR*, vol. abs/1506.07158, 2015. [Online]. Available: http://arxiv.org/abs/1506.07158

[41] S. Akoum, O. El Ayach, and R. Heath, "Coverage and capacity in mmWave cellular systems," in *Signals, Systems and Computers (ASILOMAR), 2012 Conference Record of the Forty Sixth Asilomar Conference on*, 2012, pp. 688–692.

[42] Z. Pi and F. Khan, "An introduction to millimeter-wave mobile broadband systems," *IEEE Commun. Mag.*, vol. 49, no. 6, pp. 101–107, Jun. 2011.

[43] S. Akoum, M. Kountouris, M. Debbah, and R. Heath, "Spatial interference mitigation for multiple input multiple output ad hoc networks: MISO gains," in *2011 Conference Record of the Forty Fifth Asilomar Conference onSignals, Systems and Computers (ASILOMAR)*, 2011, pp. 708–712.

[44] S. Singh, R. Mudumbai, and U. Madhow, "Interference Analysis for Highly Directional 60-GHz Mesh Networks: The Case for Rethinking Medium Access Control," *IEEE/ACM Trans. Netw.*, vol. 19, no. 5, pp. 1513–1527, 2011.

[45] T. Bai, R. Vaze, and R. Heath, "Using random shape theory to model blockage in random cellular networks," in *2012 International Conference on Signal Processing and Communications (SPCOM)*, 2012, pp. 1–5.

[46] F. Baccelli and X. Zhang, "A Correlated Shadowing Model for Urban Wireless Networks," in *IEEE INFOCOM'15*, Apr. 2015.

[47] W. Lu and M. D. Renzo, "Stochastic Geometry Modeling of Cellular Networks: Analysis, Simulation and Experimental Validation," *CoRR*, vol. abs/1506.03857, 2015. [Online]. Available: http://arxiv.org/abs/1506.03857

[48] T. Bai, R. Vaze, and R. W. Heath Jr., "Analysis of Blockage Effects on Urban Cellular Networks," *IEEE Trans. Wireless Commun.*, vol. 13, no. 9, pp. 5070–5083, Sept 2014.

[49] M. Samimi, K. Wang, Y. Azar, G. N. Wong, R. Mayzus, H. Zhao, J. K. Schulz, S. Sun, F. Gutierrez, and T. S. Rappaport, "28 GHz Angle of Arrival and Angle of Departure Analysis for Outdoor Cellular Communications Using Steerable Beam Antennas in New York City," in *Proc 2013 IEEE 77th Vehicular Technology Conference (VTC Spring)*. IEEE, Jun. 2013, pp. 1–6.

[50] G. Grimmett, *Percolation*. Springer Verlag, 1989.

[51] C. Galiotto, I. Gomez-Miguelez, N. Marchetti, and L. Doyle, "Effect of LOS/NLOS Propagation on Area Spectral Efficiency and Energy Efficiency of Small-Cells," *CoRR*, vol. abs/1409.7575, 2014. [Online]. Available: http://arxiv.org/abs/1409.7575

[52] H. Balakrishnan, V. Padmanabhan, S. Seshan, and R. Katz, "A comparison of mechanisms for improving TCP performance over wireless links," *IEEE/ACM Trans. Netw.*, vol. 5, no. 6, pp. 756–769, 1997.

[53] H. Alzer, "On Some Inequalities for the Incomplete Gamma Function," *Mathematics of Computation*, vol. 66, 1997. [Online]. Available: http://www.jstor.org/stable/2153894

[54] J. Lee, N. Lee, and F. Baccelli, "Scaling Laws for Ergodic Spectral Efficiency in MIMO Poisson Networks," *CoRR*, vol. abs/1608.06065, 2016. [Online]. Available: http://arxiv.org/abs/1608.06065

[55] A. Thornburg, T. Bai, and R. W. Heath Jr., "MmWave ad hoc network coverage and capacity," in *2015 IEEE International Conference on Communications (ICC)*, June 2015, pp. 1310–1315.

[56] ——, "Performance Analysis of Outdoor mmWave Ad Hoc Networks," *IEEE Transactions on Signal Processing*, vol. 64, no. 15, pp. 4065–4079, Aug 2016.

[57] ——, "Interference statistics in a random mmWave ad hoc network," in *2015 IEEE International Conference on Acoustics, Speech and Signal Processing (ICASSP)*, April 2015, pp. 2904–2908.

[58] H. Su and X. Zhang, "Clustering-Based Multichannel MAC Protocols for QoS Provisionings Over Vehicular Ad Hoc Networks," *IEEE Transactions on Vehicular Technology*, vol. 56, no. 6, pp. 3309–3323, Nov 2007.

[59] X. Yang and G. de Veciana, "Inducing Multiscale Clustering Using Multistage MAC Contention in CDMA Ad Hoc Networks," *IEEE/ACM Transactions on Networking*, vol. 15, no. 6, pp. 1387–1400, Dec 2007.

[60] N. Gao, L. Tang, S. Li, and Q. Chen, "A hybrid clustering-based MAC Protocol for Vehicular Ad Hoc Networks," in *2014 International Workshop on High Mobility Wireless Communications*, Nov 2014, pp. 183–187.

[61] R. K. Ganti and M. Haenggi, "Interference and Outage in Clustered Wireless Ad Hoc Networks," *IEEE Trans. Inf. Theory*, vol. 55, no. 9, pp. 4067–4086, Sept 2009.

[62] B. Nosrat-Makouei, R. K. Ganti, J. G. Andrews, and R. W. Heath Jr., "MIMO Interference Alignment in Random Access Networks," *IEEE Trans. Commun.*, vol. 61, no. 12, pp. 5042–5055, Dec. 2013.

[63] T. Bai, A. Alkhateeb, and R. W. Heath Jr, "Coverage and Capacity in Millimeter Wave Cellular Networks," *IEEE Communications Mag.*, Sep. 2014.

[64] J. Wildman, P. H. J. Nardelli, M. Latva-aho, and S. Weber, "On the Joint Impact of Beamwidth and Orientation Error on Throughput in Directional Wireless Poisson Networks," *IEEE Trans. Wireless Commun.*, vol. 13, no. 12, pp. 7072–7085, Dec. 2014. [Online]. Available: http://ieeexplore.ieee.org/articleDetails.jsp?arnumber=6835179

[65] J. Yu, Y.-D. Yao, A. Molisch, and J. Zhang, "Performance evaluation of CDMA reverse links with imperfect beamforming in a multicell environment using a simplified beamforming model," *IEEE Trans. Veh. Technol.*, vol. 55, no. 3, pp. 1019–1031, May 2006.

[66] H. Li, Y.-D. Yao, and J. Yu, "Outage Probabilities of Wireless Systems With Imperfect Beamforming," *IEEE Trans. Veh. Technol.*, vol. 55, no. 5, pp. 1503–1515, Sept 2006.

[67] "IEEE Standard for Information technology–Telecommunications and information exchange between systems–Local and metropolitan area networks–Specific requirements-Part 11: Wireless LAN Medium Access Control (MAC) and Physical Layer (PHY) Specifications Am," pp. 1–628, 2012.

[68] T. Bai and R. W. Heath Jr., "Coverage and Rate Analysis for Millimeter Wave Cellular Networks," *IEEE Trans. Wireless Commun.*, Feb 2015, Available Online: http://arxiv.org/abs/1402.6430.

[69] S. N. Chiu, D. Stoyan, W. S. Kendall, and J. Mecke, *Stochastic Geometry and Its Applications*. Wiley, September 2013.

[70] P. Stoica and N. Arye, "MUSIC, maximum likelihood, and Cramer-Rao bound," *IEEE Transactions on Acoustics, Speech and Signal Processing*, vol. 37, no. 5, pp. 720–741, May 1989.

[71] D. Ramasamy, S. Venkateswaran, and U. Madhow, "Compressive Parameter Estimation in AWGN," *IEEE Trans. Signal Process.*, vol. 62, no. 8, pp. 2012–2027, April 2014.

[72] H. Shokri-Ghadikolaei, Y. Xu, L. Gkatzikis, and C. Fischione, "User association and the alignment-throughput tradeoff in millimeter wave networks," in *2015 IEEE 1st International Forum on Research and Technologies for Society and Industry Leveraging a better tomorrow (RTSI)*, Sept 2015, pp. 100–105.

[73] H. Park, Y. Kim, T. Song, and S. Pack, "Multiband Directional Neighbor Discovery in Self-Organized mmWave Ad Hoc Networks," *IEEE Transactions on Vehicular Technology*, vol. 64, no. 3, pp. 1143–1155, March 2015.

[74] A. S. A. Mubarak, E. M. Mohamed, and H. Esmaiel, "Millimeter wave beamforming training, discovery and association using WiFi positioning in outdoor urban environment," in *2016 28th International Conference on Microelectronics (ICM)*, Dec 2016, pp. 221–224.

[75] T. Nitsche, A. B. Flores, E. W. Knightly, and J. Widmer, "Steering with eyes closed: Mm-Wave beam steering without in-band measurement,"

in *2015 IEEE Conference on Computer Communications (INFOCOM)*, April 2015, pp. 2416–2424.

[76] T. Oh, C. Song, J. Jung, and I. Lee, "A new RF beam training method for multi-user millimeter wave systems," in *2017 IEEE International Conference on Communications (ICC)*, May 2017, pp. 1–6.

[77] J. P. Beltran, D. D. Donno, and J. Widmer, "Tracking mm-Wave Channel Dynamics: Fast Beam Training Strategies under Mobility," *CoRR*, vol. abs/1612.07957, 2016. [Online]. Available: http://arxiv.org/abs/1612.07957

[78] J. Bae, S. H. Lim, J. H. Yoo, and J. W. Choi, "New Beam Tracking Technique for Millimeter Wave-band Communications," *CoRR*, vol. abs/1702.00276, 2017. [Online]. Available: http://arxiv.org/abs/1702.00276

[79] V. Va, J. Choi, and R. W. Heath, "The Impact of Beamwidth on Temporal Channel Variation in Vehicular Channels and Its Implications," *IEEE Transactions on Vehicular Technology*, vol. 66, no. 6, pp. 5014–5029, June 2017.

[80] F. Devoti, I. Filippini, and A. Capone, "Facing the Millimeter-Wave Cell Discovery Challenge in 5G Networks With Context-Awareness," *IEEE Access*, vol. 4, pp. 8019–8034, 2016.

[81] H. Shokri-Ghadikolaei, C. Fischione, G. Fodor, P. Popovski, and M. Zorzi, "Millimeter Wave Cellular Networks: A MAC Layer Perspective," *IEEE Transactions on Communications*, vol. 63, no. 10, pp. 3437–3458, Oct 2015.

[82] Q. Li, H. Shirani-Mehr, T. Balercia, H. Niu, A. Papathanassiou, and G. Wu, "Millimeter wave channel model and system design considerations," in *2015 IEEE International Conference on Communication Workshop (ICCW)*, June 2015, pp. 1214–1219.

[83] C. A. Balanis, *Antenna Theory: Analysis and Design*. Wiley-Interscience, 2005.

[84] D4.1 Preliminary radio interface concepts for mmwave mobile communications. [Online]. Available: https://bscw.5g-mmmagic.eu/pub/bscw.cgi/d127361/mmMAGIC_D4.1.pdf

[85] A. Thornburg and R. W. Heath Jr., "Capacity and Coverage in Clustered LOS mmWave Ad Hoc Networks," in *2016 IEEE Global Communications Conference (GLOBECOM)*, Dec 2016, pp. 1–6.

[86] A. Thornburg, R. Daniels, and R. W. Heath Jr., "Capacity and scaling laws of dense mmWave and interference alignment ad hoc networks," in *MILCOM 2016 - 2016 IEEE Military Communications Conference*, Nov 2016, pp. 319–324.

[87] A. Thornburg and R. W. Heath Jr., "Ergodic Rate of mmWave Ad Hoc Networks," *submitted to IEEE Trans. Wireless Commun.*, 2017.

[88] M. Haenggi and R. Smarandache, "Diversity polynomials for the analysis of temporal correlations in wireless networks," *IEEE Transactions on Wireless Communications*, vol. 12, no. 11, pp. 5940–5951, November 2013.

[89] Y. Li, F. Baccelli, J. G. Andrews, and J. C. Zhang, "Directional cell search delay analysis for cellular networks with static users," *CoRR*, vol. abs/1709.00779, 2017. [Online]. Available: http://arxiv.org/abs/1709.00779

[90] K. Roth and J. A. Nossek, "Arbitrary Beam Synthesis of Hybrid Beamforming Systems for Beam Training," *IEEE Wireless Communications Letters*, vol. PP, no. 99, pp. 1–1, 2017.

[91] A. Nosratinia, T. E. Hunter, and A. Hedayat, "Cooperative communication in wireless networks," *IEEE Communications Magazine*, vol. 42, no. 10, pp. 74–80, Oct 2004.

[92] H. Nishiyama, M. Ito, and N. Kato, "Relay-by-smartphone: realizing multihop device-to-device communications," *IEEE Communications Magazine*, vol. 52, no. 4, pp. 56–65, April 2014.

[93] S. Biswas, S. Vuppala, J. Xue, and T. Ratnarajah, "On the Performance of Relay Aided Millimeter Wave Networks," *IEEE Journal of Selected*

Topics in Signal Processing, vol. 10, no. 3, pp. 576–588, April 2016.

[94] USRP X-Series. [Online]. Available: https://www.ettus.com/product/category/USRP-X-Series

[95] mmWave Transceiver System. [Online]. Available: http://sine.ni.com/nips/cds/view/p/lang/en/nid/213722

Publications

Publications related to the dissertation

1. A. Thornburg, T. Bai, and R. W. Heath Jr., "Coverage and Capacity of mmWave Ad Hoc Networks," *in Proc. of 2015 IEEE International Conference on Communications (ICC)*, Jun 2015, pp. 1310-1315.

2. A. Thornburg, T. Bai, and R. W. Heath Jr., "Interference Statistics in a Random mmWave Ad Hoc Network," *in Proc. of 2015 IEEE International Conference on Acoustics, Speech, and Signal Pro- cessing (ICASSP)*, Apr 2015, pp. 2904-2908.

3. A. Thornburg, T. Bai, and R. W. Heath Jr., "Performance Analysis of Outdoor mmWave Ad Hoc Networks", *in IEEE Transactions on Signal Processing*, vol. 64, no. 15, pp. 4065-4079, Aug 2016.

4. A. Thornburg and R. W. Heath Jr., "Ergodic Capacity in mmWave Ad Hoc Network with Imperfect Beam Alignment", *in Proc. of 2015 IEEE Military Communications Conference (MILCOM)*, Oct 2015, pp. 1479-1484.

5. A. Thornburg and R. W. Heath Jr., "Capacity and Coverage in Clustered LOS mmWave Ad Hoc Networks", *in Proc. of 2016 IEEE Global Telecommunications Conference (GLOBECOM 2016)*, Dec 2016, pp. 1-6.

6. A. Thornburg, R. Daniels, and R. W. Heath Jr., "Capacity and Scaling Laws of Dense mmWave and Interference Alignment Ad Hoc Networks", *in Proc. of 2016 IEEE Military Communications Conference (MILCOM)*, Oct 2016, pp. 319-324.

7. A. Thornburg and R. W. Heath Jr., "Ergodic Rate of mmWave Ad Hoc Networks", *submitted to IEEE Transactions on Wireless Communication*, 2017.

8. A. Thornburg and R. W. Heath Jr., "Analysis of Mobility and Beamforming in mmWave Mobile Ad Hoc Networks", *submitted to IEEE Transactions on Wireless Communication*, 2017.

Other Publications

1. A. Thornburg, A. Bovik, and R. W. Heath Jr., "Multi-User Real-Time Wireless Video with Perceptual Constraints", *in Proc. of 2013 Asilomar Conference on Signals, Systems, and Computers*, Nov 2013, pp. 1183-1187.

Vita

Andrew Scott Thornburg completed his Bachelors of Science in Electrical and Computer Engineering at the University of Pittsburgh in 2010. He worked as an Electronic Warfare Engineer at Edwards Air Force Base from 2010 – 2012. His research interests span much of wireless communications with a current focus in future mmWave networks. He received the MSEE from the University of Texas in 2014. He spent a year working at PHAZR as a Senior Engineer, a millimeter wave startup in Allen, TX from 2016 – 2017. He currently works for AT&T Labs in Austin, TX as a Senior Member of the Technical Staff.

Permanent address: andrew.thornburg@gmail.com

This dissertation was typeset with LaTeX[†] by the author.

[†]LaTeX is a document preparation system developed by Leslie Lamport as a special version of Donald Knuth's TeX Program.